LIÈGE université Library

http://lib.uliege.ac.be http://matheo.uliege.be

Master thesis : Study of a IR reflective optical system for Earth observation from a 3U CubeSat

Auteur : Calozet, Donatien
Promoteur(s) : Loicq, Jerome
Faculté : Faculté des Sciences appliquées
Diplôme : Master en ingénieur civil en aérospatiale, à finalité spécialisée en "aerospace engineering"
Année académique : 2017-2018
URI/URL : http://hdl.handle.net/2268.2/4675

Avertissement à l'attention des usagers :

Tous les documents placés en accès ouvert sur le site le site MatheO sont protégés par le droit d'auteur. Conformément aux principes énoncés par la "Budapest Open Access Initiative"(BOAI, 2002), l'utilisateur du site peut lire, télécharger, copier, transmettre, imprimer, chercher ou faire un lien vers le texte intégral de ces documents, les disséquer pour les indexer, s'en servir de données pour un logiciel, ou s'en servir à toute autre fin légale (ou prévue par la réglementation relative au droit d'auteur). Toute utilisation du document à des fins commerciales est strictement interdite.

Par ailleurs, l'utilisateur s'engage à respecter les droits moraux de l'auteur, principalement le droit à l'intégrité de l'oeuvre et le droit de paternité et ce dans toute utilisation que l'utilisateur entreprend. Ainsi, à titre d'exemple, lorsqu'il reproduira un document par extrait ou dans son intégralité, l'utilisateur citera de manière complète les sources telles que mentionnées ci-dessus. Toute utilisation non explicitement autorisée ci-avant (telle que par exemple, la modification du document ou son résumé) nécessite l'autorisation préalable et expresse des auteurs ou de leurs ayants droit.

MASTER THESIS

Study of a IR reflective optical system for Earth observation from a 3U CubeSat

---

SUPERVISOR: LOICQ J.

JURY: CLERMONT L.
HABRAKEN S.
KERSHEN G.

CALOZET DONATIEN

Master in Aerospace Engineering

Academic year 2017-2018

Contents

List of Figures

Abstract

This master thesis is about the optical design that would be used in the scope of the OUFTI-NEXT mission. Its goal is to capture image in the MWIR window of agricultural fields, looking at their gradient of temperature from one pixel to another aiming to monitor the field irrigation. Different optical designs are considered and analyzed through different tools. The feasibility of the mission is confirmed and then the performances are described.
In the end, this work is unfinished, and the final design can still be improved. The ground sampling distance could be lowered for a more efficient observation and there is room for improvements concerning the tolerances analysis.

Key words : OUFTI-NEXT, CubeSat, optical design, MWIR, geometrical aberrations, Airy Disk, reflective optics.

Aknowledgement

First of all, I would like to thank my supervisor Jerome Loicq for helping me all the way along this master thesis.

Then, I would like to thank the whole OUFTI-NEXT team, which was present at all the "midi OUFTI" meeting. It greatly helped to present the progress in our respective master thesis to each other.

I would like to thank two of my friends. Pierre Remacle who gave me a ride everyday to go to our internship where most of the master thesis was done. Baptiste Seynaeve, my roommate, writing his thesis this year as well, and providing a great source of motivation.

Finally, I would like to thank both my parents, providing me with the pressure needed to get to work by asking me everyday how my thesis was going.

Chapter 1

Introduction

This master thesis is actually about the OUFTI-NEXT project. This project was thought as a continuation of OUFTI-1, a success project launched in April 2016. This project started in November 2016, many proposals were made to collect general ideas to select a specific mission objective. Eventually, the idea of Bernard Tychon was retained: to detect hydric stress in agricultural fields and, by such, helping in monitoring the fields irrigation. This decision concluded the phase 0 of the project.

Last year, the phase A of the mission occurred. The feasibility of the mission was made based on a parametric study. Such a study is quite complex because there is not much to start from and the outcome of the study is of great importance. It will indeed defined is the mission can be considered or should be abandoned. Fortunately, the first results were quite positive and the feasibility of the mission is now almost certain. Phase A is coming to its end and the Phase B is coming up. Indeed, this year was about the preliminary definition of the mission.

The preliminary definitions must cover all the satellite fields, from the thermal analysis to the attitude control passing through the optical properties. It is hard for one person to focus on all the fields at the same time, this is why the different task are allocated to different studies. The optical properties will be the main focus of this master thesis.

First, the general satellite environment will be defined, slowly aiming to the specific properties needed in the creation of an optical design. Once the optical background is well stated, different designs will be considered and analyzed. Out of those designs, one of them will be selected for a thorough analysis and eventually subject to tolerances.

The aim of this master thesis is to assess the feasibility of the mission concerning the optical properties (Phase A). As it will turn out to be feasible (However by loosing up a few top level requirements), the preliminary computations and design making will be defined (Phase B).

Chapter 2

CubeSat

A CubeSat is a type of nanosatellite ($1 - 10$ [kg]) which is actually a miniaturized satellite made of multiple units, U. The main advantage of such small and light satellites is their low cost since they can easily be launched as secondary payloads or deployed from the International Space Station (*ISS*) and, yet, still accomplish several high-level goals such as Earth observation, scientific tests, biological research,... However, their are small, this is why the structure and the systems aboard must be cleverly and well designed in order to counterbalance the lack of space. CubeSats are composed of different subsystems depending on the mission goals.

1 CubeSat subsystems

Structure

As said earlier, a CubeSat is composed of multiple units, U. One such unit is a cubic box of size $10 \times 10 \times 10$ [cm] and of no more than 1.33 [kg]. Therefore, a 3U CubeSat is a layout of 3 units. FIGURE 2.1 represents the skeleton structure of 1U, 2U and 3U CubeSats.

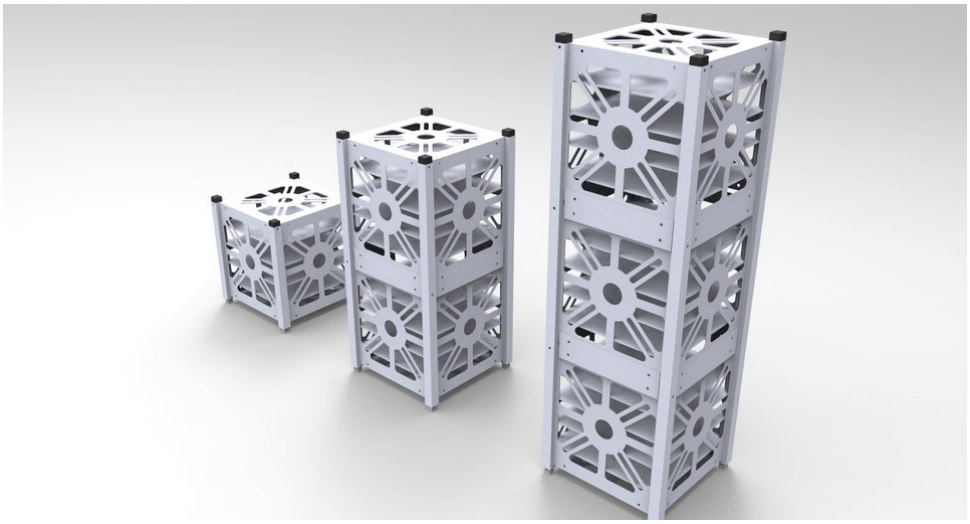

Figure 2.1: Structures of 1U, 2U and 3U CubeSats. [1]

ADCS

The ADCS, standing for Attitude Determination and Control Subsystem is necessary to control the attitude of the satellite. Its purpose is to stabilize the satellite against any disturbances (external or internal). It requires sensors in order to measure the orientation of the satellite such as sun sensors or star trackers. Once the orientation is known, it also requires actuators applying torques around the center of gravity to reach the orientation needed. Those actuators can be reaction wheels or magnetorquers. Also called the AOCS (Attitude Orbit Control System), it ensures the satellite remains in its due orbit. The better the ADCS, the better the pointing accuracy which is a big issue in satellites. [2]

EPS

The EPS stands for Electrical Power System. The best way to store power is by means of solar panel and by taking advantage of the solar flux. Therefore, the types of solar panels and their position is a big issue, they should be as large as possible and be pointing towards the sun as much as possible. However, the solar panels alone is usually not sufficient to power the whole satellite. This is why batteries are also needed, where the energy can be stored and then use in case of emergency or when the satellite is in eclipse. Then, this system obviously needs a Power Control and Distribution Unit (PCDU) to manage all that power.

Thermal control

All of the satellite's subsystems and components actually have an operational temperature range. Therefore, the thermal control makes sure it stays in this range during the whole mission. The thermal environment depends highly on the orbit and on the position with respect to the sun. The analysis must meticulously be done for all modes. The sun synchronous orbits are usually very popular because, in such orbit, the satellite passes over the same spot on the ground at the same solar time of day, helping the thermal control computations along.

There are different means of thermal control depending on the heat exchange and the tightness of the allowable temperature range. Ideally, the thermal control should only use passive systems such as coatings, radiator or straps since they are simplest, light, cheap and not involving constraints on the satellite. However, if the passives means are not sufficient to respect the requirements, actives systems must be used such as Peltier, heaters or coolers even though they imply large powers and attitude control. [3]

Payload

The optical instrument is the main payload, guiding the photons to the detector in the best way possible depending on the mission strategy. It is a key parameter since the success of the mission will depend on its efficiency. Indeed, a flaw optical design would ruin the entire mission while the better the payload, the better the results with a higher amount of reliable information. It is composed of an assembly of optical surfaces which can be reflective, refractive or diffractive. The number of different possible designs is limitless.

Data handling

The payload allows to collect the data needed for the mission, but then all that data must get back to Earth to be used and analyzed. First, the data is stored in the On Board Computer System (OBC) and memory where it will be processed. Then, it is eventually tracked back to Earth thanks to the communication system. It arrives directly to the ground station by means of different possible bands, depending on the frequency.

Mechanism

Mechanisms are used for the moving parts of the CubeSats. Usually, the main mechanisms are the one to deploy the solar panels or the antennas. There are also present in most actuators such as reaction wheels. Even though mechanisms are necessary in most space missions, they must be totally reliable because they will introduce vibrations and mechanical noise which must remain under control or failure is bound to happen. [4]

Propulsion

The propulsion system is actually uncommon for CubeSats. They are usually launched in their orbit as secondary payload and will not need any propulsion system which are large and demand lots of power which goes against the CubeSat's philosophy.

2 OUFTI-NEXT mission

As mentioned in the title, this master thesis will be based on a 3U CubeSat but more precisely, it will actually be about the OUFTI-NEXT mission which will most likely be a 3U CubeSat. When designing its payload, it is compulsory to learn about the mission of the satellite beforehand. Indeed, each satellite is different depending on its mission and its top level requirements.

This OUTFI-NEXT will actually be a demonstrator which will need to prove the use of a thermal detector in Middle Wavelength InfraRed (MWIR) (also called the Thermal Infrared) by taking images of fields that are scientifically exploitable, leading to the potential OUFTI mission as a constellation. Those images will measure the surface temperature, showing the gradient of temperature as accurately as possible. Then, we would be aware of when a field needs to be irrigated and that could greatly improve the different agricultural method, maintenance and their production. The best way to check the water in agricultural fields is by observing its leaves, preferably at certain time of the day. Also, the satellite should focus on specific areas in the world (Maroc, Australia, South America) which will be highly demanding on the orbit's choice and the attitude control.

The observations are made in the MWIR including the wavelength from $3\mu m$ to $5\mu m$. As it can be seen in FIGURE 2.2, the MWIR is dominated by water vapor and carbon dioxide absorption which makes it an appropriate wavelength choice to observe the quantity of water in fields.

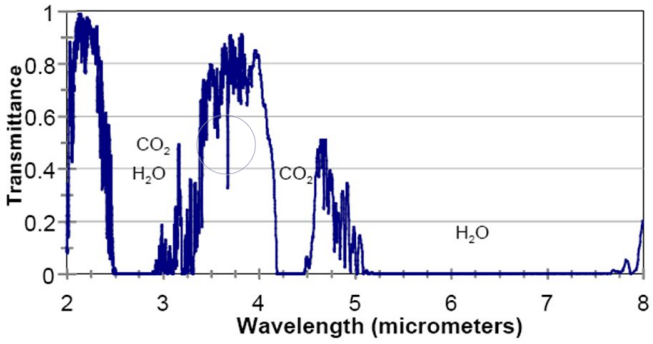

Figure 2.2: Aborption in MWIR [5]

Then, the better the image and thermal resolution and the better it will be able to distinguish the different gradient of temperature in the fields resulting in more precise and reliable results. The ideal aims are a Ground Sample Distance (GSD) of 20 [m][1] for the image resolution and a thermal resolution of about 1K.

3 Team

A satellite is not designed by one person alone but actually by a group of engineers, each having their specialty and field of work. Concerning OUFTI-NEXT, the team is made up of several people :

- The system engineer: he is is the conductor of the mission. He looks for different orbits depending both on the requirements and on launchers availability. He must also ensure the total energy needed for the satellite can be provided. He sets the size of the solar panels and their configuration. His job is also to make sure the project is on the right track with everyone working in symbiosis.

- The thermal engineers: they will study how the heat is spreading in the satellite and make sure it stays in its operational temperature range. One of them will study the general thermal state of the satellite while another one will focus on the cooling of the detector. Indeed, temperatures in satellite are a major factor to ensure the satellite operates correctly. The detector is one of the most important tool aboard the satellite because all the information is going through it and it will not work well unless it is cold enough. Moreover since we are in CubeSat, it is a lot preferable to cool it down by using only passive systems instead of active ones such as a stirling because it influences the state of the whole satellite.

[1] It will be seen later that such GSD can not be reached and the mission's goal must be lowered to a GSD of about 100 [m].

- The attitude engineer: his goal is to make sure the satellite is always pointing where we want it to be pointing otherwise the whole mission is irrelevant. Instabilities can not be avoided. They can be created when mechanisms are deployed, moving the center of gravity and source of vibrations. Loss of stability can also come from outside the satellite due to the harsh space environment. The whole point is to be aware of those possible instabilities so they can be counter in order to keep the satellite in its duty.

- The optical engineers: their job is to make the optical design of the payload. In the scope of the project, two studies will be made corresponding to refractive optics : the first using casual lenses and the other using Fresnel lenses. Finally, the third engineer will be working with reflective optic, using mirrors, which will be the subject of this master thesis.

However, a satellite is not designed by simply adding everyone's individual work together at the end. Indeed, the team work is essential along the whole project. The team must constantly communicate with each other in order to reach a common goal with common restrictions. Satellites are all about compromises. For example :

- Usually, the bigger the component, the better its performances. However, the lack of space is a big challenge. Allocating more space to a certain component will result in decreasing another one;

- When the optical engineer would prefer a lower orbit, this will have an impact on the lifetime of the satellite;

- The energy consumption is also a big challenge in satellite and especially in CubeSats. The total energy is defined by the solar panels surface and position and must then be spread between the different components depending on how important they are and how much energy they require to work well.

- When designing a satellite, components with a big temperature gap should not be placed next to each other in order to avoid high heat transfer which would give a hard time to the thermal engineer.

- The use of different mechanisms can be an asset to move components or to deploy solar panels or even mirrors but on the other hand, it will have some impacts on the attitude of the satellite which must be taken care of. The mechanisms also take some space in the satellite.

In the end, when a modification would be absolutely convenient to one engineer, there is always another engineer to whom it would not suit at all. Then, it is all about finding the best balance for everyone in order to reach the most effective and reliable satellite in the end.

Chapter 3

State of the art

This section will identify other CubeSat missions in order to get familiar with the subject. In order to be relevant, those missions must be about observation so they are equipped with an optical design, subsystem of main interest in the scope of this thesis. Indeed, it is always interesting to be aware of the technologies used in other missions. Then, the actual satellite can be inspired from other satellites that already proved their worth.

1 ASTERIA

Overview

The Arcsecond Space Telescope Enabling Research in Astrophysics (*ASTERIA*) is a 6U CubeSat NASA project ($\simeq$ 12 [kg]) which was launched with Falcon-9 in August 2017 to the International Space Station (ISS) and then deployed from the station in November of the same year. It will then operate in Low Earth Orbit (LEO). This satellite has a demonstrator purpose for astrophysical measurements with a lifetime of 90 days. As stated in its name, the ASTERIA's main challenge is to achieve a line-of-sight pointing error of no more than one arcsecond on top of a very stable focal plane temperature control. Indeed, in astrophysical, precision photometry is a key to observe interesting phenomena such as transiting exoplanets or stellar activities. [6]

Figure 3.1: ASTERIA CubeSat. [6]

Payload

As stated in the overview, the pointing accuracy is the main challenge in this mission. The optical design needs to be very efficient. The telescope used is presented in FIGURE 3.2 and its position in the CubeSat could be seen in FIGURE 3.1. Even though, it is a 6U CubeSat, the telescope still fits in 1U in width, leaving room for the other components. The telescope is actually composed of a baffled assembly using a single lens as well as a Complementary Metal–Oxide Semiconductor(CMOS) imager for pointing control. CMOS actually tracks different guiding stars and then the focal plane is shifted in order to counterbalance the potential residual pointing error. For high thermal control, the payload is isolated from the rest of the satellite. It uses mostly passives systems. [6]

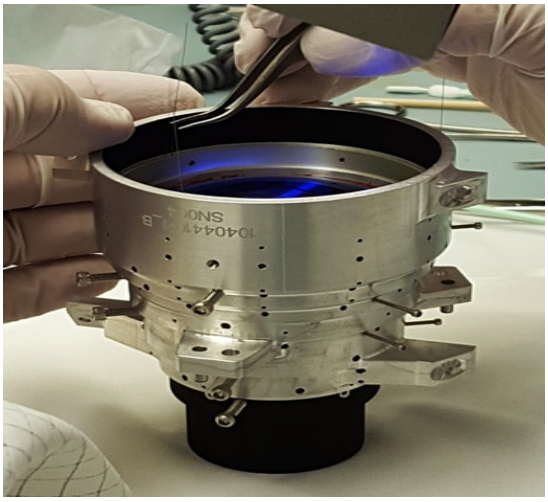

Figure 3.2: Telescope of the ASTERIA CubeSat. [6]

2 ARKYD-6

Overview

The 6U CubeSat Arkyd-6 was successfully launched earlier this year, on January 12, it was sent on a sun-synchronous orbit at an altitude of 505 [km]. This CubeSat is interesting to study since its mission is very similar to OUFTI-NEXT. It will indeed operate in MWIR, this region is sensitive to the presence of water (including that in hydrated minerals) and thermal energy. It can be used as a tool to search for water on Earth and beyond. The main goal will be on the latter, searching for water on near-Earth asteroids. If an actual source of water were to be found on asteroids, it would be the first step to creating a civilization in space. It the system operates well, it also plans to capture MWIR images of targets on Earth's surface, including agricultural land.

Figure 3.3: Artist's rendition of Arkyd-6. [7]

Eventually, the Arkyd-301 mission should be launched in 2020 to explore the potential asteroid with water sources. It will also carry piggyback miniprobes, which will deploy from their mothership and burrow into their target asteroid to get even closer looks at the space rocks.

Payload

The satellite is composed of a mid-wave infrared sensor, second-generation avionics, power systems, communications (only 115 kbit/s S-band terminal), and attitude determination and control systems. It uses a body mounted and two deployable solar arrays (delivering an orbit average power of 35 W). It weights around 10 [kg] overall.

The Arkyd instrument (FIGURE 3.4) is a broadband imager spanning 3.4 to $5.1\mu m$. From its altitude of 505 [km], it still achieves a great ground resolution of 26 [m], overcoming the diffraction limit issue[1]. It also has a quite high EFL of 200 [mm], an Indium-Antimonide detector array of 640×540 pixels (Same array as the one that will be used for OUFTI-NEXT), which is cooled to 77 K with a Stirling cryocooler. Enventually, the instrument captures imagery of a 19×15 [km] ground footprint.

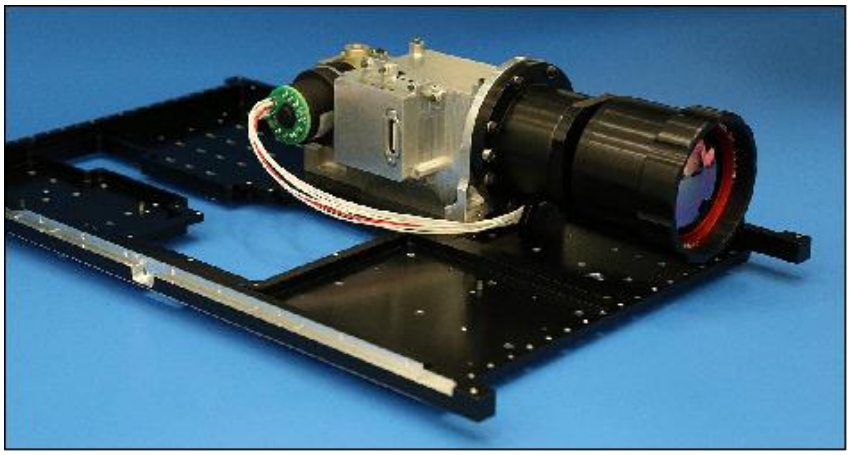

Figure 3.4: Arkyd's MWIR imager. [7]

It can be seen that even though the CubeSat is made of 6U instead of 3U (in the case of OUFTI-NEXT), the instrument still fits only in one side of the satellite, taking about 2U in length. Therefore, it is not taking much more space than the instrument aboard a 3U, leaving more room for other systems and subsystems.

[1] Such a high GSD is indeed fairly impressive seeing how the diffraction limit will turn out to be a big issue (especially when observing in MWIR) in designing the optical design for OUFTI-NEXT.

3 CIRAS

Overview

The CubeSat Infrared Atmospheric Sounder (CIRAS) which will be launched in late 2018 is a 6U CubeSat designed to measure the infrared radiation of the Earth in MWIR. A schematic view of the satellite is shown in FIGURE 3.5. The observation of this region of the spectrum fulfills different features such as weather forecast or information about the water vapor and temperature of the lower troposphere. This CubeSat is a NASA mission which is actually a first step in initiating Earth Observation Nanosatellite - Infrared (EON - IR). [8]

Figure 3.5: CIRAS CubeSat. [6]

Payload

The main issue in this mission is the wavelength in which the observation are done : $3 - 5\mu m$. It presents three key technologies :

- Two High Operating Temperature Barrier InfRared Detector (HOT-BIRD) photosensitive materials are used in a 2D array. They are very cheap and induce little noise. They also present a high uniformity and a high operational temperature range.
- An infrared black body made of black Silicon mounted in a flat plate having a really high emissivity, used for calibration.
- The MWIR Grating Spectrometer (MGS) holds in a CubeSat and provides imaging spectroscopy for atmospheric sounding. The MGS is fixed and the grating allows a reduction of the distortion. However, it only works in the spectral range included between 4.8 and $5.1\mu m$. [9]

The payload actually includes a mirror which can fully rotate around itself allowing to observe both Earth and deep space. It uses a single aluminum mirror which is coated with gold because it is highly reflective in the CIRAS band[2]. Then the energy coming from the telescope is focused in the entrance slit of the MGS. Moreover, there is a window at the interface between the optics and the detector and a cold filter next to the focal plane for thermal control. Indeed, the gradient of temperature between the optics and the detector is quite significant. The closer they are to each other the greater the heat transfer. This is an issue for all payloads design.

[2]Gold coating will also be used for OUFTI-NEXT, very efficient in MWIR band

4 Lunar Icecube

Overview

Since most CubeSats do not have any propulsion system (too large and energy demanding), they are usually send to an insertion orbit as secondary payload and then are able to drift to their required position. [10]. However, the age of CubeSats for deep space exploration sees the light of the day. Lunar IceCube is a 6U satellite among the first small satellites exploring deep space. As its name suggests, the mission's goal is to search for water ice on the surface of the moon. It will follow a path using the gravity of the Earth, the Sun and the Moon before reaching its lunar orbit. The satellite includes a low-thrust electric propulsion system. Besides scientific research, the mission will also provide information aiming to send human further into the solar system. [11]

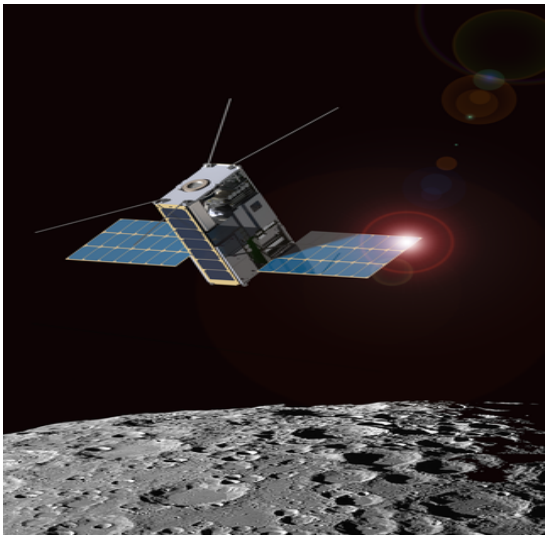

Figure 3.6: Artist's rendition of Lunar Icecube. [11]

Payload

Although missions such as the Lunar Prospector, Chandrayaan-1, and Lunar Reconnaissance Orbiter, discovered traces of water on the moon surface, their payload was not optimized for observing the elements in the infrared wavelength bands (ideal for detecting water). Lunar Icecube will be using the Broadband InfraRed Compact High-Resolution Exploration Spectrometer (BIRCHES) which was specifically designed to distinguish forms of water. It is actually a compact version of the volatile-seeking spectrometer on New Horizons which could be improved thanks to the recent technological advances, especially in miniaturization. Moreover, the study is not confined to the Moon's shadowed area. [11]

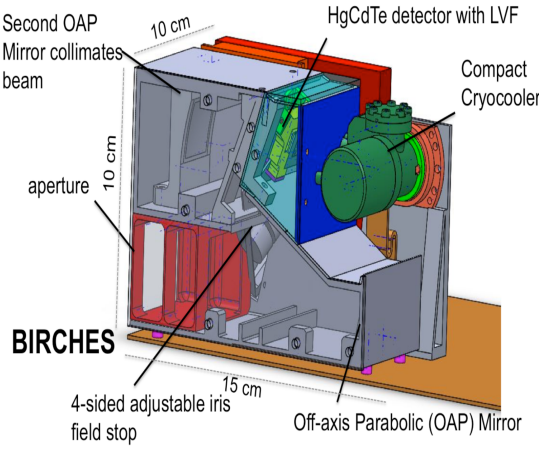

Figure 3.7: BIRCHES prototype. [12]

BIRCHES is an incredible instrument which can fit in 1.5U, weight no more than 2.5 kg and does not need more than 5W to operate. It has the following characteristics:

- It has a high-resolution spectrometer with compact microcryocooler (keeping its temperature below 140K) with a spectral resolution of 5 [nm] which is sufficient to distinguish important volatiles and mineral bands.

- A HgCdTe detector for broadband measurements mostly in the infrared ($\simeq 1 - 4\mu m$).
- An optical box system with an aperture of about a half U and composed of two Off-Axis Parabolic (OAP) mirrors with high flexibility in maintaining the spot size[3] to $10km \times 10km$ even if the altitude is modified by up to five times its value. [12]

[3]The concept of spot size will be explained in details in CHAPTER 3

Chapter 4

Optics : Theory

The optics is the science dealing with the propagation of light, the changes that it undergoes and produces as well as other phenomena associated to it. More than a science, it is part of our everyday life. Indeed, the human eye is no other than an amazing natural optical system. It allows us to see the visible light which gives a meaning to our world. If they were not any sources of light we would be constraints to live in an infinite darkness. But thankfully, the light sources such as the sun or simply any kind of lamps allow us to see the world as it is.

However, as good as it is, the human eye has its limitations just as any optical system does. It only allows us to observe in the visible light and only as far as it can see. This is where the artificial optical design comes into play. By using the right instruments and transformation of light, scientific are able to observe phenomenon at other wavelength, giving significant data. For example, the UV spectral region allow to detect the presence of H and He in the atmosphere while an application of thermal infrared observation would be to study surfaces temperature [13]. In the scope of OUFTI-NEXT, observing in mid-infrared is a good way to analyze the vegetation cover and the biological properties such as the percentage of water in different fields, as explained in CHAPTER 2. The other main purpose of optical design is obviously to observe any object from very far away out of the human's eye reach. This is actually how the astronomers are able to map the universe bit by bit and how remote objects such as other planets or asteroids can be studied.

However, the conception of an optical design is only possible based on a thorough understanding of the light and its properties. The purpose of this chapter is to establish a strong basis of the optics theory. Only then, the conception of the optical design will be possible followed by smart analysis based on the knowledge acquired in this chapter.

In the scope of this project, the optical design needed must concentrate the light rays in one focus. A simple such design is shown in FIGURE 4.1.

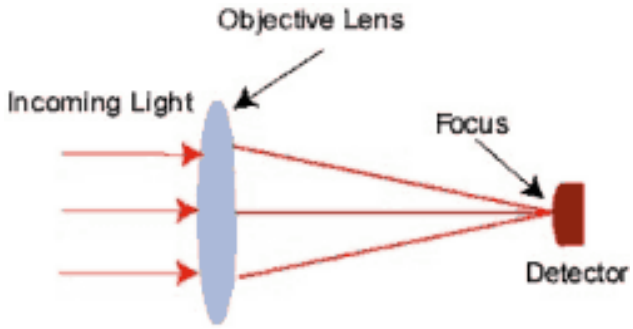

Figure 4.1: Basic optical design configuration [14].

This simple design uses one lens which focuses all the light rays straight into the detector. The object observed is considered at infinite distance resulting in the incoming rays parallel to each other. One of the main optical parameter is the focal length (f) which is the distance between the center of the lens and the focus point. Actually, in real case scenatio, the focus point will not exactly be a point. Its surface can be represented on the focal plane and is called the spot size. The whole purpose of the optical design will be to have that spot size as small as possible to obtained the best performances possible. However, different phenomena will tend to increase that spot size.

The light is a wave propagating through space but it can also be considered as a ray or even as a corpuscle in order to fully understand its behaviour and characteristics. The different forms of light will be studied one at a time allowing to understand the different related phenomena and eventually the performance of the optical design, as analyzed in CHAPTER 7.

1 Light = wave

1.1 Diffraction phenomenum

For a good understanding of the wave and diffraction concepts, let us first introduce a simple situation. When throwing a stone in the middle of lake, this latter will produce concentric waves equidistant from each other (representing the wavelength) and perfectly circular (assuming a very still lake), if nothing comes in the way of those waves and if the lake is big enough, very far from the position of the rock, the wave will appear parallel to each others. However if those parallel wave must go through a narrow entry, the obstacle will generate new concentric waves behind it. This phenomenon is called diffraction. It happens when going through an opening of finite length.

In space observation, the point source of light which can be compared to the rock, are usually observed from very far away. Therefore, the wave of the point source reaching the optical system will be straight and parallel carrying the information about the point source. However, the optical system is composed of sharp edges which will influence the wave propagation and make it impossible for the optical system to reach an infinite resolution [15]. Indeed, going through the optical aperture of the system will be similar to going through a narrow obstacle, involving new concentric wave. The bigger the entrance pupil diameter and the less the optical

system will suffer from the effects of diffraction. With big entrance pupil diameter, the wave is less perturbed when going through. Moreover, this also strongly depends on the wavelength. The diffraction effect, as well as the effects of the aperture size and the wavelength are shown in FIGURE 4.2.

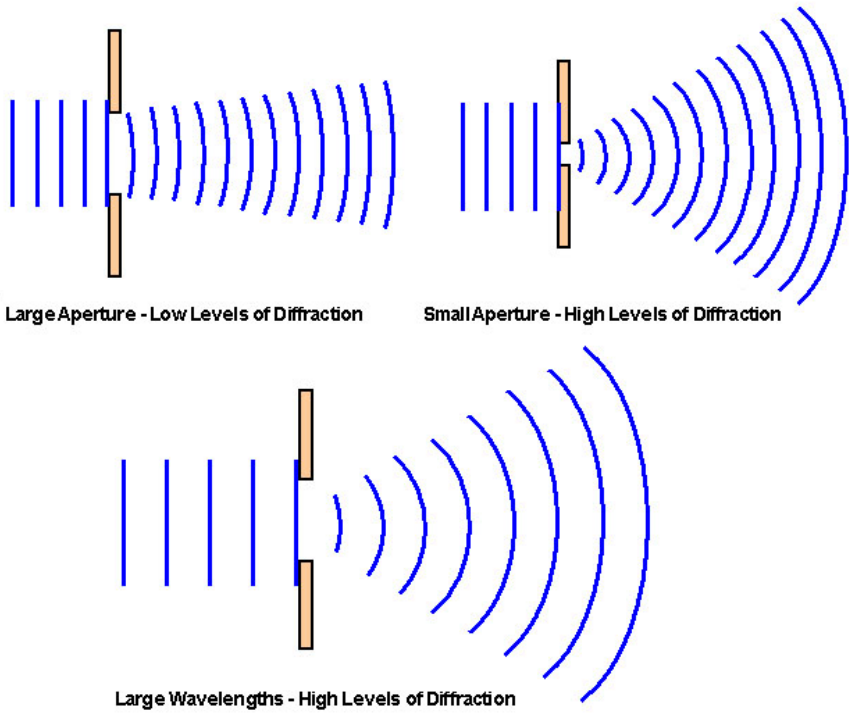

Figure 4.2: Diffraction effect for different parameters [15].

It shows how smaller aperture and larger wavelength involves higher levels of diffraction. In this picture, the rays are actually coming perpendicular to the wave front meaning a very far away source of light. Int the end, the wave contains the information about the object observed, and when diffraction occurs, it modifies the information by decreasing the image resolution. Diffraction must be avoided.

A better way to consider the diffraction phenomenon is to use the Point Spread Function (PSF). This function defines the image that will be obtained on the focal plane [1]. The diffraction pattern observed in the focal plane is the Fourier transform of the aperture field distribution. In the most common case of circular aperture, the diffraction pattern is represented in FIGURE 4.3.

[1] It actually represents the image considering all the phenomena including the geometrical aberration introduced in the next section. But for now, the diffraction PSF will be considered meaning the component due to the geometrical aberrations are not taken into account yet. So this section focus on the diffraction phenomenum only

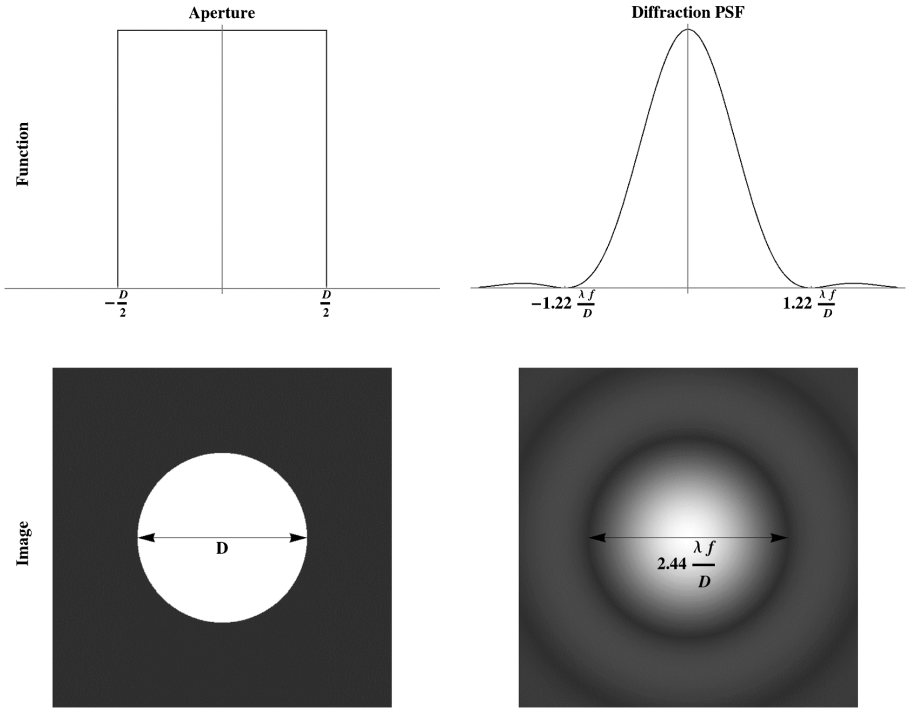

Figure 4.3: PSF function and corresponding diffraction pattern [16].

It represents the shape of the aperture and the corresponding shape of the diffraction PSF on the focal plane, called an Airy pattern. The top row is a cross-section of the functions and the bottom row shows an intensity plot of the functions. The Rayleigh criterion is defined by the first zero of the PSF : $\pm 1.22\lambda(f/D)$ with f the focal length and D the entrance pupil diameter. When the system is aberration-free, the diffraction blur is dominated by the diffraction pattern, the system is said diffraction-limited. In that case, the physical diameter of the Airy disk, D_A (representing the difference between the two first minima), which is twice the Rayleigh criteria, will define the best image resolution possible and is expressed by EQUATION 4.1.

$$D_A = 2.44\lambda\frac{EFL}{D} \tag{4.1}$$

Where

- λ represents the wavelength;
- D represents the aperture diameter;
- EFL represents the effective focal length. It is the same as the focal length f in the case of a single thin lens/mirror system. The effective focal length for an optical system in air is the distance over which initially collimated (parallel) rays are brought to a focus. It defines the optical power of the system, the shorter it is and the closer the rays will focus meaning a strong optical power. In complex optical design with many mirrors and lenses, the computation of the effective focal length becomes very complicated. The software usually compute it itself [17].
- The fraction $\frac{EFL}{D}$ is often renamed $F\#$, called the $F - number$.

Therefore, this airy disk diameter must remain as small as possible for a more accurate focus enabling a good image resolution. Otherwise, this will result in a blurry image which is not acceptable in most missions. When designing an optical design, one will want the smallest airy disk diameter possible. There are only 3 ways to decrease it, by referring to EQUATION 4.1.

1. Decrease the wavelength;
2. Increase the effective focal length;
3. Increase the pupil entrance diameter.

However those 3 reduction methods are almost always fixed by the mission's top level requirements. Indeed, the range of wavelength observed is part of the mission statement and can not be modified. The effective focal length is directly linked to the altitude, the GSD and the pixel size of the detector which are 3 parameters with usually low margin of modification. Finally, in the case of CubeSats, the pupil entrance diameter can hardly be bigger than 10 [cm] except if deployable optics is considered but then bringing other issues such as the mechanisms and the stability. Moreover, as it will be seen in the next section, increasing the pupil's size strongly increases the geometrical aberrations, tarnishing the image quality.

The resolution of a system is its ability to distinct two points source at a considered distance. This distinction limit is defined by the Rayleigh criterion. Indeed, the FIGURE 4.3 considers only one point source. Let us now considered two points source with the same diffraction PSF and therefore both producing a perfect diffraction pattern representing the Airy disk. The Rayleigh criterion says that if the maxima of the second source is further than the first minima of the first source, then the two points are resolvable. It comes back to say that the distance between both peaks must be higher than the radius of the Airy disk. FIGURE 4.4.

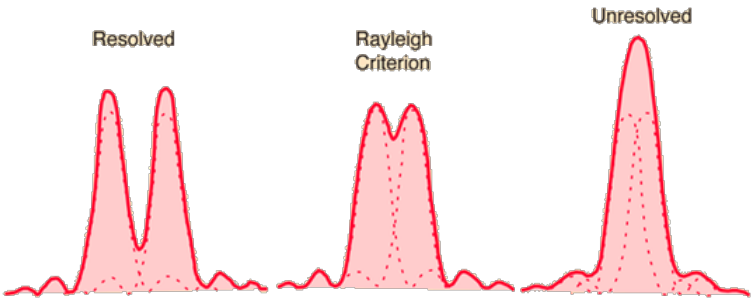

Figure 4.4: PSF function and corresponding diffraction pattern [18].

1.2 MTF

It is also very helpful to understand how the imaging system is modifying the contrast of the spatial frequencies of the scene by calculating the Fourier transform of the system PSF. It gives the system transfer function which is called the Optical Transfer Function (OTF). The PSF is actually a 2D distribution of light, it contains all the combined information related to the transmission through the optical system of an object point source [3]. Therefore, the PSF and its corresponding OTF have a direct impact on the image quality. For instance, a broader PSF

translates into an OTF that drops off more rapidly in the higher spatial frequencies, resulting in a blurrier image.

The Modulation Transfer Function (MTF), the modulus of the complex OTF, is a great tool to show how the transfer function modifies the contrast of each spatial frequency. When considering a specific pattern wave (sine shape), the modulation is defined by EQUATION 4.2 according to FIGURE 4.5. This latter assumed an optical system with aberrations, resulting in a loss of intensity in the image modulation. [19]

$$M = \frac{I_{max} - I_{min}}{I_{max} + I_{min}} \tag{4.2}$$

It actually represent the image contrast with I_{max} and I_{min}, respectively the highest and lowest intensity.

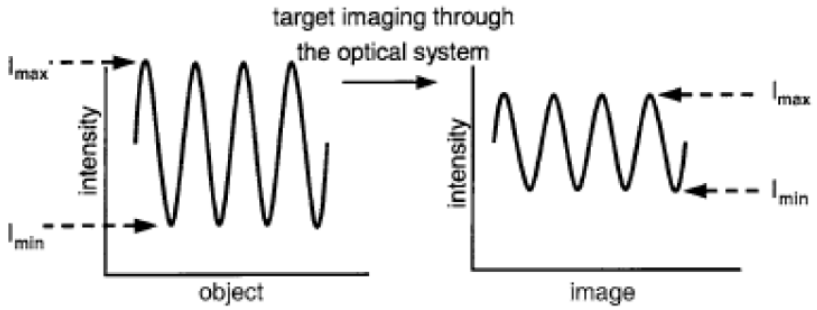

Figure 4.5: Intensity of image and object wave [20].

Then, the MTF is actually the fraction of the image modulation over the object modulation. A MTF of 100% can happen at very low frequency and meaning the pattern is unattenuated through the optical system and that it retains full contrast. But usually, when going through the optical system, the MTF considerably drops. The following FIGURE 4.6 shows the difference between the perfect object contrast and then a 20% contrast for the image which only partially retain the contrast.

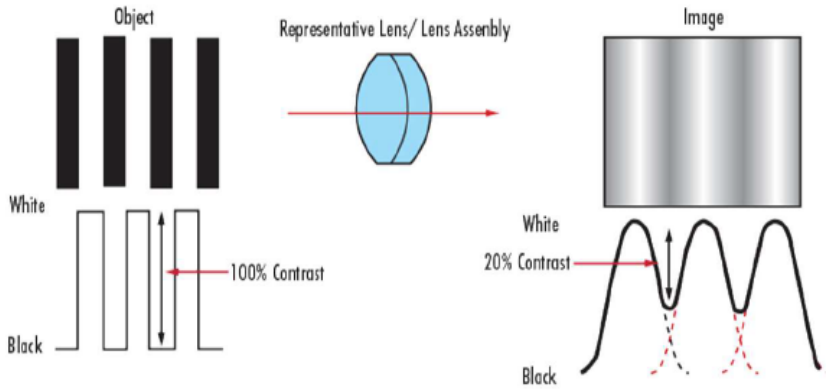

Figure 4.6: Contrast intensity for object and image [3].

In optical software, the MTF are usually represented in graphics as shown in FIGURE 4.7 which greatly helps for the analysis since the results are much easier to analyze.

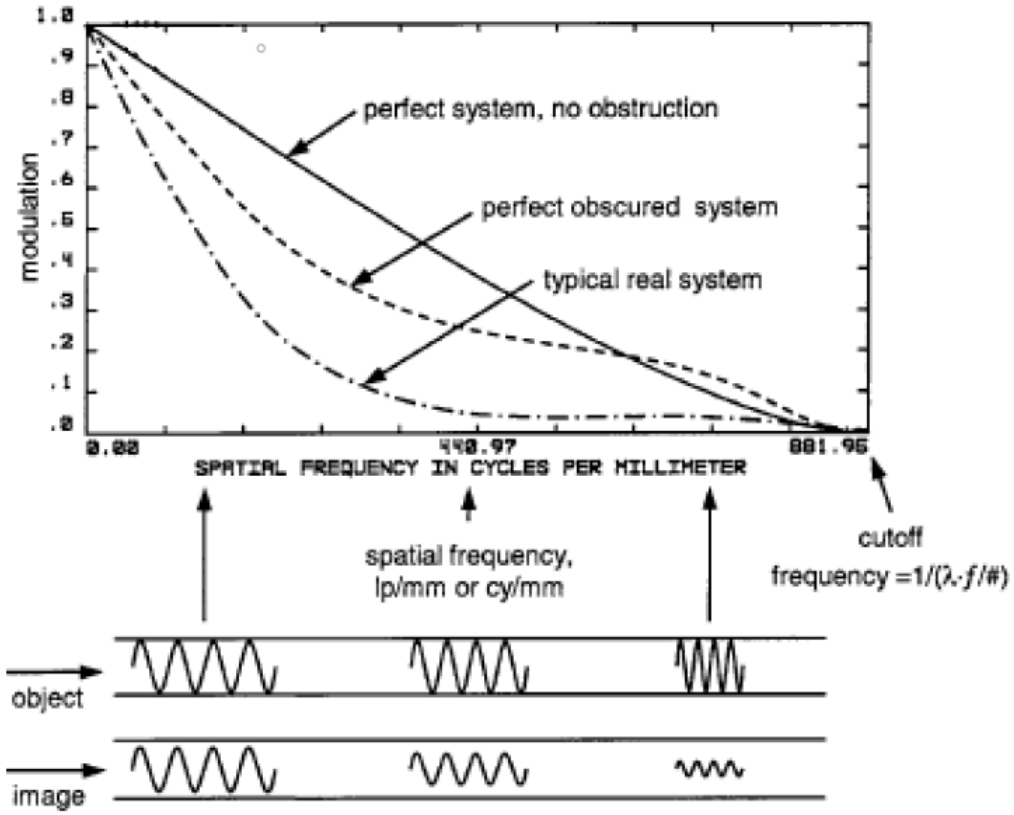

Figure 4.7: MTF values with respect to the spatial frequency for different cases [20].

The diffraction-limited curve is obtained when considering a perfect system, it represents the best MTF that can be reached with respect to the spatial frequency ([number of cycles/°] or [number of cycles/mm]). When the frequency increases, the image contrast decreases as shown in the waves below the graphic for different frequencies. An aberration-free system presenting obscuration will have a lower MTF. The obscuration can be introduced from surfaces standing in the way of the light rays[2]. Then the MTF of a typical real system with aberrations is even lower and drops quicker. Therefore, a real optical system wants its MTF to be as close as possible to the diffraction-limited one[3].

When contrast drops to zero, it is called the cutoff frequency which is given by EQUATION 4.3.

$$\nu_{cutoff} = \frac{1}{\lambda f\#} \tag{4.3}$$

However, using a pixelated sensor will actually limit the cutoff frequency to the Nyquist frequency. The Nyquist frequency ν_N is the maximum spatial frequency allowed without intro-

[2]For instance, the Cassegrain telescope introduced later presents some obscuration due to its secondary mirror standing up front and preventing some light rays to reach the primary mirror.

[3]It can be seen in FIGURE 4.7 that at higher frequencies, the perfect obscured system will actually exceed the diffraction-limited curve. This is due to the light inside the first the Airy Disk transferring to the outer one. In such case, finer details can be obtained than the diffraction limit. [20]

ducing errors, defined by EQUATION 4.4.

$$\nu_N = \frac{1}{2p_s} \quad \text{with } p_s \text{ the pixel size.} \tag{4.4}$$

That way, the signal modulation has its maxima and minima in distinct pixels. If the frequency increases, one pixel could be in presence of a maximum and a minimum at the same time resulting in a blurry resolution. So, the Nyquist frequency represents the maximal acceptable frequency, it is also called the pixel cutoff frequency. [21]

2 Light = ray

As said in the previous section, light is a wave phenomenon propagating through space and through optical designs. However, the design of optical systems are mostly made considering the ray nature of the light. This section will be based on geometric optics. Therefore, those rays are simply following a straight line in space. The issues will come up as soon as it encounters a surface where it will either change its direction of travel (refraction or reflexion) or it will be absorbed. In optical design, one wants as little light as possible to be absorbed by the mirrors or the lenses. The absorptivity will take place at the detector level. The upcoming section will focus on the change of direction of the light rays. Property that will be used to focus the light rays as accurately as possible.

2.1 Refraction & Reflection

Since the speed of light changes from one medium to another medium, when the light enters another medium, its direction changes according to Snell's law (EQUATION 4.5). Each medium has its index of refraction, n, which is set to 1 for vacuum. Then, the denser the medium, the higher its index of refraction. It is also a function of the angle of incidence, i, which is always taken with respect to the normal line.

$$\frac{\sin i}{\sin r} = \frac{n_2}{n_1} \tag{4.5}$$

In some cases, the critical angle is reached and instead of refraction, the light will reflect on the surface, in that case, the law is very simple since the angle of incidence equals the angle of reflection : $i = -i$. This is under this assumption that light is either reflected or refracted but both can occur simultaneously. Therefore, in addition to the Snell's law, the Fresnel equations will define the ratio of light reflected and transmitted.

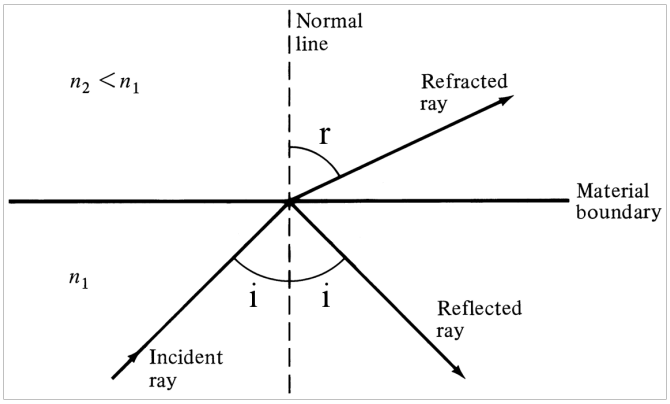

Figure 4.8: Refractive vs Reflective : Snell's law [22]

Even though the light is considered as a ray in this section, some materials will show different properties to the light depending on its wavelength. The atmosphere itself is a good example, indeed, and fortunately for us, it is completely opaque and therefore absorbs 100% of all the harmful X-rays, Gamma-rays and most of the ultraviolet rays. It also blocks most of the infrared radiation and the very low energy radio wave. On the other hand the visible light can go through as well as the radio waves, allowing the astronomers to observe the universe at those wavelength from Earth. The opacity of the atmosphere with respect to the wavelength is represented in FIGURE4.9.

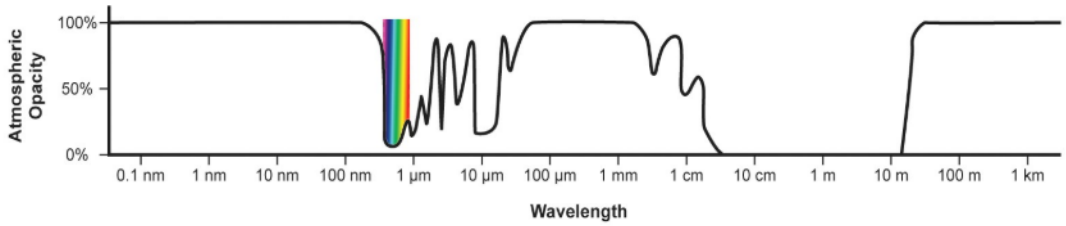

Figure 4.9: Atmospheric opacity [20].

Basically, everything we know about the Universe comes from studying the light or the electromagnetic radiation emitted by objects in space. To get a complete picture of the Universe, we need to see it in all of its light, at all wavelengths. This is why it is so important to send satellites into space, to get above our atmosphere which prevents a lot of this valuable information from reaching us. [23]

Some materials can actually show some very interesting properties. For instance, the semiconductor silicon (Si) has the property to be transparent in the low energy infrared of the spectrum, so the infrared rays will go through, while it is opaque to photon in the visible region of the spectrum so it will prevent such light to go any further by reflecting it. This property is very handy for optical design meant to study in the infrared region of the spectrum without involving any perturbations from the visible light. [24]

When both concept of reflection and refraction are well mastered, one will be able to "play" with the light and guide it the way he wants it, this is the whole point of optical design, using

that geometrical characteristic of the light in order to observe things the eye would be unable to see. However, the light is tricky and it is not as easy to play with it. Indeed, this geometrical optics comes with a lot of aberrations tarnishing the true nature of the light, resulting in the image deterioration of the initial object observed.

2.2 Aberrations

Using such geometrical optic for the light is subject to a few assumptions :

- To prevent diffraction phenomenon, the wavelength is considered very small compared to the components size of the optical design which is usually true;
- The light rays are independant and do not interact with each others;
- In homogeneous medium, light travels in straight line (as in vacuum) and at a flat interface between two mediums, it will follow Snell's law and the Fresnel equations.
- The light reversibility principle is applicable, stating that light will follow exactly the same path if its direction of travel is reversed.

The geometrical aberrations mostly appear when ray angle is large or off-axis. It is interesting to first approximate an ideal system free of aberrations. Therefore the actual locations of the object and the focus plane can be determined. This approximation can be done thanks to the paraxial optic which assumes very low ray angles remaining close to the optical axis, as shown in FIGURE 4.10. Moreover, it allows to determine the clear aperture and the separation between the optical elements and also the optical power leading to the radiometric budget.

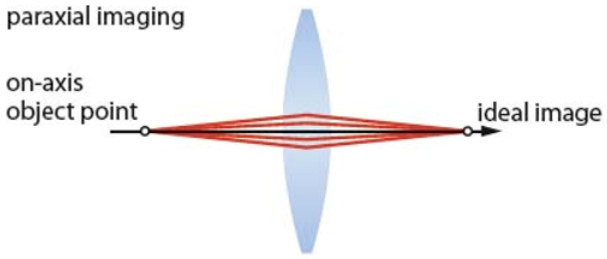

Figure 4.10: Paraxial approximation for low ray angle [25].

The paraxial approximation quickly becomes inaccurate when the ray angle increases or away of the optical axis, this is where the aberrations appear. A specific aberration is the chromatic aberration which is the most sensible one. It already shows up at very low angle of incidence. However, this kind of aberration is only produced through refractive optics. It will happen because the index of refraction depends on the wavelength. Fortunately, this master thesis is about reflective optics so such aberrations will not have to be dealt with. However, there are

still plenty of aberrations left.

All the following aberrations about to be introduced are called monochromatic aberrations and occur both in refracting and refracting systems. It happens when light of one wavelength is involved, out of the paraxial approximation. This time the sine of the Snell's law will not be simplified to the angle ($\sin i \simeq i$) but will use the sine decomposition : $\sin i = i - \frac{i^3}{3!} + \frac{i^5}{5!} - ....$ Therefore, there is an infinite number of aberrations but only the third order aberrations, called the Seidel's aberration, will be presented. The fifth order ones and more can almost always be neglected. Those aberrations are actually defined by their deviation from the paraxial ray trace and strongly depends on the optics shape, the field angle and the aperture size.

Spherical aberration

The spherical aberration is an axial one, contrarily to the other Seidel's aberrations which are all off-axis aberrations. FIGURE 4.11 shows the difference between a perfect lens and a lens causing spherical aberrations. It occurs when light rays parallel to the optical axis at different height enter the system but focus at different point along the axis, the outer rays intersect each other closer than the inner rays. Rays very close to the optical axis intersect at the paraxial focus meaning the further they are from the center, the more aberrations they produce. This is actually due to the prismatic effect since the ray passing through the edges are more deviated. The best focus plane will move up front of the paraxial focus. On that plane the other rays spread apart from the focus point in a concentric way. Hence the name of "Spherical aberrations".

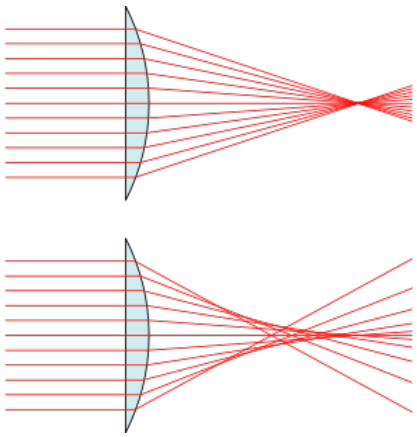

Figure 4.11: Aberrations free vs Spherical aberrations [26].

There are two main ways to get rid of such aberration or at least to minimize them. The first way is to use aspherical lenses or mirrors, the complex surface of such element allow to reduce the spherical aberration. It can be seen in FIGURE 4.12A that the focus point is identical for all rays. The second way to reduce spherical aberration is to reduce the entrance pupil, which is called diaphragming the aperture, so the longitudinal aberration will not be as bad. It is shown in 4.12B. Theoretically, it should be reduced to the paraxial approximation in order to be totally aberration free. However such a reduction should be done very carefully since the reduction of the pupil entrance brings other issue concerning the Airy's pattern (related to the Airy disk EQUATION 4.1) and the radiometric budget. Indeed the entrance pupil diameter is

a very important parameter when designing an optical design as it will be seen in the further chapters.

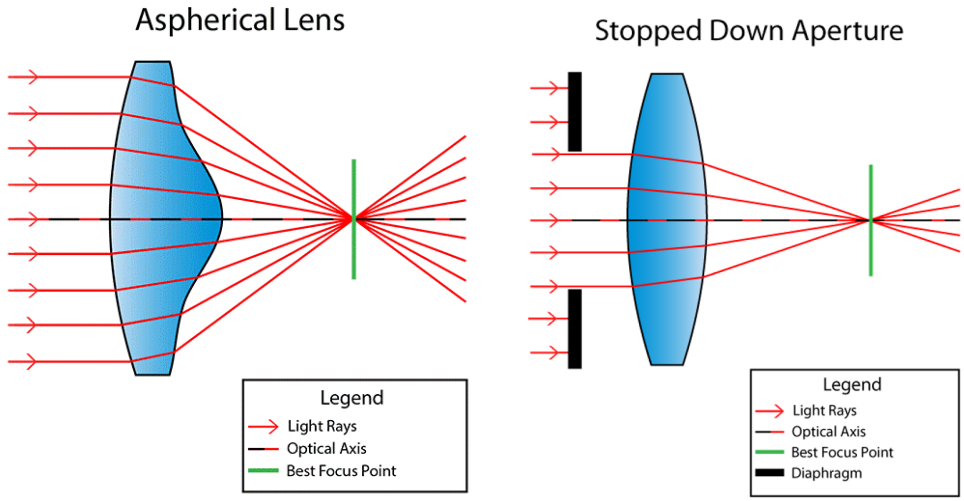

(a) Aspherical lens (b) Smaller pupil entrance

Figure 4.12: Ways to reduce spherical aberrations [26].

Coma

Coma occurs when the intersection of ray is not symmetrical, in an oblique bundle of light. It involves the off-axis rays passing near the edge of the lens and intercepting the image surface at different heights than those going through the center of the aperture. This aberration results in an image in comet-like shape, a light core with a spreading tail which is quite noticeable when analyzing the spot size : red mark in FIGURE 4.13. Similarly to the spherical aberration, the rays passing at the periphery are the more deviated. On the other hand, the focus is laterally displaced instead of longitudinally.

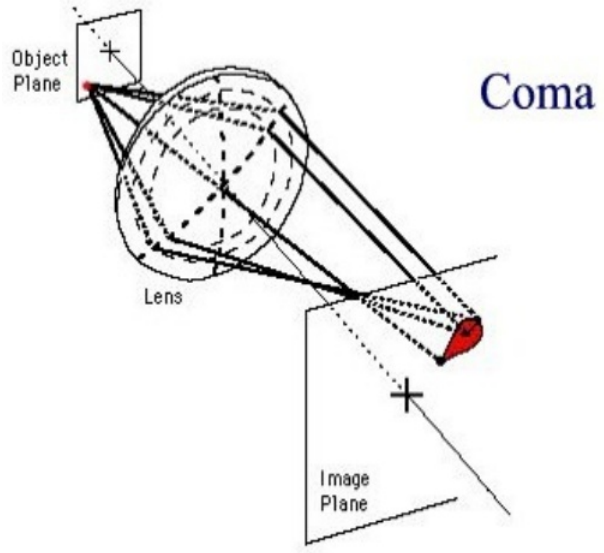

Figure 4.13: Coma aberration with its comet-like shape [27].

This aberration is very troublesome because not only is the off-axis image unsharp but it is also asymmetric. Therefore, coma aberration prevents from getting accurate results which makes it impossible to locate stars or planets. It gets even more troublesome when combined with spherical aberrations and the position of the aperture stop becomes critical. The coma aberration can also be reduced by diaphragming the aperture. Again, this solution does not work well for the diffraction limit or the signal to noise ratio.

Astigmatism

In order to understand the astigmatism aberration, it must be explained in 3 dimensions. It appears when there is a difference between the optical power of the system in the tangential plane (along the height of the pupil) and the sagittal plane (along the width of the pupil). Both of them have their own focal surfaces which are not superimposed but causing a defocus : FIGURE 4.14.

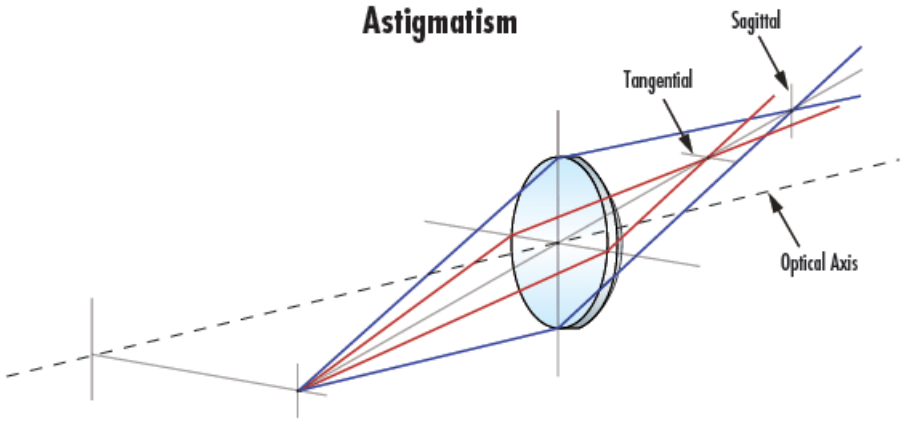

Figure 4.14: Astigmatism aberration [28].

Mid-way between the tangential and sagittal focus line, that's where the blur of light reaches its smallest dimension and therefore where the best focus plane lies. The size of the pupil entrance has no effect of this aberration. It will become worse with higher power lenses.

Field curvature

Actually, the sharpest image is formed on a curved focal surface. This is why a flat focal plane will induce aberration due to the field of curvature. The curved image surface where the ray intercept is called the Petzval surface [27] and is represented in black dotted line in FIGURE 4.15.

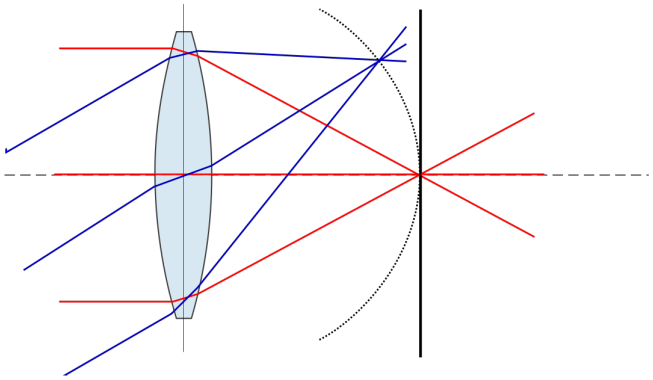

Figure 4.15: Field curvature aberration [29].

Practically, it can not be totally corrected. In telescope design, the use of detector with curved surface can be an efficient option, as it was used in the Proba satellite. Moreover, the curved image also reduces the astigmatism aberration.

Distortion

Distortion is not quite an image aberration since it influences the image scale and not its sharpness. The image will be deformed instead of being blurry. Distortion can happen when the image is too large, then it is referred to positive (or pincushion) distortion (which happens with a convex lens) or when the image is too small, then we are dealing with negative (or barrel) distortion (which happens with a concave lens). Both distorsion are represented in FIGURE 4.16. Indeed, the image scale varies with the distance to the optical axis.

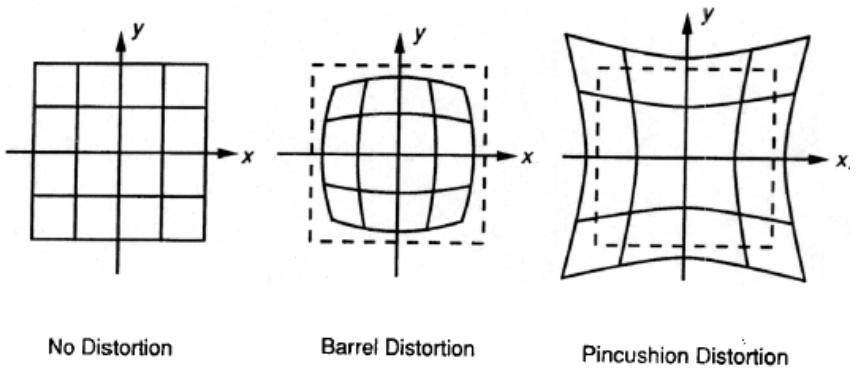

Figure 4.16: Both cases of distortion aberrations [30].

Spot diagram

In the end, the quality of an optical system, is defined by the residual image aberration. In the absence of diffraction, the perfect optical system would produce a point image in the focal surface for a source point. However, such performance can hardly be achieved. In the presence of aberrations, the supposed point source becomes a blur representing a scattered figure. It actually arises from a combination of aberrations and it becomes difficult to figure out which part of the scattering figure results from which aberration.

The spot diagram is the best known tool to simulate the size, shape and light distribution in the image surface. Using the geometric optics, the bundle of rays going through the optical system reaches the focal plane. Then, their distribution on this latter plane, from a point source, is called the spot diagram. A few of them are represented in the following FIGURE 4.17 for which the causing aberrations can sometimes be deduced.

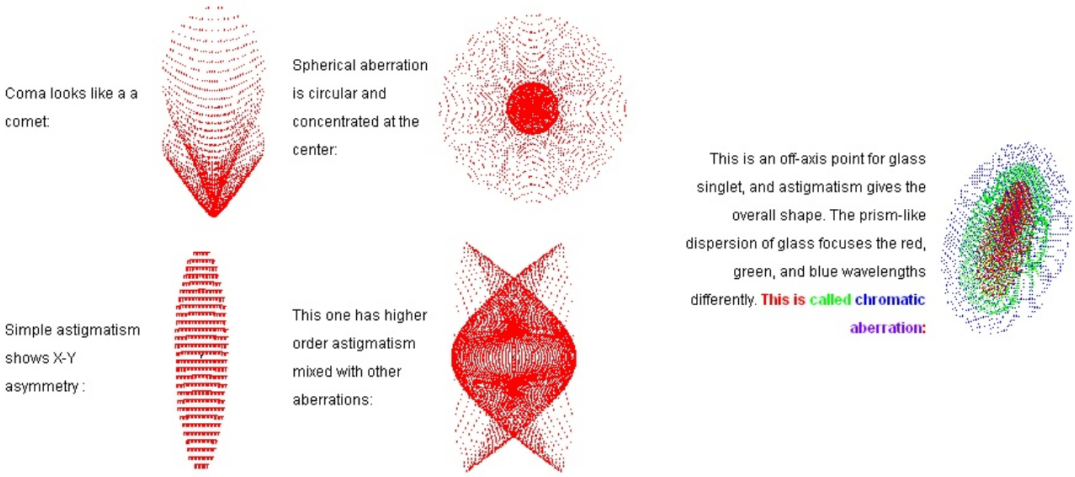

Figure 4.17: Different spot diagrams and their cause [31].

Therefore, the bigger the spot size and the greater the aberrations meaning a worse image quality. In order to have acceptable aberrations through the optical system, the spot size must be

smaller than the pixel size of the detector. This statement will be very useful in CHAPTER 7, in order to find an operational design.

It must be kept in mind that in a real case, all the components of the entire imaging system have to be taken into account in order to assess the optics quality, both concerning the aberrations and the diffraction. For instance, the sensors and the electronics also have degrading effects that should be included in the analysis.

3 Light = corpuscule

The light can also be considered as small discrete particles, then it enters the corpuscular theory of light. Therefore, it has a quantized energy and will be able to interact with matter. Even if considered as a particle, it is tiny and when going through an atom, some light particles will encounter matter (Nuclei, electrons,..) while some will go through. Actually, when light reaches a matter, it will have three options : FIGURE 4.18

- Light reflection;
- Light emission;
- Light absorption.

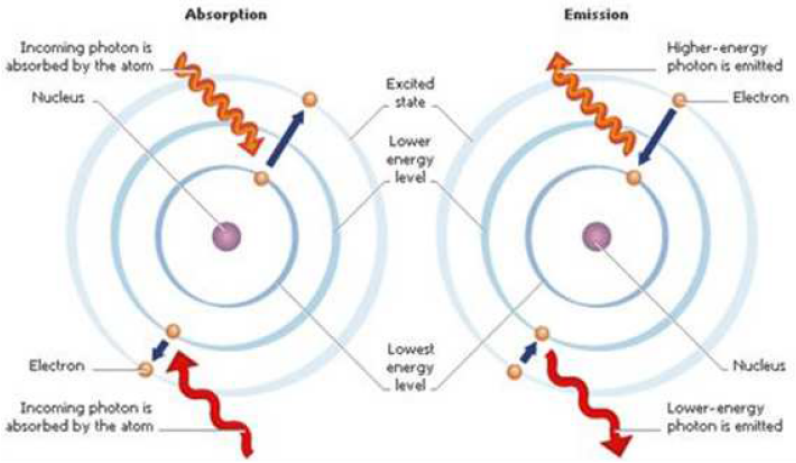

Figure 4.18: Interaction light-matter [3].

This theory will actually be of use when the light eventually interacts with the detector's sensors. This is where the photons information is transformed into electrons by means of interactions. However, this theory can not explain diffraction, refraction, interference and polarization, so it will not be of much interest to consider the light as a corpuscule in the scope of purely optical designs.

4 Telescopes

A main optical instrument is the telescope, such an optical system is made of a combination of lenses and mirrors. They have two functions :

- To enlarge the apparent angle subtended by a distant object. In other word, the image of something (planet, asteroid, natural satellite,..) viewed through a telescope will appear much larger and enables to observe things where the human eye alone would be blind.
- To increase the amount of light reaching the observer's eye or the detector. This second function will make an observed star appearing much brighter when using the telescope than with unaided eye. [17]

There is an infinite number of ways to combine lenses and mirrors to design an optical system. The whole point is to find the best assembly depending on the mission's goal and its requirements and limitations. However, some basic telescope structures have already proven their worth. Therefore, when making a new optical design, it can be very interesting to start from one of those well known telescopes. Two of them, working with reflective optics only, will quickly be introduced.

Newtonian

This telescope was the first successful reflective telescope made by Newton in 1668. It usually has a paraboloid primary mirror (mirror first intersected by the light rays) and then it adds a flat, diagonal secondary mirror to the optical path. That secondary mirror will move the focal plane out of the telescope as it can be seen in FIGURE 4.19. The blue and green lines represent two rays of light coming at different angle and the red mark representing the image size, where the detector should be placed.

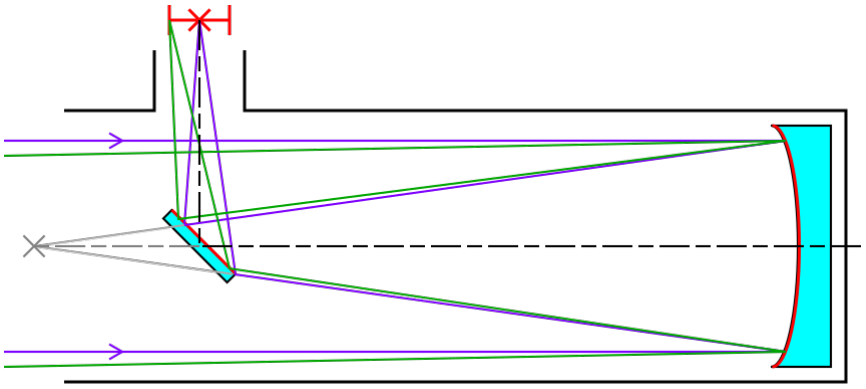

Figure 4.19: Light path in a Newtonian telescope [32].

Advantages :

- Shortens telescope;
- Focal plane out of telescope;
- Inexpensive, easy to make;
- Collimation is relatively easy;
- Instruments can be placed on fixed external platform (depending upon telescope mounting).

Disadvantages :

- Central obscuration;
- Diffraction spikes from supports;
- Strong coma aberration.

Cassegrain

The classic Cassegrain telescope has a parabolic primary mirror, and a hyperbolic secondary mirror. This secondary mirror reflects the light back through a hole in the primary mirror. It is represented in FIGURE 4.20 with the same notations as the Newtonian.

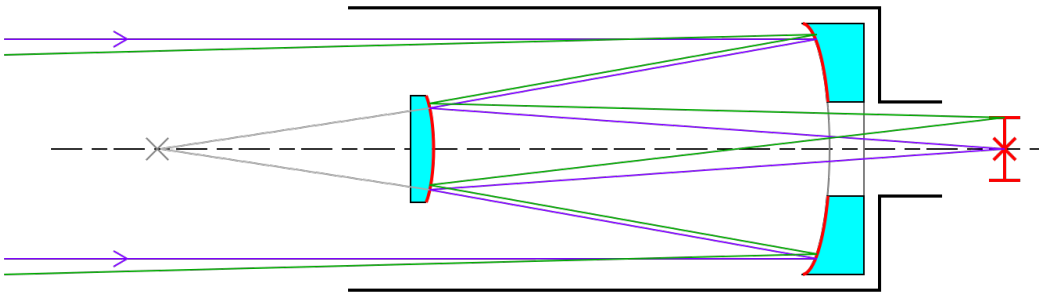

Figure 4.20: Light path in a Cassegrain telescope [32].

Advantages :

- Very compact;
- Long focal length while short tube length;
- Inexpensive, easy to make;
- Collimation is relatively easy;

Disadvantages :

- Central obscuration;
- Diffraction spikes from supports;
- Suffers from astigmatism and coma aberrations

The Ritchey–Chrétien telescope is identical except for the primary mirror which is also hyperbolic and actually lowers both the coma and astigmatism aberrations.

The Gregorian telescope is also very similar to the Cassegrain one but the secondary mirror is placed after the focus of the primary mirror. Then, its concave surface allows it to reflect the image back through a hole in the primary mirror, producing an upright image.

The Matsukov-Cassegrain and the Schmidt-Cassegrain are also based on the Cassegrain telescope. Then, there is the Nasmyth telescope which incorporates features of both Cassegrain and Newtonian telescopes, using a tertiary mirror. This actually proves how many designs can already ensue from such basic telescopes.

To conclude this chapter, the two main issues when working on an optical design are to obtain a good image resolution, limited by the diffraction and to obtain the best image quality possible defined by the different aberrations. However other parameters can degrade the performance of the optical design such as the surface inaccuracies, the deviations in assembly, the misalignment, the environmental change, the jitter, the stray lights, the non 100% reflectivity of the mirrors, the ghosts,...

Chapter 5

Optical Design : Preliminary computations

Before starting the optical design strictly speaking, the mission and its purposes must be well stated and understood. Therefore, the optical design will have different restrictions and requirements which will already allow to define different parameters. Some of those parameters will be fixed for the whole mission while other parameters can vary.

The requirements will be of two main kinds : the room available and the performances to reach. This actually represents an everyday problem in technology, one will always aim for the device which is both small and reliable.

1 Structure

OUFTI-NEXT is a 3U CubeSat and half of it (1.5U) is designated for the optical. payload. This must include the telescope assembly as well as the optical instrument such as the detector and its cooling system. In most optical design, the detector will stand behind the optical design meaning this latter must fit in 1U and may slightly exceed it depending on the optical instrument size. Out of the 150 [cm] in length allowed for the whole payload, 120 [cm] can be dedicated for the optical design itself.

Of course, the different mirrors have a thickness, usually around a few millimeters. Therefore it reduces the maximum distance allowed between to mirrors. On the other hand, the diameter of the mirrors is allowed to reach up to 10 [cm], corresponding to 1U. Therefore, the maximum pupil entrance diameter, D_p will be 10 [cm]. The only way to exceed that maximum entrance pupil will be by using deployable optics. The idea of deployable optics will be considered in CHAPTER 9.

Space telescope mirrors must usually endure the extremely frigid temperatures in space, be highly reflective, tough and lightweight. The material used to make the mirrors must be chosen wisely to cope with those constraints as well as possible. Different materials are considered.

- A common choice is to use Aluminum (Al) due to its wide range of performances, low

price and it is an ordinary material. It is non magnetic and good conductor of electricity and heat.

- The Beryllium (Be) which is very strong for its weight and good at holding its shape across a range of temperatures. It is also non magnetic and good conductor of electricity and heat. However, such materials is quite rare. For instance, this material was used for the James Webb Space Telescope (JWST) [33].
- The ZERODUR is an inorganic, non-porous Lithium Aluminum Silicon oxide glass ceramic. It presents a good homogeneity for mirror applications. It provides an extremely low coefficient of thermal expansion. It is ideal for applications where the optical mirror is exposed to high temperature fluctuations. It is also an ultra-light weight option. It can be polished extremely smoothly into a wide range of precise geometrical shape. The ZERODUR is available in the market at moderate prices. [34]
- The fused Silica provides a high degree of purity, exceptional environmental durability, and a low coefficient of thermal expansion. Such material is very expensive though. [35]

Independently of the material selected, it will need a reflection coating to ensure an optimal reflection. Therefore, the choice will mostly be based on the density (see weight analysis in CHAPTER 7 and their coefficient of thermal expansion (see environmental analysis in CHAPTER 8). An idea of their price is also important. They are compared in the following TABLE 5.1.

Material	Density [g/cm³]	Coefficient of thermal expansion [10^{-6}/K]	Cost
Aluminum	2.7	21-24	Low
Beryllium	1.84	12	High
ZERODUR	2.53	$\simeq 0.1$	Moderate
Fused Silica	2.203	0.52	High

Table 5.1: Material properties.

Even if aluminum is cheap, it provides the worst properties so it will be rejected. Than, it will actually be seen in the further chapters that the main issue between the weight and the thermal expansion is the latter one. Therefore, the choice will mostly be based on the coefficient of thermal expansion. The best material is then the ZERODUR. Moreover, the density were all quite similar and the ZERODUR is actually not as expensive as the Beryllium or the fused Silica.
Concerning the coating, there are three main choices when dealing with InfraRed (IR) wavelength : Silver (Ag), Gold (Au) or Dielectric. However, the former and the latter are more used for application involving laser while the gold is actually ideal in the MWIR range and will therefore be chosen. [36]

2 Performance

The first and most important parameter of the mission influencing the optical design is the orbit of the satellite and especially the altitude. The altitude will help define the ground sample

distance (GSD), the pixel size (P_s), the effective focal length (EFL) and the instantaneous Field of View (iFoV). Those parameters are linked as shown in the FIGURE 5.1 and in EQUATION 5.1 (where α actually represents the iFOV).

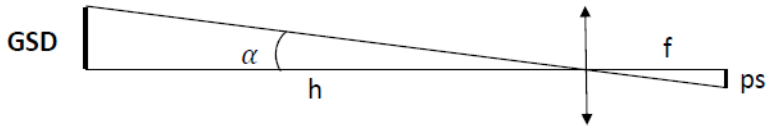

Figure 5.1: Geometrical relation between h, EFL, GSD and P_s.

$$\tan\alpha = \frac{GSD}{h} = \frac{P_s}{EFL} \tag{5.1}$$

Since OUFTI-NEXT is a nano-satellite, it will most likely be launched as a secondary payload and therefore, the orbit will depend on the available launches at the time. The altitude was therefore a subject of discussion throughout those last months. Eventually, three altitudes stand out from the crowd:

- 800 km : lots of satellite sent in SSO orbit at such altitude;[1]
- 600 km : or around that altitude which is a widespread altitude for most CubeSats;
- 350 km : lots of launches going to the International Space Station (ISS) and therefore very common to set satellite into orbit from there which will then follow the ISS orbit. [37]

However, OUFTI-NEXT is a demonstrator, so its main goal is to prove the interest and the feasability of the mission. In the first place, a working altitude must be selected. Then it will be different for the constellation which will make a real use of the data obtained.
Concerning the detector, the parameter influencing the optical system is the pixel size. It will have a direct influence on the EFL as well as the GSD (EQUATION 5.1) and the shape of its array which will help to define the field of view and the swath, as shown in FIGURE 5.2.

[1] However, this altitude of 800 [km] will eventually have to be rejected because sending OUFTI-NEXT so high will actually extend its lifetime over the acceptable limit.

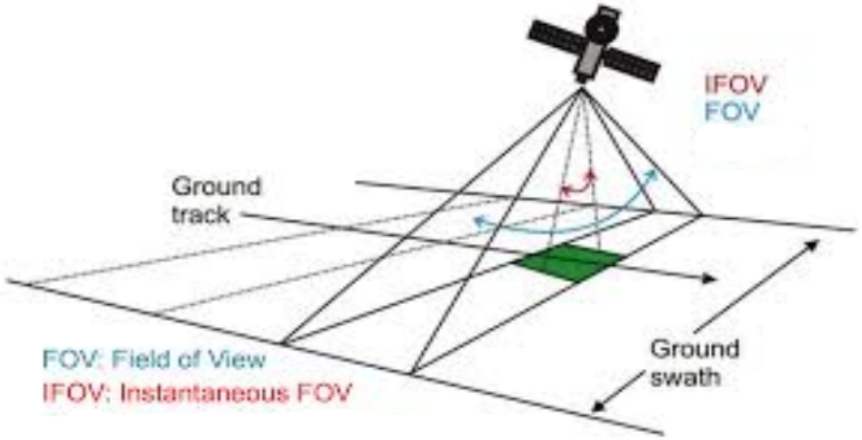

Figure 5.2: Swath and Field Of View (FoV) [38].

The green area is the GSD and it is what will be represented by one pixel. The ground track is the projection of the satellite's orbit onto the surface of the Earth.
A trade-off study was made and eventually, the choice inclined towards a detector with a 2D arrays of 640 pixels by 512 pixels ($m \times n$), representing the number of pixels in each direction and the pixel's size will most likely be 15 [μm]. Therefore, both the swath and the Field of View (FoV) must be defined in both directions: EQUATIONS 5.2.

$$\begin{aligned} FOV_m &= m \times \alpha & Swath_m &= m \times GSD \\ FOV_n &= n \times \alpha & Swath_n &= n \times GSD \end{aligned} \tag{5.2}$$

Since the detector array is rectangular, it will provide $FOV_m > FOV_n$ and $Swath_m > Swath_n$. In the further analysis, the larger field of view (and swath) is kept since it will be the most restrictive one. Indeed, the larger the field of view, the harder it is to focus all the rays coming through the aperture of the telescope because the more aberrations will be produced.

Concerning the GSD, as stated in CHAPTER 2, in order to provide very interesting results, the GSD should be about 20 [m]. However that represents a very small distance for which a good image resolution can very hardly be obtained. Eventually it was decided that if the GSD could get close to 100 meters, it would already be sufficient for the demonstrator. The following FIGURE 5.3, using EQUATION 5.1 and **??**, represents the EFL and the FoV with respect to the GSD for the three possible altitudes. As said earlier, the pixel size will be $P_s = 15\mu m$ along the whole project.

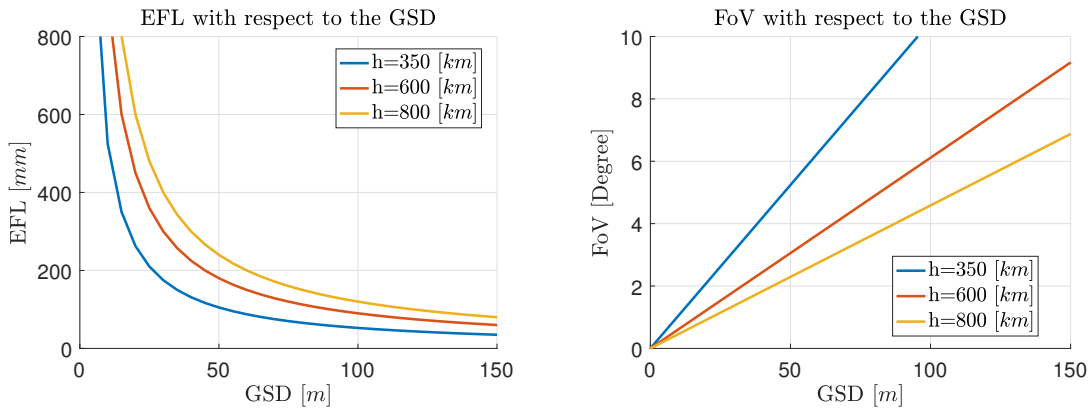

(a) Effective focal length

(b) Field of View

Figure 5.3: Parameters with respect to the GSD at different altitudes. $P_s = 15\mu m$

As it can be seen, to decrease the GSD, the EFL focal length must be as big as possible. The EFL depends on the mirrors position and curvature and on the focus point. In order to reach high EFL, more than one mirror can be used. Then, at fixed EFL a better GSD can be obtained at lower altitudes as demonstrated in TABLE 5.2 for a particular EFL of 120 [mm]. Such an EFL was arbitrarily chosen because it represents the maximum EFL considering the simplest design of one lens at the entry of the optical design with it focus point at 120 [mm]. Then, the following TABLE 5.3b shows that to obtain a GSD of 100 [m], the FoV will decrease with the altitude contrarily to the EFL.

EFL [mm]	Altitude [km]	GSD [m]
120	350	43.75
120	600	75
120	800	100

Table 5.2: GSD and h for fixed EFL

GSD [m]	Altitude [km]	FOV [°]
100	350	4.58
100	600	6.11
100	800	10.47

Table 5.3: GSD and h for fixed FOV.

A high EFL can be managed through an appropriate design within some limitations (a EFL larger than 400 [mm] could hardly be obtained). Moreover, the smallest FOV would entailed the lowest geometrical aberration. Therefore, with those information, a small GSD seems quite easy to obtained but that is leaving aside the diffraction limit which will come into play to make the problem a lot more complex. Indeed, the key parameter driving the performances and the limitations is the F#.

The best way to compute the diffraction limit is with the Airy disk diameter, as explained in the wave-like light theory. It highly depends on the wavelength which is between $3 - 5\mu m$ in MWIR. The higher the wavelength, the tighter the constraints. Therefore, all the computations and designs will be made assuming $\lambda = 5\mu m$. Eventually the Airy disk diameter directly depends on the f# (EFL and entrance pupil diameter) :

$$D_A = 2.44 \times 0.005 \times f\# \tag{5.3}$$

Using EQUATION 5.3 directly leads to the FIGURE 5.4a representing the Airy disk diameter with respect to the EFL for different entrance pupil diameter. Then, in FIGURE 5.4b, the Airy disk diameter is this time plotted with respect to the GSD that could be recovered from the EFL through EQUATION 5.1 assuming the altitude of $h = 600$ [km] and still a pixel size of $15\mu m$.

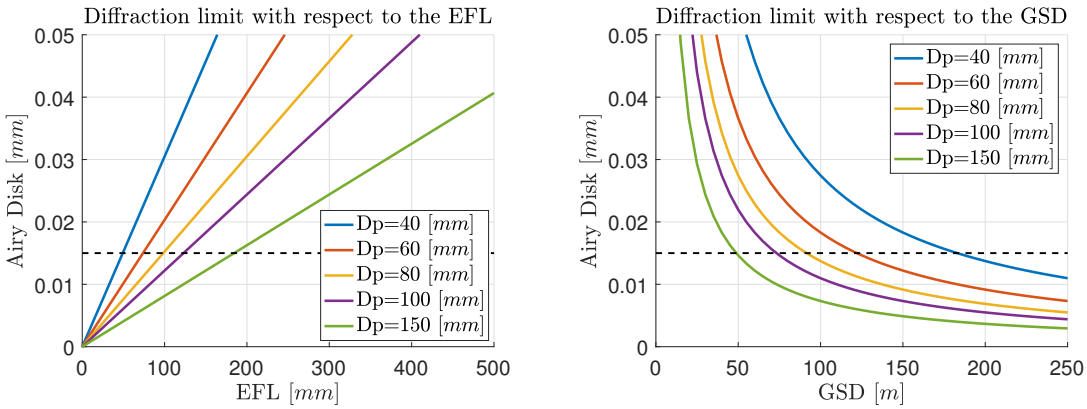

(a) EFL limit

(b) GSD limit ($h = 600km$, $P_s = 15\mu m$)

Figure 5.4: Diffraction limit for different parameters. Pixel size ($15\mu m$ represented by the black dotted line

A good image resolution can only be obtained if the Airy disk diameter is below the pixel size (represented by the horizontal black dotted line). Therefore, the EFL must be as low as possible unfortunately having as a consequence that the GSD is bigger. Concerning the pupil entrance diameter, it must be as large as possible, as it can be seen in the FIGURE 5.4. An entrance pupil of 150 mm was also considered to have a grasp on the benefits of deploybale optics. TABLE 5.4 shows the best GSD reachable and its corresponding EFL for each pupil entrance diameter, so assuming an Airy disk diameter of $15\mu m$ (still with $h = 600km$). The red line marking the transition to deployable optics.

Entrance pupil diameter (D_p) [mm]	EFL [mm]	GSD [m]
40	49.18	183
60	73.77	122
80	98.36	91.5
100	122.95	73.2
150	184.43	48.8

Table 5.4: Best GSD reachable within diffraction limit for different pupil size.

The previous results were made for an altitude of 600 [km] only. Therefore, the following FIGURE 5.5 presents the best GSD reachable with respect to the altitude, assuming the biggest entrance pupil diameter possible, out of the scope of deployable optics: $D_p = 10[cm]$. Therefore, using EQUATION 4.1, the EFL is fixed to 122.95 [mm].

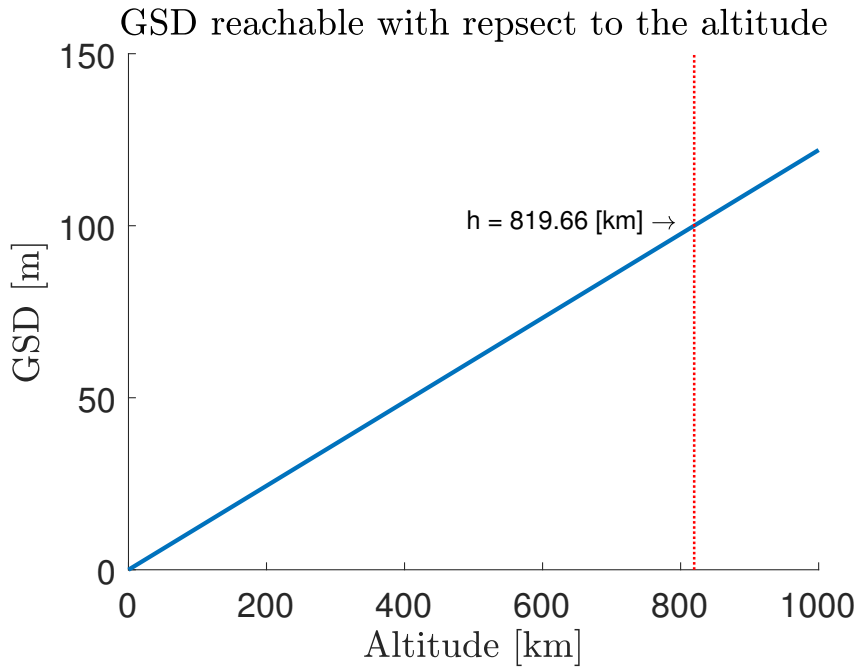

Figure 5.5: Best GSD with respect to the altitude. $D_p = 10$ [cm]. $P_s = 15\mu m$. $EFL = 122.95$ [mm].

Obtaining a GSD of at most 100 meters on ground will not be physically possible with a satellite in orbit higher than 819.66 [km]. Of course, this plot represents the theoretical results obtained assuming an aberration free system with the biggest entrance pupil diameter of 10 [cm]. It also assumed paraxial approximation. TABLE 5.5 shows the best theoretical GSD reachable for each target altitudes with their corresponding FoV.

Altitude [km]	GSD [m]	FoV [°]
350	42.7	4.47
600	73.2	2.61
800	97.6	1.96

Table 5.5: Best theoretical GSD reachable for each target orbit altitude. D_p, EFL and P_s constant.

In a real case scenario, as it will be seen in CHAPTER 7, a much lower altitude is needed to reach such a GSD. However, at lower altitude, a larger FOV is needed, resulting in more geometrical aberrations.

Besides, as defined in the CHAPTER 4, the Nyquist frequency (EQUATION 5.4) can be computed:

$$\nu_n = \frac{1}{2p_s} = 33.3 \quad \text{line pairs/mm} \tag{5.4}$$

while the cutoff frequency (EQUATION 5.5) will still depend on the $f\#$ which will remain in the interval [0.5 , 5], leading to

$$\nu_{cutoff} = \frac{1}{\lambda f\#} = [40, 400] \quad \text{line pairs/mm} \tag{5.5}$$

According to the diffraction theory, a lower $f\#$ would be preferable. Both those frequencies will be used when analyzing the MTF diagrams in CHAPTER 8.

3 Radiometric budget

OUFT-NEXT is an observation satellite. The information of the area observed is actually contained in the photons, transmitting light. Those photons will go through to optical system and eventually generates electrons at the detector (Thanks to the corpuscular theory of light from CHAPTER 4). The radiometry budget will actually be the study of the electrons generated at the detector through the computation of the Signal to Noise Ratio (SNR).

First the irradiance from the area of the Earth observed reaching the satellite will be computed. Then the actual signal generated when going through the optical system and reaching the detector will be considered. Eventually the signal to noise ratio will be computed.

Satellite irradiance

The irradiance comes from two different sources :

- The direct emmisivity of the Earth to the satellite
- The reflection of the photons coming from the Sun, called the albedo.

However, the ground is not easy to model. Indeed, the emissivity and transmitivity can vary a lot from one component to another. In the scope of OUFTI-NEXT, fields will be observed and they will be assumed to be divided into plants or land, with the following data[2] listed in TABLE 5.6.

Plant emissivity ϵ_p	0.95
Land emissivity ϵ_p	0.95
Plant albedo τ_p	0.05
Land albedo τ_l	0.1
Plant coverage τ_c	70%

Table 5.6: Data concerning the emissivity and albedo of the ground.

Those data assume the MWIR spectrum. Also, the plant coverage is the one seen from a nadir pointing which will be the case of OUFTI-NEXT.

However, the light still has to go through the atmosphere before reaching the satellite. The atmosphere is a very complex environment which will not let all the photons go through in the MWIR band. As shown in FIGURE 5.6a, the transmission coefficient of the atmosphere is quite hard to evaluate which is why a simpler model will be used as represented in FIGURE 5.6b.

[2] All those assumptions were given by Bernard TYCHON, with expertise in Environmental Science, Irrigation and Water Management, Plant Protection and Animal Health

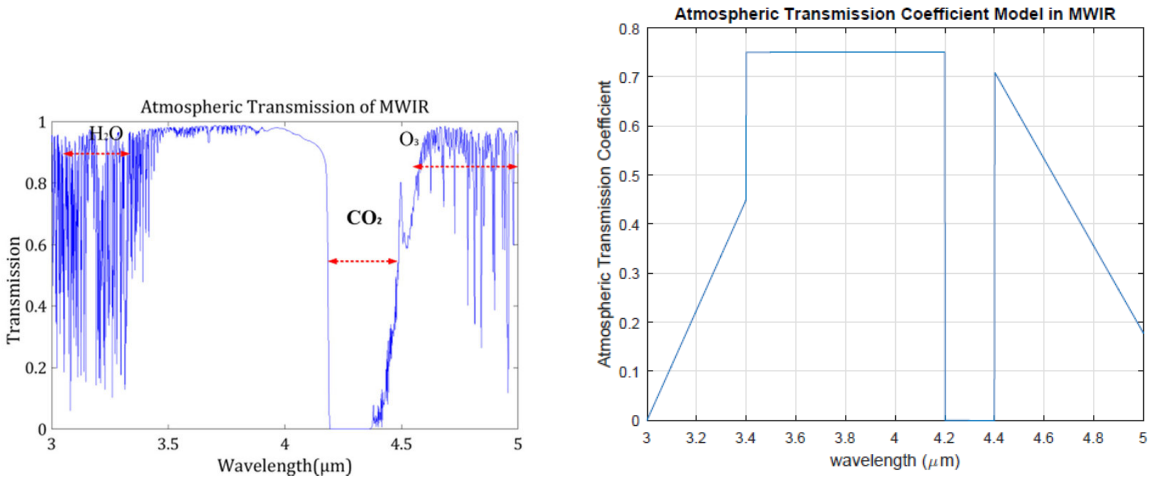

(a) Real [39] (b) Model [40]

Figure 5.6: Earth transmission coefficient in MWIR.

In FIGURE 5.6a, the constituents appearing are the main atmospheric constituents absorbing the photons in the corresponding wavelength For instance, it can be seen that from a wavelength of 4.2 to 4.5 $[\mu m]$, no observation can be made since it is all absorbed by CO_2.

Ground emitted radiance

The Earth radiance will depend on the emissivity of the ground, the temperature of the ground and the wavelength. Moreover, the Earth is considered as a grey body, so its spectral radiance in wavelength is given by EQUATION 5.6

$$B_{\lambda,Earth}(\lambda, T_g) = \frac{2hc^2}{\lambda^5(exp\left(\frac{hc}{\lambda k T_g}\right) - 1)}\epsilon_{p,g} \quad [W/sr^{-1}m^{-2}\mu m^{-1}] \tag{5.6}$$

with

- $h = 6.32 \times 10^{-34}$ [J.s] : The Planck constant;
- $c = 2.998 \times 10^{8}$ [m/s] : The speed of light in vacuum;
- $k = 1.38 \times 10^{-23}$ [J.s] : The Boltzmann constant;
- $T_g = [270 - 335]$ [K] representing the ground temperature.

Once the radiance is obtained, it can be computed for each wavelength using the model of the atmospheric transmission coefficient such as

$$L_{Earth \to Sat} = B_{\lambda,Earth}\tau_A tm \tag{5.7}$$

The results is shown in FIGURE 5.7.

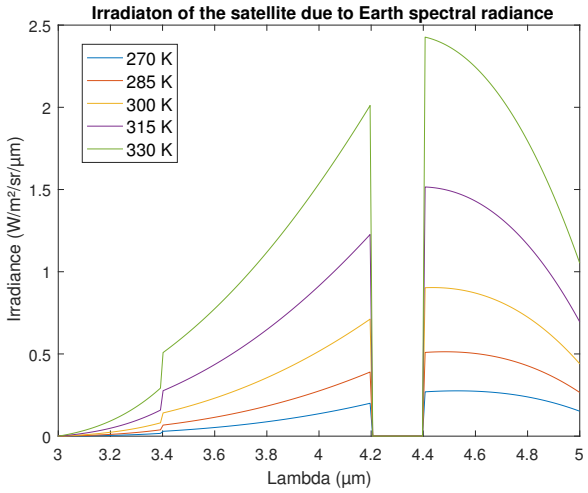

Figure 5.7: Irradiance of the satellite coming form the Earth radiance alone for different ground temperatures. [41]

Sun reflected radiance

The sun is considered as a black body and follow the Planck law of blackbody radiation represented in FIGURE 5.8.

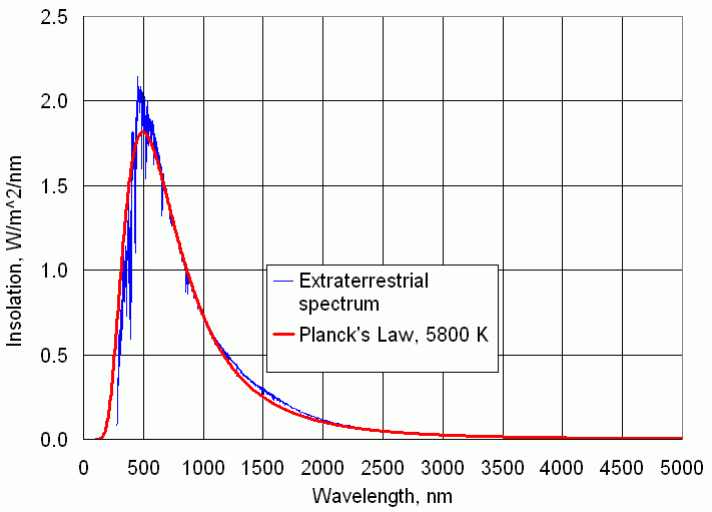

Figure 5.8: Planck law for the sun radiation ($T \simeq 5800$ [K] and actual radiation. [42]

The theoretical result is really close to the actual results, represented by the extraterrestrial spectrum blue function. As it can be seen, the black body mostly radiates in the visible light while the radiation becomes very small in MWIR. But even if small, it still radiates in the MWIR window and it must be taken into account. Planck's law for blackbody is given by EQUATION 5.8.

$$B_{\lambda,Sun}(\lambda) = \frac{2hc^2}{\lambda^5(exp\left(\frac{hc}{\lambda k T_{sun}}\right) - 1)} \quad [W/sr^{-1}m^{-2}\mu m^{-1}] \tag{5.8}$$

This equation presenting the same parameters as EQUATION 5.6 except for the temperature of the Sun: $T_{Sun} = 5778$ [K]. From there, the radiance (times steradian) at the Top Of the Atmosphere can be computed by means of EQUATION 5.9.

$$B_{TOA} = B_{\lambda,Sun}\Omega_{Sun-Earth} \quad [W/m^{-2}\mu m^{-1}] \tag{5.9}$$

With $\omega_{Sun-Earth} = \pi R_{Sun}^2/(1AU)^2$ the solid angle between the Sun and the Earth[3].
Then, once the radiance is at TOA, the light still has to go through the atmosphere then reflected by the ground (plant and land albedo) and eventually back through the atmosphere until reaching the satellite. Such modification are given by EQUATION 5.10.

$$L_{Sun\to Sat} = B_{TOA}\tau_{Atm}[\tau_p\tau_c + \tau_l(1-\tau_c)]\tau_{Atm}/2\pi \quad [W/sr^{-1}m^{-2}\mu m^{-1}] \tag{5.10}$$

Where the solid angle between the Earth and th satellite is a whole hemispher (2π [sr]). And the atmospheric transmission coefficient was indeed used twice. In the end, the irradiance arriving to the satellite from the Sun is plotted in FIGURE 5.9 with respect to the wavelength.

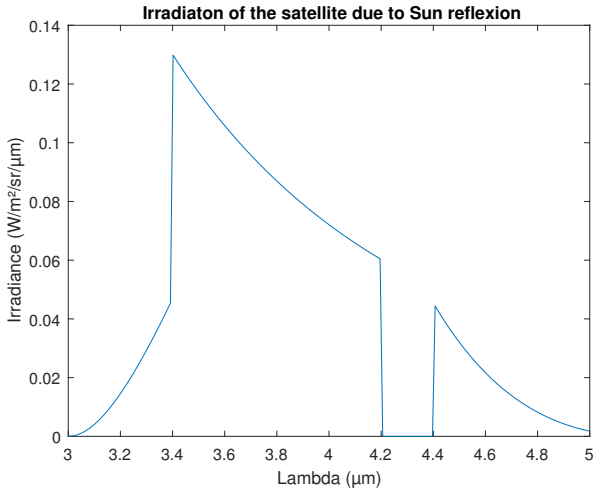

Figure 5.9: Irradiance of the satellite coming from the reflection of the Sun radiance ($T_{Sun} = 5778$ [K]). [41]

Now that both sources of irradiance have been computed, adding them will lead to the total irradiance of the satellite.

$$L_{Sat} = L_{Sun\to Sat} + L_{Earth\to Sat} \tag{5.11}$$

This is done in FIGURE 5.10.

[3]AU is the astronomical representing the average distance between the Sun and the Earth. It is about 150 millions [km].

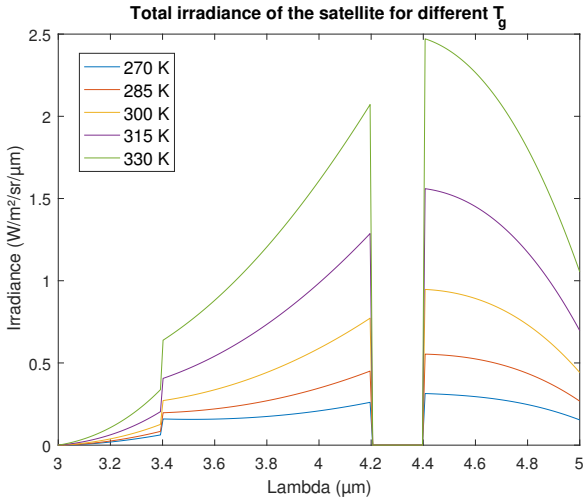

Figure 5.10: Total irradiance of the satellite coming from the Sun reflection and the Earth emission for different T_g with respect to the wavelength. [41]

It can be seen that the shape is similar to the FIGURE 5.7 obtained with the Earth Emission only. This is simply because the contribution of the Sun to the total irradiance is a lot smaller. This is mostly due to the fact that the spectral range is in MWIR. So far, the irradiance do not give much information about the actual signal received at the detector. Now, the radiometric budget computations will occur at the satellite level.

Signal

The computation of the signal will actually represent the signal reaching one pixel. It is based on different parameters:

- The irradiance of the satellite, computed in the previous section.
- The altitude alt, between 350 and 800 [km];
- The GSD considered equal to 100 [m] so far;
- The transmission coefficient of the filter τ_F which is needed to select the desired spectral range. It is set to $T_F = 0.8$;
- The detector temperature T_D which will vary through time and depending on the efficiency of its cooling system. Its average value is set to 140 [K];
- The detector quantum efficiency $Q_{eff} = 0.7$
- The pixel size $P_s = 15$ [μm];
- The pixels array of the detector 640;
- The wavelength range 3 to 5 [μm];
- The surface of collection of the optical system S_{eff} which will depend on the optical design;

- The optical transmission τ_O which will also depend on the optical design;
- The integration time T_I which will depend on the scanning method used. In case of a linear scan, it will simply represent the time spend above the GSD. $T_I = GSD/v_{sat}$

First the photons must go through the optical system. The flow of photons reaching the detector must be computed. The surface of collection must be reduced considering one pixel (EQUATION 5.14). The new surface is called the $etendue$ (E).

$$E = P_s^2 \Omega_{pix} \quad [m^2 sr] \tag{5.12}$$

$$= \frac{p_s^2 S_{eff}}{f^2} \tag{5.13}$$

$$= \frac{S_{eff} GSD^2}{alt^2} \tag{5.14}$$

Then the power reaching the detector is given by EQUATION 5.15.

$$P_\lambda = L_{Sat} E \tau_O \quad [W/\mu m] \tag{5.15}$$

Then the photons are converted into electrons in the detector. Integrating them over the wavelength will give the flow of electrons following EQUATION 5.16

$$F_{e^-} = \int_{\lambda_{min}}^{\lambda_{max}} \frac{P_\lambda Q_{eff} \lambda}{hc} d\lambda \quad [e^-/s] \tag{5.16}$$

Eventually, the electrons flow simply needs to be multiplied be the integration time and the filter transmission in order to find the actual Signal at one pixel: $S = F_{e^-} T_I \tau_F$.

The numerical results corresponding to the signal will be given in CHAPTER 7. By then, the parameters concerning the optical design will be evaluated (S_{eff} and τ_O).

Noise

Actually the signal computed will be strongly influenced by the different noises present in the satellite. The noises are irregular fluctuations that accompany the transmitted signal but are not part of it and tend to obscure it. They can be generated from many sources.

First the shot noise N_S which is the noise produced by the signal itself. Since the signal of photons arriving at the detector is governed by the Poisson statistics distribution of light, the shot noise is the given in EQUATION 5.17[43]

$$N_S = \sqrt{S} \tag{5.17}$$

Another important noise, arising from the detector is the Dark Current Noise N_{DC}. It is due to the electrons thermal excitement converted from the photons. A good approximation of this noise is given by EQUATION 5.18. [40]

$$I_{DC} = c P_s^2 T_D exp\left(\frac{-\Delta E}{T_D}\right) \quad [A] \quad \rightarrow \quad N_{DC} = I_{DC} \frac{T_I}{Q_{e^-}} \quad [e^-] \tag{5.18}$$

with ΔE the bandgap energy[4] and $Q_e = 1.6e^{-19}$ [C], the electron's charge.

The last main noise is the Read Out Noise N_{RO} which represents the noise coming from all the electronics aboard the CubeSat. Indeed, the electronics generates electrons as well which could interfere in the signal. For OUFTI-NEXT, it is assumed $N_{RO} = 850$ [e^-/pixel]

Eventually, the total noise will be computed from the different noises just introduced. It is given by EQUATION 5.19.

$$N = \sqrt{N_S^2 + N_{DC}^2 + N_{RO}^2} \tag{5.19}$$

However, the total noise computed here neglects the other sources of noise such as the thermal noise, the jitter noise or any potential mechanisms noise.

Signal to Noise Ratio (SNR)

Quite naturally, the Signal to Noise Ratio is obtained by EQUATION 5.20.

$$SNR = S/R \tag{5.20}$$

This parameter is of great importance when designing a satellite. It represent the ratio of the meaning full information divided by the unwanted signal. It should indeed be as big as possible. If the SNR is too low, then the whole mission would be doomed to failure since no readable information could be retrieved from it. As it was described, both the Signal and the Noise depends on many parameters. Even a small modification in the satellite's configuration will most likely have an impact on the SNR.

[4]For the InSb Focal Plane Array (FPA), the Energy activation $\Delta E = 0.16[eV] = 2.56 \times 10^{-20}[J]$

Chapter 6

Optical Design : Presentation

1 Design process

Now the basics of optics and the most important parameters value have been introduced, it is going to be possible to engage in the actual design making. Of course, this will not be done by hand in order to get a working design and to get it before 2050. Indeed, when making such sophisticated design, requiring very high accuracy and reliability, software will be used. Two powerful software in the field of optics are *CODE V* and *ASAP*. The first one will be used along the whole design.

1^{st} step : Basic parameters

This first step was actually to get accustomed to the mission and to make the preliminary computations in order to get the essential parameters needed to start the actual design. The basic parameters were actually presented in the previous CHAPTER 5. When starting with *CODE V*, the field angle must be precised to the software, so it knows the field of view and the size and shape of what it is observing. Then, the wavelength and the pupil diameter must also be plugged into *CODE V*.

2^{nd} step : Geometry generation

Then the different surfaces and their characteristics must be specified. The software offers some preconceived design of all kind which can turn out to be a good starting point. It is also possible to start a whole new design from blank. The kind of mirrors/lenses used must also be specified as well as the material between two surfaces (if nothing is said, the software will consider air in between). The different optic conventions must be precised concerning the signs. It is indeed possible to have "negative" distances or heights :

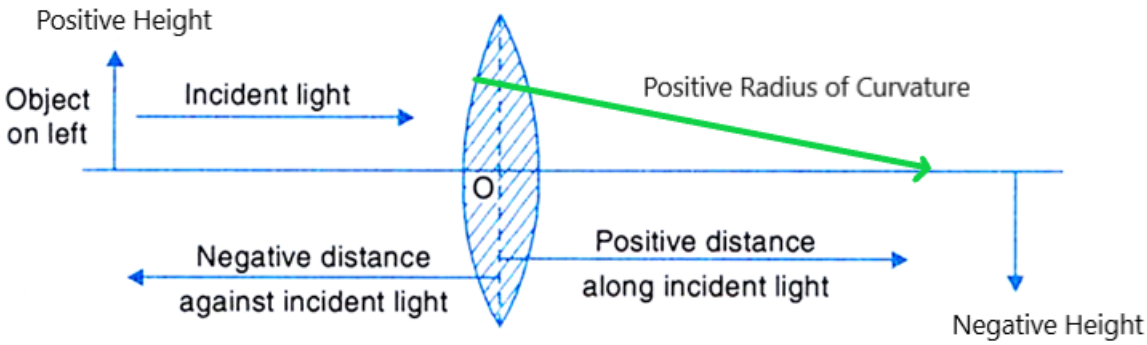

Figure 6.1: Sign conventions in optical design [44].

All distance are measured from the optical center of the mirror/lens. So, the radius of curvature also follow the rule, positive in the direction of the ray and negative in the opposite case. Also, the fact that distances are taken from the optical center means that the thickness of the mirror do not influence the optical performance nor the results obtained. The thickness can still be specified for a more practical view of the design.

An important thing to know about *CODE V* is that it is a sequential ray-tracing software contrarily to *ASAP*. Sequential ray-tracing means the surface order is of major importance. The surfaces must be specified in the order the light rays will hit them (object, primary mirror, secondary mirror,... , image). However, as soon as it touches a mirror and reflected on it (or refracted in the case of a lens), it forgets about it. Hence, if some rays were to come back in its direction, they would go through it like it was not there at all. Same thing if, for instance, the secondary mirror creates an obscuration of the the primary mirror. The incoming ray would not see it and go straight to the primary mirror as if the other surfaces did not exist.

Many mirrors' geometries can be defined. Instead of spherical, the mirrors can be defined as conic. Then, the conic constant must be specified. Different values are represented in FIGURE 6.2.

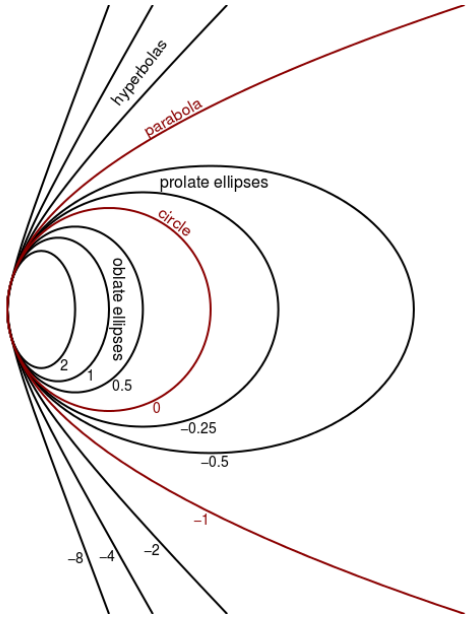

Figure 6.2: Representation of various conic constant [45].

It can be seen that a conic constant of zero comes back to a spherical mirror. Also, the radius of curvature is defined from the spherical mirror and independant of the conic constant. The geometry of the mirror can become even more specific when using an aspherical mirror. Then, 10 more parameters can be defined to establish the exact mirror's geometry. Usually, when using aspherical mirrors, up to three aspherical parameters are used.

3^{rd} step : Optimization

Once the whole design is defined, the software can run its optimization tool. It aims to find the best configuration for the best focus point with the least geometrical aberrations possible. All the parameters must be specified as variable or frozen so the software knows with which parameters it can play to reach the best configuration. However, the optimization starts from the initiated design and looks for the closest optimized solution which will not especially be the best optimized solution. In other words, the software will modified the variable parameters until reaching a minimum of the performance error function meaning that modifying any parameters would actually exacerbate the solution. So it stops even though an other optimized solution with better properties could exist. FIGURE 6.3 allow to understand the concept better.

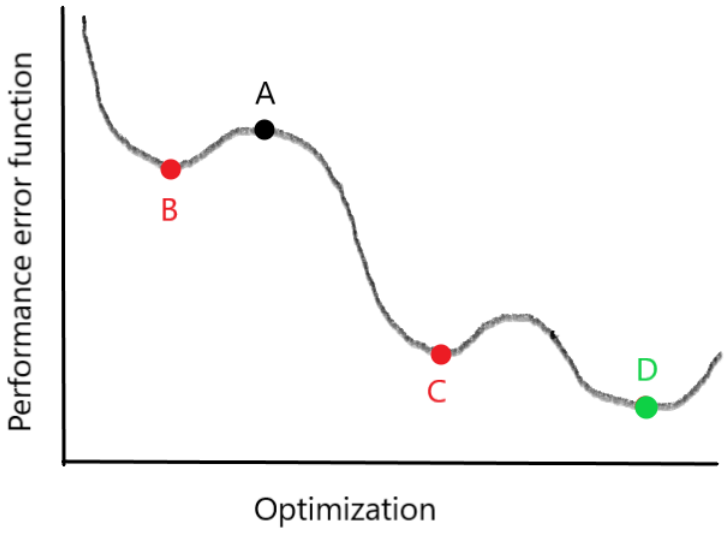

Figure 6.3: Optimization process in *CODE V*

If the design is at point A, the optimization will either lead to point B or point C (being already much better than B) before it stops. However, there actually is the solution D which is even better and there might be even more optimized configuration further.

Therefore, one must not blindly relies on the optimization tool of the software since the starting point is of significant importance. A critical mind must be kept in order to reach a truly optimized configuration.

Once a decent optimized configuration is achieved, the software offers many analysis tools either concerning the geometry or concerning the diffraction, the two main issues. For instance, there are the spot diagram, the encircled energy, the MTF plot, the ray trace curves,...

4^{th} step : Tolerances

Once the design has been analyzed and actually fulfills all the mission's goal and requirements. The sensitivity analysis must be carried out. This analysis is actually a tolerances study. It will study the impact of a tiny variation of one parameter over the performances of the entire system. In some way, it will define the robustness of the design in case of manufacture or assembly imperfections.

Moreover, *CODE V* uses by default a temperature of $T = 20°C$ and a pressure of $p = 760$ [mm Hg]. Then a thermal analysis must be performed in order to make sure the optical design would still be operational in the possible range of environmental changes it could suffer from.

5^{th} step : Manufacture

Eventually, this fifth step is the actual assembly phase of the design. High precision work is required and, even then, tests must be run on the final design to make sure the optical performances were well predicted.

Summary

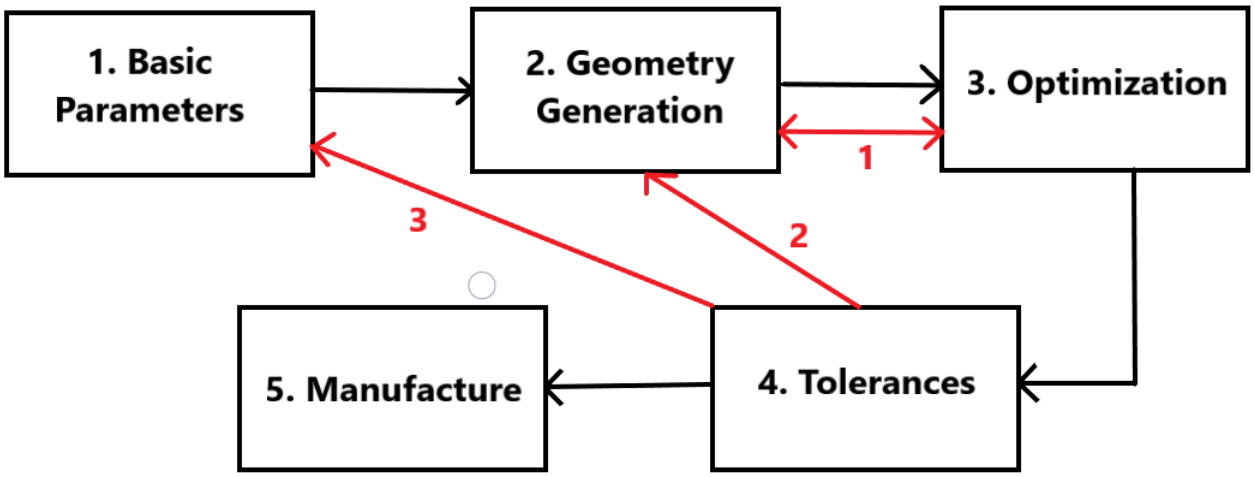

Figure 6.4: Summary of the design process.

Obviously, moving forward through the different steps can only be considered assuming the previous step is well done. However, the optimization does not gives reliable results all the time. Therefore the optical engineer will often need to go back and forth between step 2 and 3 before reaching an acceptable optimization. Then if the tolerances analysis are a failure, it means the configuration the designer must go back to step 2. If step 4 keeps being a barrier to the acquisition of an operational design, then it might mean the requirements of step 1 were too tight. So, the whole mission must be reviewed before going back into the design process loop from step 1.

The more parameters are used (many mirrors, aspherical mirrors using all 10 parameters and so on) and the most precise the configuration and the geometry will be. A very specific design configuration should actually give great optical performances. Such a design will quickly reach the tolerances step. However, the fact that many parameters are used means the odds are high that one of them will be very sensitive to the tolerances analysis. Therefore, a design with too many parameters might appear really good concerning its performance but will never be able to go past the tolerances analysis. This would result in a pointless design. A good compromise must be made between simplicity and high optical performances.

2 Main designs

Before worrying about placing the different surfaces, the first question is where to place the camera of the optical payload. There are two possibilities as shown in FIGURE 6.5. Indeed, half of the satellite is provided to organize the payload.

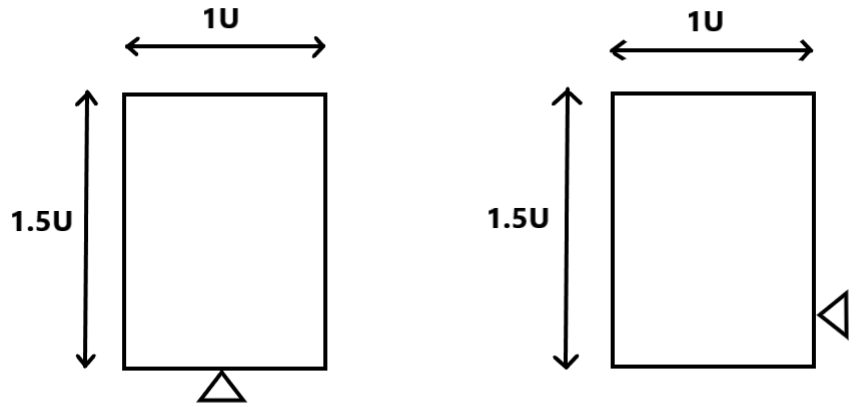

Figure 6.5: Possible positions of the camera (Left: bottom of CubeSat. Right: side of the CubeSat).

The first option has as an advantage that the design can go further into the CubeSat, in the direction of the rays. On the other hand, the second option would need a slanted mirror[1] at some point in order to use the whole space available. Moreover, when the camera is placed at either side (second configuration), it is an impediment for body mounted solar panels that would not be able to use that space to extend as much as possible. Anyways, all three design's configurations about to be presented in the next sections all fit better when the camera is at the bottom of the CubeSat. The first option will be selected.

1^{st} design

When getting familiar with *CODE V* it is much easier the first time to start from one of the preconceived design offered by the software. It happens one of them is actually the Cassegrain telescope, the very simple and handy design introduced in CHAPTER 4. Knowing its properties, it seemed like a great first design to start from.

The design was remodelled in order to fulfill the present conditions as best as possible. The design's shape is represented in FIGURE 6.6 for 3 rays coming at $0°$, $1.5°$ and $3°$ and an EFL of 480 [mm].

[1] A slanted mirror is a mirror at different angle to the light rays. For instance, a mirror presenting a 45 degrees angle, will reflect the light at 90 degrees of its incidence ray.

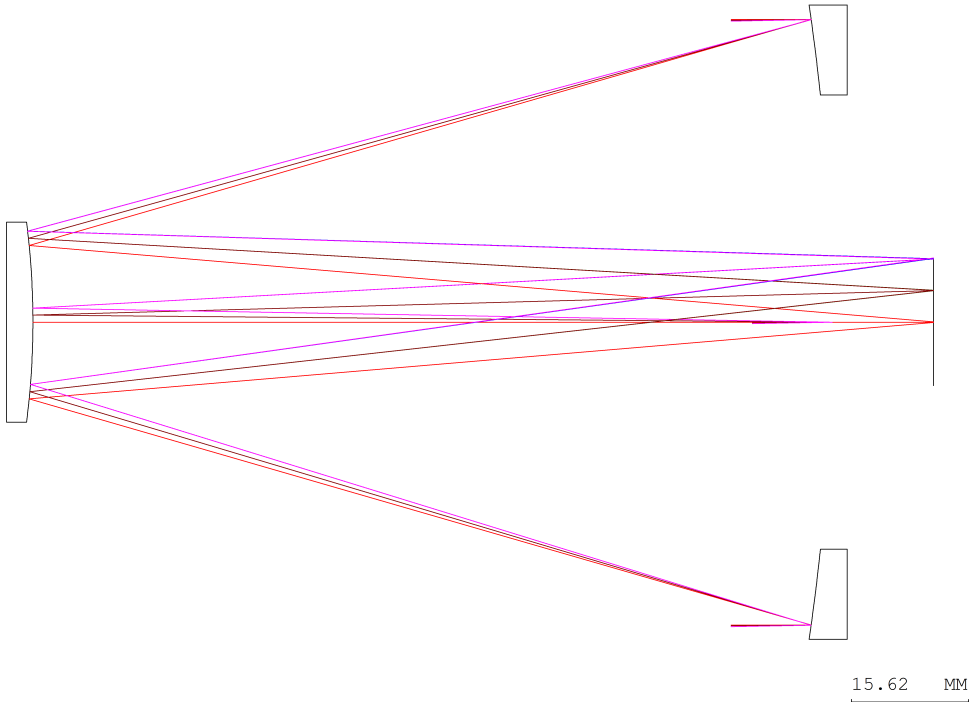

Figure 6.6: First design : D1. $EFL = 480$ [mm], $FoV = 3°$.

The advantage of this design comes from its big entrance pupil diameter which can actually go up to the CubeSat size : 10 [cm]. It also allow large EFL and do not require too much mirrors surface. On the downside, the secondary mirror is up front in such configuration, resulting in obscuration. Even though it does not impact the diameter of the entrance pupil strictly speaking, it will have an impact on the radiometric budget, decreasing it. Also, the Cassegrain is good for very small FoV but quickly becomes inaccurate when observing larger fields as it will be demonstrated in the analysis section. Concerning the backfocus, behind the secondary mirror, it must still fit the detector, therefore it is constrained to no more than 120 [mm]. Then the detector can fit behind without overstepping the 1.5U given for the payload.

2^{nd} design

Since the first design was not good with larger FoV, other designs where thought of. After getting used to *CODE V*, it was possible to start from blank in order to considerate new ideas of designs. Still with the Cassegrain telescope in mind, this second design will be referred as "Backward Cassegrain". Both mirrors position will be switched: the primary mirror will become the secondary one and conversely. It is represented in FIGURE 6.7 for an EFL of 60 [mm] and a field of view of $5°$ represented by 3 rays.

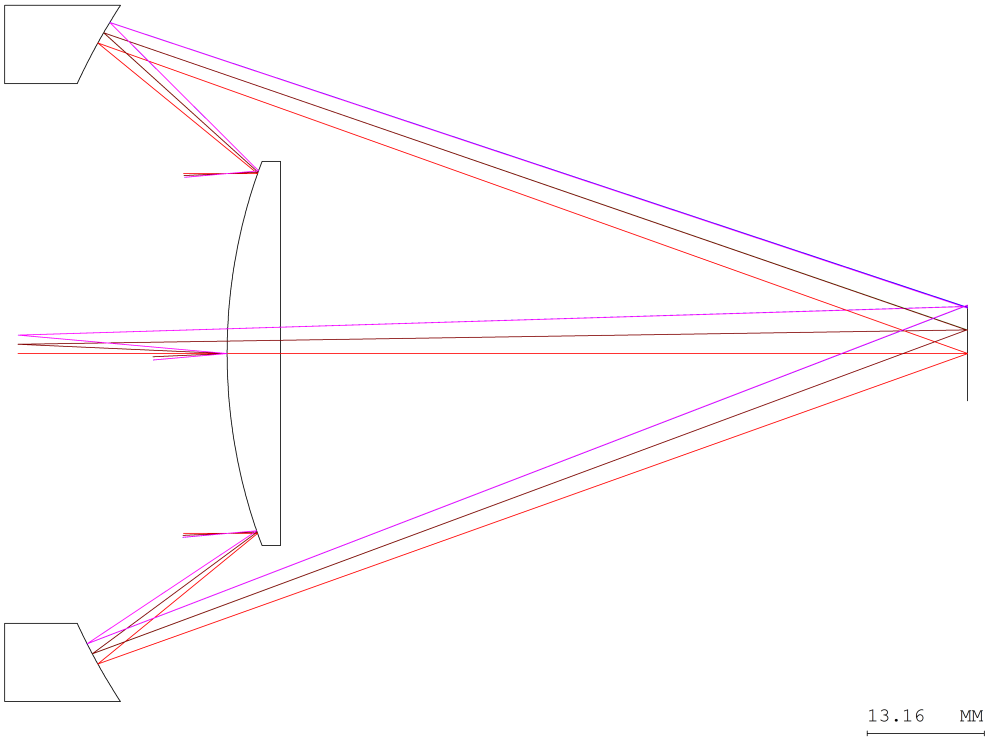

Figure 6.7: Second design : D2. $EFL = 60$ [mm], $FoV = 5°$.

This design reveals much lower EFL than the first one because the distance between both mirrors is much smaller. This design is still very sensible to large FOV. It does not present any obscuration anymore since the secondary mirror is not in the way. However, it comes with a price since the entrance pupil diameter can not meet the CubeSat size anymore and will be lower then 10 [cm]. Again, the backfocus can go up to 120 [cm] to leave room for the detector which seems to be quite a constraint for the design which always uses that maximum length when the optimization is run.

3^{rd} design

Usually, when designing a telescope, it is always better to try to find a working design using as few mirrors as possible. Simply because more mirrors means more manufacture, more risks for imperfection, more weight, more expensive. But sometimes, when the aberrations are still too important, there are no other ways than adding a surface. For instance, when a 2 mirrors telescope does not meet the expectations, the Three Mirrors Anastigmat (TMA) is widely used in space observation due to its high efficiency.

So, since the two first designs will not prove to be that good with large FOV because of big aberrations of all kind produced, the idea of placing a third mirror will be contemplated. But instead of starting from blank, it will stem from the second design. Indeed, the optimization of the second design actually put both mirrors really close to each other in the front part, leaving quite some room behind it. Moreover, its main issue was concerning not having length to focus further. Therefore, a third mirror will be placed more or less instead of the focus plane and

focus the different rays back inside the optical design, as shown in FIGURE 6.8. The idea to "extend the length of the focus that was restricted before".

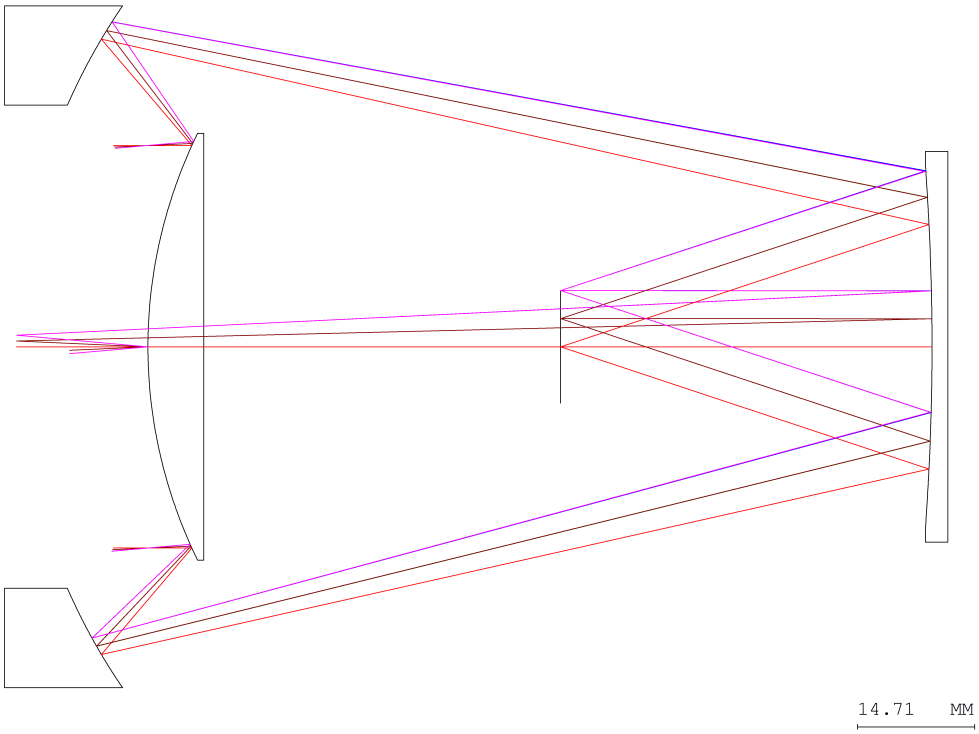

Figure 6.8: Third design : D3. $EFL = 80$ [mm], $FoV = 5°$.

Indeed, this design will turn out be a lot more efficient concerning the geometrical aberrations. Similarly to the second design, the pupil entrance diameter is lessened but it does not present any kind of obscuration, all surfaces considered. The double-edges characteristic of this third design is that the detector must actually be inserted inside the optical design. The good point is that the configuration can go a little further since it does not require to leave room for the detector behind it. The disadvantage of it is to hold the detector there and to make sure it does not bother the whole optical system. But it is feasible and not an absurd idea. It can indeed be held there by using completely transparent materials to the wavelength observed that would not impact the light rays' path through the optical design. Still, one more constraint when optimizing this third design is to ensure the detector will fit inside and will not prevent any ray from making its way to its sensors.

Chapter 7

Optical Designs : Analysis

Three designs have been introduced in the previous CHAPTER 6, they each present different characteristics, performances and reliability. Therefore, all three of them will be studied in this chapter in order to eventually stick with the best one out of those 3. Different analysis will be made concerning different aspects. Firstly, they will be a geometrical analysis, considering the light as rays. It will resume the different aberrations produced mostly thanks to the spot diagram tool. Secondly, a study will be made when considering the diffraction limit but still by looking at the geometrical aberration at the same time. Thirdly, the structure itself of the designs will be compared such as the volume needed for the mirrors and their weight. Lastly, the radiometric budget will be computed for each design studied.

1 Geometrical aberrations

This first analysis will be made by focusing on the geometrical aberrations only. Therefore, an object angle field will be specified, it actually allows to quantify the field of view. As said in CHAPTER 4, a larger field of view will produce more aberrations because it is harder to focus rays coming from highly different angles. The detector uses a rectangular 2D array, defining the swath on ground and its corresponding FoV. The considered angle field will be defined as shown in FIGURE 7.1.

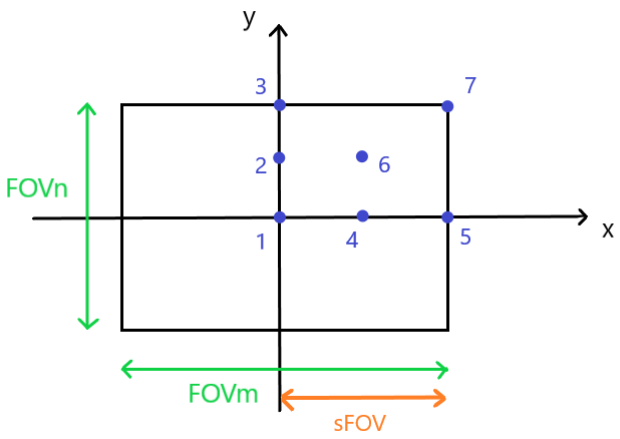

Figure 7.1: Thorough angle field, including the whole array.

Since the four quarters of this array are the same by symmetry, studying one of them comes back to studying the entire field. The different point selected represent the extreme angles from where the most aberrations should come. So, such a choice of angle field takes the worst case into account by analyzing the ray coming from the very corner. For instance, TABLE 7.1 represents the angle field when the length of the array is a $1°$ FOV meaning a sFoV of $0.5°$. It must be mentioned that each point is actually normalized by the FoV_m (so the largest of the two FoV) explaining the coordinates.

Field position	X coordinate [°]	Y coordinate [°]
1 (0,0)	0	0
2 (0,0.4)	0	0.2
3 (0,0.8)	0	0.4
4 (0.5,0)	0.25	0
5 (1, 0)	0.5	0
6 (0.5, 0.4)	0.25	0.2
7 (1, 0.8)	0.5	0.4

Table 7.1: Angle field corresponding to each point in FIGURE 7.1

However, in the following analysis, it will appear that this extreme corner angle (field position 7) is actually subject to most of the aberrations, every time, and will then strongly reduce the efficiency of each design. This is why this second object angle field, FIGURE 7.2 will also be used, identical to the previous one but not taking into account the rays coming from the very corner of the array. This loss of information can actually be greatly counterbalanced by the gain in image quality.

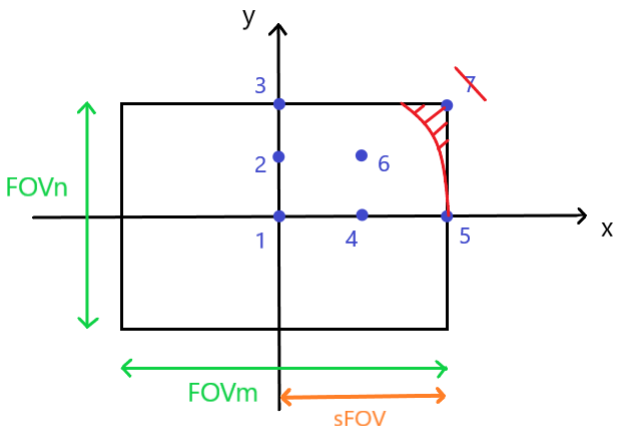

Figure 7.2: Loose angle field, excluding the corners.

For more clarity, the first angle field taking the whole array into account will be referred as the "Thorough angle field" while the second one will be refered as "Loose angle field". Excluding the corner position can be obtained by limiting the aperture to the loose angle field, allowing to strongly reduce the aberrations. However, going from the thorough angle field (FIGURE 7.1) to the loose angle field (FIGURE 7.2) means losing some information. Therefore it will result in induced intentional vignetting and light energy is reduced inside the system, but this is the cost to pay in order to obtained a decent image quality.

Now that the field positions have been defined, they will be used for each design optimization. The field of view will be increased little by little and the spot size will be analyzed each time in order to see from which FoV the aberrations will start to be too great.

First design

Concerning the first design, similar to the Cassegrain telescope, the first concern was the choice of both mirror's surface. In *CODE V*, the default settings use spherical mirrors. FIGURE 7.3 actually shows different spot diagrams obtained from the first design for 4 different mirrors surface configuration. As explained in CHAPTER 4, the bigger the spot size the more aberrations are produced. Actually, the spot size is considered acceptable as long as it is smaller than the pixel size. Therefore, the image quality is good and reliable. This statement will actually lead most of the analysis through this chapter.

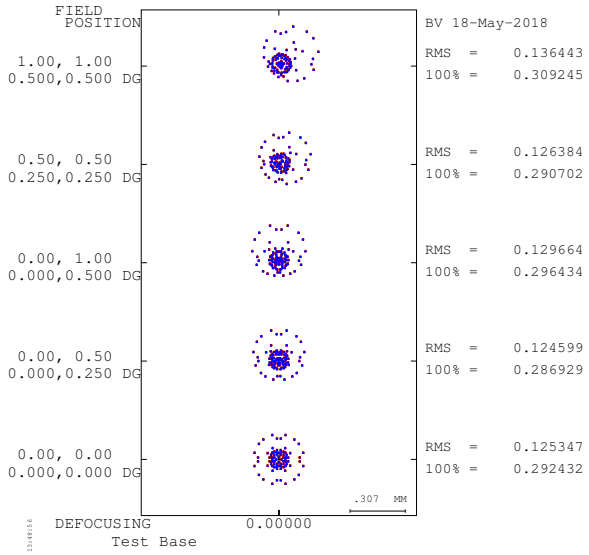

(a) Spherical mirrors

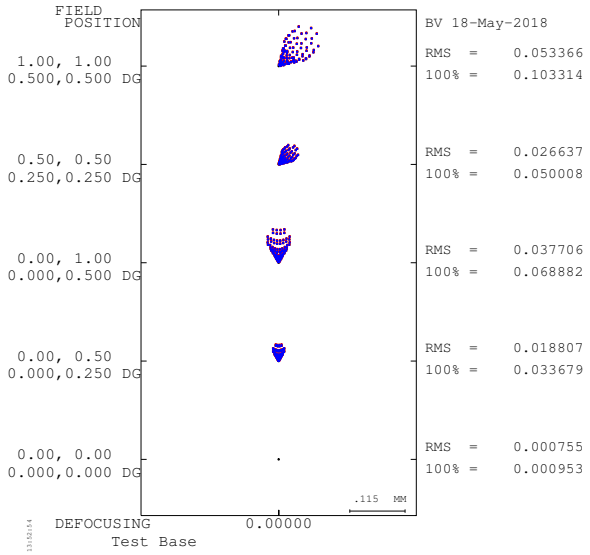

(b) 1^{st} mirror parabolic & 2^{nd} mirror spherical

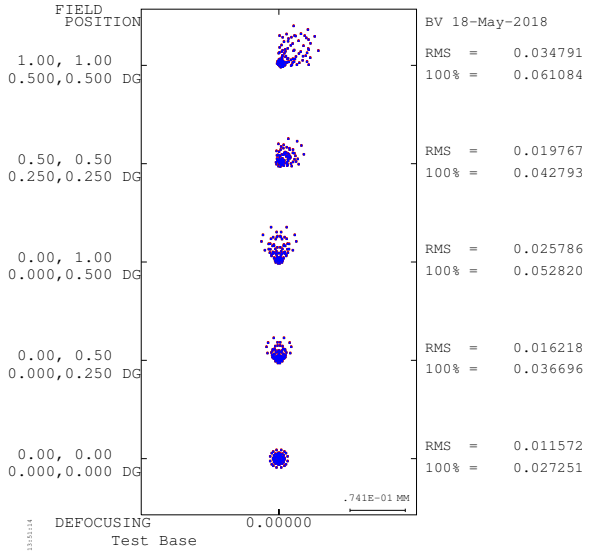

(c) Conic mirrors

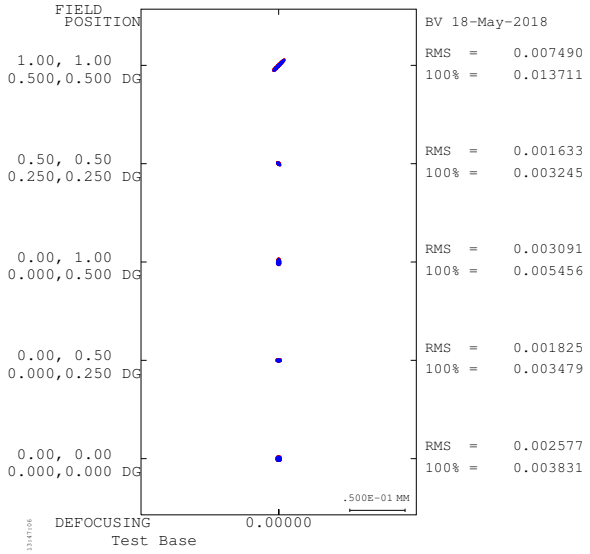

(d) Aspherical mirrors

Figure 7.3: Spot diagram for different mirrors properties : Conic, Spherical, Aspherical

The figure represents the spot size for 5 field positions, with the upper one the most extreme position, usually the cause of most aberrations, as explained before. Then on the right, two spot sizes are defined :

- The RMS : The Root Mean Square diameter, in millimeters, represent the diameter of the circle in which about 67 % of the rays are focused. It already gives a great deal of information about the image quality.
- 100% : It gives the diameter of the circle needed in order to encompass every single ray. This measure is then very complete but can become quite innacurate in the event of singular rays off focus.

It can be seen that using spherical mirrors only results in spot sizes 3 times bigger than any of the three other configurations. Moreover, the shape of the spot diagram is due to spherical aberrations as it could have been guessed. The second configuration is actually the same as the Cassegrain telescope as described in CHAPTER 4: the primary mirror is parabolic while the secondary one remains spherical. It already reduces the aberrations by a lot. It can be seen that the spot diagrams have the comet shape, meaning the main aberration is the coma. Then, the third configuration, using both conic mirrors, gives smaller spot sizes but still represents an awful image quality. Eventually, the last option using two aspherical mirrors produces spot sizes fitting in a pixel size of $15\mu m$. Indeed, both the RMS and the 100% function are smaller than the pixel size for each field position. Therefore, the results are acceptable. Actually, aspherical mirrors are very useful to get rid of aberrations with the off-axis rays. They will therefore be used in each design.

One surprising thing to notice is that the second configuration is actually the best one for the zero field : (0,0). This means that the Cassegrain telescope as it is (parabolic primary mirror and spherical secondary mirror) is really efficient at very low field of view but then the aberrations increase more and more with the field of view.

Now that the first design has been optimized through a lot of trials and errors (back and forth between step 2 and 3 of the design process), the spot sizes can be analyzed with respect to the field of view, as shown in FIGURE 7.4. This was done independently of the altitude but still for different EFL[1] and strictly geometrically wise (diffraction not taken into account).

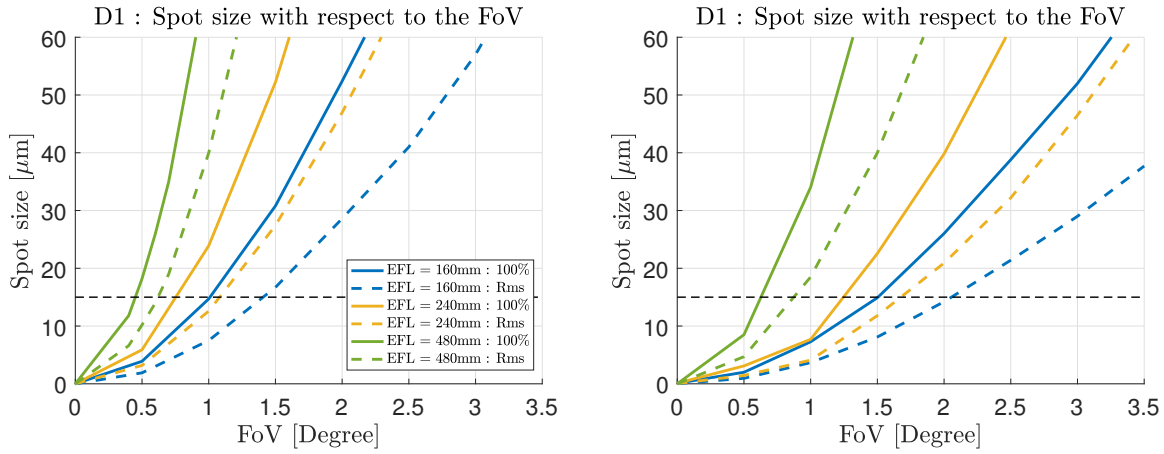

(a) Thorough angle field

(b) Loose angle field

Figure 7.4: D1 : Spot sizes with respect to the field of view. $D_p = 80$ [mm]

It must be mentioned that the analysis of this first design were made with a pupil entrance diameter D_p of 80 [mm]. In the graphics, the black dotted line represents the pixel size at $15\mu m$. Therefore, the image quality will be sufficient only if the spot size is below that line. For instance, with the design corresponding to an EFL of 160 [mm]. In order to focus 100%

[1]Obviously, once the EFL is chosen, it actually directly defines the field of view required, but this section focuses on the geometrical aberrations and will still consider a wide range a field of view

of the rays within the pixel size, the field of view can not be higher than $1°$ when referring to the thorough angle field and $1.5°$ in the loose angle field while the RMS spot size can go up to respectively $1.5°$ and $2°$.

Also, the graphics shows the results for 3 different EFL. When optimizing a design, some constraint can be given to the software. Those constraints can be of many kind: surface properties, mirrors positions, aperture,.. But the most important constraint to give to the software is actually the EFL. Then the trials and errors can start until reaching what seems to be the most optimized solution (remember the optimization tool only go to the closest performance error function, CHAPTER 6). Sometimes, the difference in structure from one design to another can seem really small while the performance results are actually strongly different. Eventually, when what seems to be the ideal design is found, one can not simply modify the EFL in the constraints in order to shift from one optimized design with such EFL to another optimized design with another EFL, the whole process must be reiterated (it can still start from the same basic initial structure, though).

Eventually, all three optimized designs seem in agreement with the fact that, within those EFL range, the smallest EFL would give the best geometrical results. Of course, smaller EFL were therefore tried. But it would actually change the whole nature of the telescope with the back-focus in front of the secondary mirror, preventing the detector to be placed correctly and even deteriorating the geometrical performances.

Second design

The same analysis will be made on the second design, the backward Cassegrain. Again, using both aspherical mirrors turns out to be the best option for better performances. It will be independent of the altitude and focus on increasing the FOV and study their corresponding spot diagrams. This will be shown in FIGURE 7.5 for two different EFL (much smaller than the first design) and on both the thorough and loose angle fields. Both design are analyzed with an entrance pupil diameter of 40 [mm].

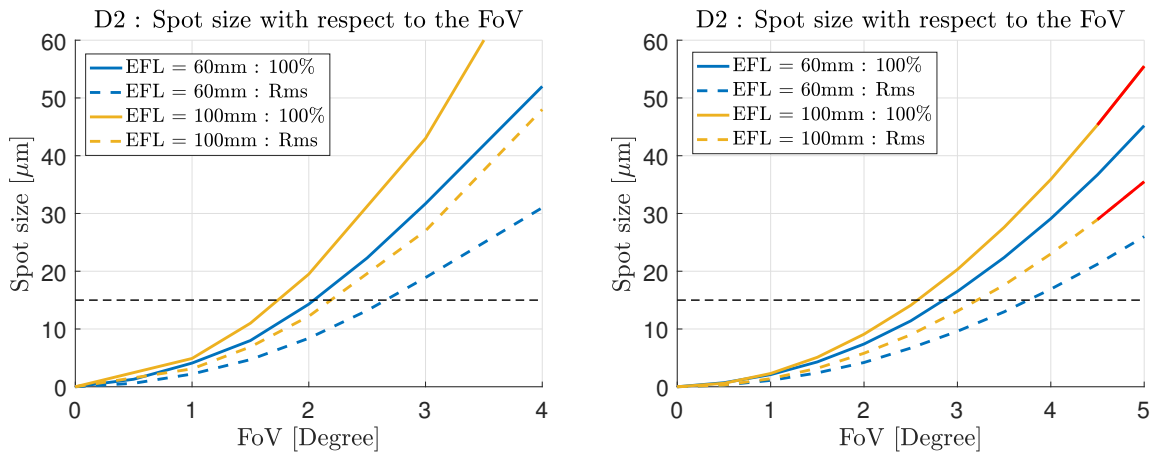

(a) Thorough angle field

(b) Loose angle field

Figure 7.5: D2 : Spot sizes with respect to the field of view. $D_p = 40$ [mm].

This time, the spot size curves go a bit further before oversizing the pixel size (black dotted line). Its geometrical performances are almost twice as good as the first design. Again, in such range of EFL, the smallest one is less affected to the different aberrations. An EFL of 60 [mm] being already quite small, trials with shorter ones actually gave bad results with no possible optimization. While trying longer EFL would not work well either because it would need to go beyond the length constraint of 120 [mm] in order to be interesting.

In the loose angle field, the curves are indeed lower and therefore, some computations were made at a FoV up to $5°$. However, concerning the design with the EFL of 100 [mm], when the FoV is reaching $4.5°$, the rays going from the secondary mirror to the focus point would actually hit back the primary mirror in their way. This is called vignetting and is represented by the red marks in FIGURE 7.5B. However, the spot size were still computed by the software which is due to the sequential ray-tracing of *CODE V* meaning each surface "disappear" after being used once. The only way to notice such intersection was by drawing a view of the design as it can be seen in FIGURE 7.6 for a FoV of $5°$.

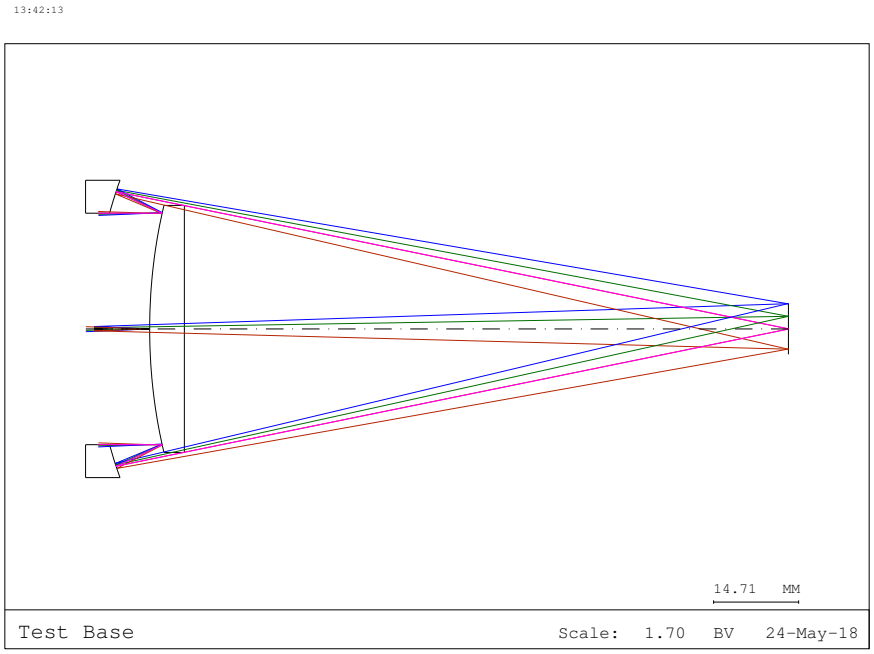

Figure 7.6: Unwanted intersection between light rays and primary mirror.

This case actually happened more quickly when the EFL was increased for other designs which were therefore rejected.

Third design

Since this third design is composed of 3 mirrors, it makes the whole design process the more complicated. The software has a lot more variables on which it can play to find the optimal configuration. There are a lot more possibilities to place the mirrors and to define them initially. Again, aspherical mirrors were used along the process.

This design was actually improved several times through the whole master thesis. Thanks to getting more accustomed to the software *CODE V* and by getting more familiar with the subject of optical design through a more subtle knowledge. At first, a quite good optimization was made. Indeed, as it can be seen in FIGURE 7.7, the results are already a lot better than the previous two designs. They correspond to the thorough field of view and represent the 100% maximum spot size, for an entrance pupil diameter of 40 [mm].

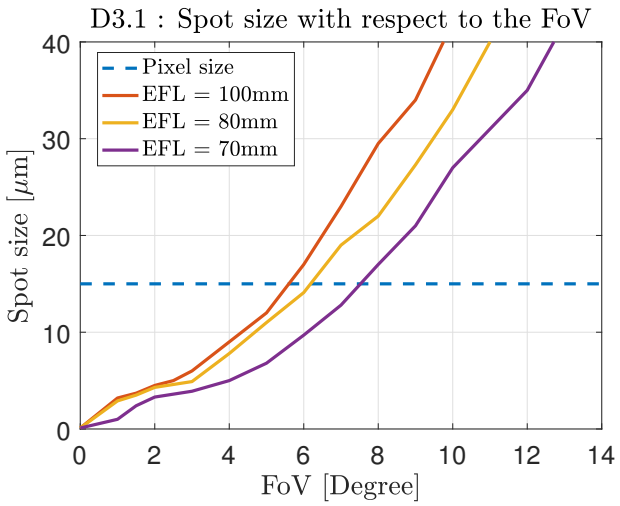

Figure 7.7: D3.1 : Spot size (100%) with respect to the field of view (Thorough angle field). $D_p = 40$ [mm].

This design was already thought to be one of the best optimization since the performances are more than 3 times better. But it is actually quite common to obtain much better geometrical results by adding a surface to the design.

It appeared the design could still be improved by playing with tiny details, but tiny details that mattered. Indeed, the results presented in FIGURE 7.8 shows off its performances for three different EFL, each considering a larger entrance pupil diameter of $D_p = 50$ [mm].

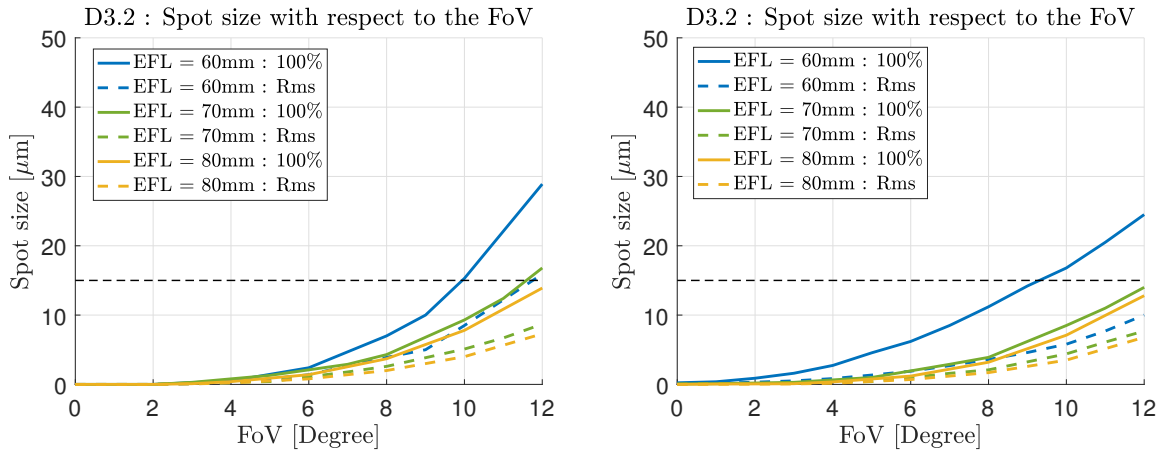

(a) Thorough angle field

(b) Loose angle field

Figure 7.8: D3.2 : Spot sizes with respect to the field of view. $D_p = 50$ [mm].

It can be seen right away that this design is really good concerning the geometrical issues. It is close to aberration-free up to a FoV of $4°$. Moreover, it was not relevant to go much higher than a FoV of $12°$, where the analysis was stopped.

So far, the constraint of a maximum length of 120 [cm] inside the CubeSat was still applied. However, as said in CHAPTER 6, the fact that the detector will actually be placed inside the optical design, frees some space. Therefore the design 3 will ultimately be improved by allowing the distance between the secondary and tertiary mirror to go up to 140 [cm] which will result in the following graphics of FIGURE 7.9.

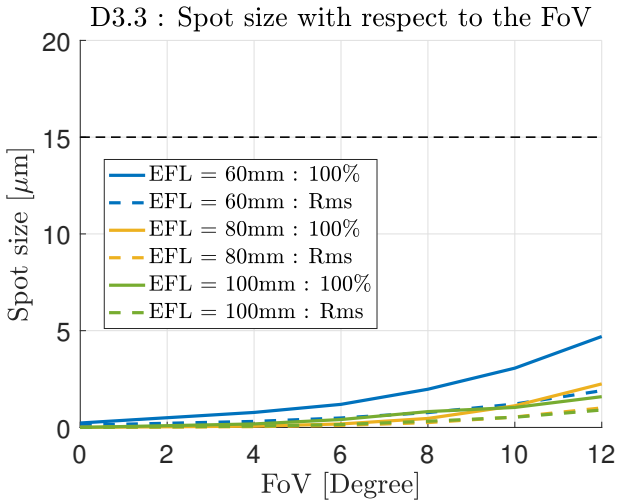

Figure 7.9: D3.3 : Spot size with respect to the field of view (Thorough angle field). $D_p = 50$ [mm].

This time, the spot size are impressively low, meaning the system is really good with geometrical aberrations. Indeed, there were no need to compute the results concerning the loose angle field since the full one was already so well represented. Also, thanks to the new constraint, higher EFL could be reached without changing the whole basis structure of the design. Each EFL considering an entrance pupil diameter of 50 [mm]. However, the design concerning the EFL of 100 [mm] would not be able to welcome the detector inside itself above a FoV of 8°. At such FoV, the ray angles would become too wide and the detector would be in the way.

Such good performance results are quite promising because it leaves some slack in the design meaning some parameters, such as the entrance pupil diameter or any critical mirror's values might be modified. It will most likely increase the spot diagrams, but their size will still remain below the pixel size and ensure an operational design. Quite obviously, from now on, when talking about the 3^{rd} design, the latter one will be considered in all the following analysis.

It must be mentioned that through all of those improvements, the design kept the same shape all along. Indeed, the modifications mostly came from the distances between the mirrors or from their characteristics, it was all about combining the right ones at the right places.

In the following analysis, the loose angle field will mainly be used because providing much better results for an almost insignificant loss of information. Moreover, the RMS spot size will be used because of the unreliability of the 100% one. Indeed, if only a few rays happen to be out of focus by a lot, it will greatly increase the spot size even though every other ray might actually be well focused inside the pixel size. So, the RMS seemed more appropriate even if it gives more of a global idea of the spot diagram than its entirety.

2 Diffraction limit

Now that the geometrical aberrations have been analyzed alone, the diffraction limit can be added to the analysis. Therefore, this time, more parameters will come into play, especially the altitude and its corresponding field of view (depending on the EFL) and also the entrance pupil diameter. This latter has a major role in computing the Airy disk as computed in EQUATION 4.1 in CHAPTER 5.

First, an altitude will be considered, then, the different EFL of each design will define the GSD and also the FoV which will therefore be fixed in the object field angle. It leaves one more parameter to play with in order to reduce the diffraction limit: the entrance pupil diameter. However, as explained in CHAPTER 4, increasing this latter will increase the production of aberrations of all kind. In the end a compromise will have to be found, respecting both restrictions of image quality EQUATION 7.1 and of image resolution: EQ.7.2 (Spot size = S_s) :

$$\text{Geometrical aberration limit : } S_s < P_s \tag{7.1}$$

$$\text{Diffraction limit : } D_A < P_s \tag{7.2}$$

The following TABLE 7.2 lists all the corresponding field of view that will need to be used for each design at each EFL, and the associated GSD depending on the altitude.

	Design 1			Design 2		Design 3		
EFL [mm]	160	240	480	60	100	60	80	100
FOV_m [°]	3.44	2.29	1.15	9.17	5.5	9.17	6.88	5.5
GSD_{800} [m]	75	50	25	200	120	200	150	120
GSD_{600} [m]	56.25	37.5	18.75	150	90	150	112.5	90
GSD_{350} [m]	32.81	21.88	10.94	87.5	52.5	87.5	65.63	52.5

Table 7.2: FoV for each design at each EFL and the associated GSD

First design

This time, the EFL and the pixel size will indeed set the FoV and the maximum spot sizes are computed for different pupil sizes. At the same time, the Airy disk diameter is also plotted with respect to the pupil size as well. This is shown in FIGURE 7.10 for each EFL.

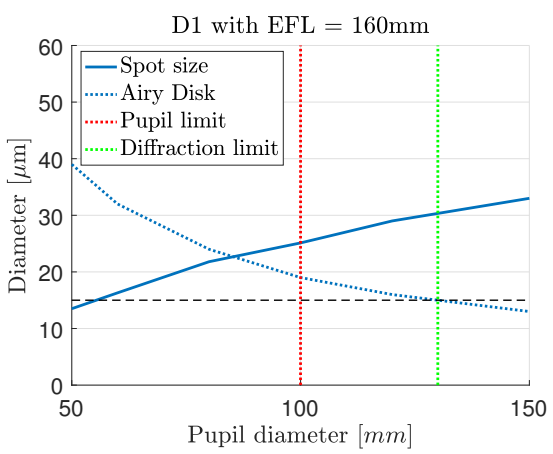

(a) EFL = 160 mm

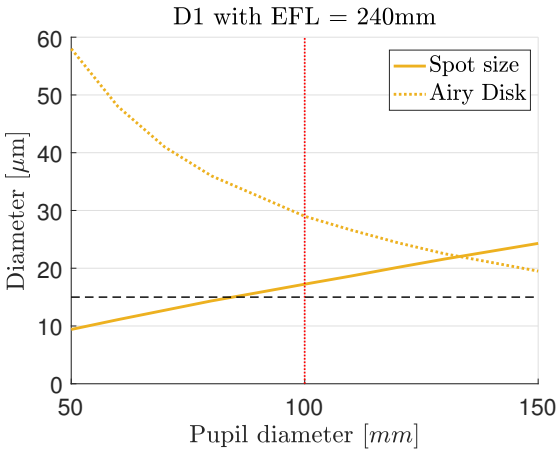

(b) EFL = 240 mm

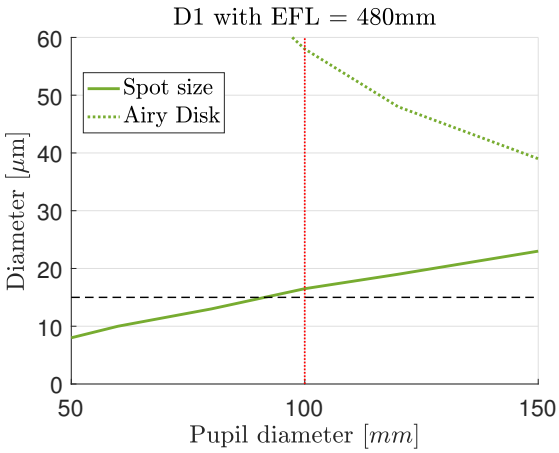

(c) EFL = 480 mm

Figure 7.10: D1 : Spot size and airy disk diameters.

In the graphics, the plain line represents the spot diagram diameter (computed by ray tracig) and the dotted one represent the Airy disk diameter. In order to have a working design, they must both be under the pixel size meaning the image quality is good (Light = ray) and the image resolution is reliable (light = wave). In this first design, the pupil entrance is defined by the primary mirror which can actually go up to 10 [cm] before oversizing the CubeSat. The pupil limit is represented by the red dotted line. It means a higher pupil entrance diameter would require the use of deployable optics.

The airy disk goes down with increasing pupil entrance while the spot size goes up. For each EFL, it can be seen that the curves intersect over the pixel size limit which means the design can not be accepted even if deployable optics was used.

Second design

The same graphics will be plotted for the second design, represented in the following FIGURE 7.11 for an EFL of 60 and 100 [mm].

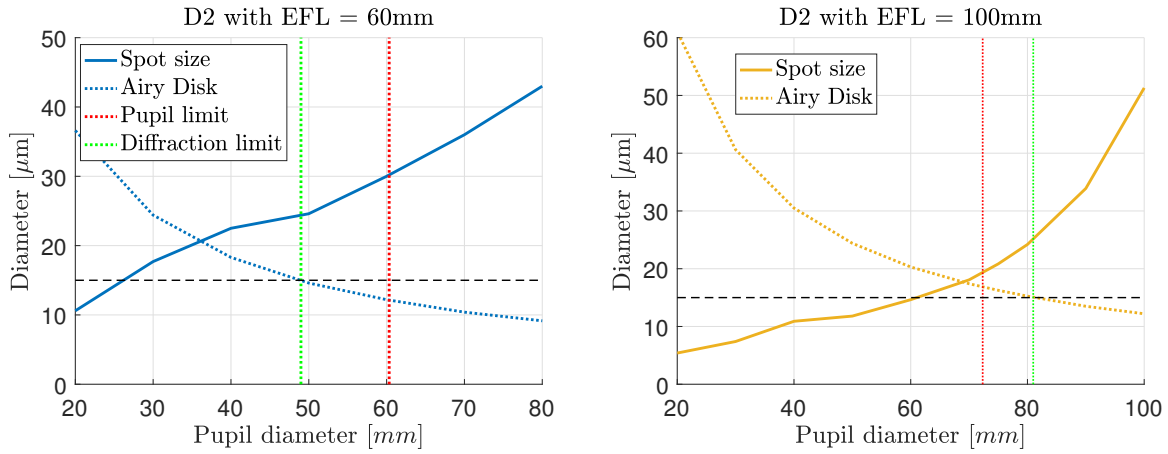

(a) EFL = 60 mm (b) EFL = 100 mm

Figure 7.11: D2 : Spot size and airy disk diameters.

Again, both curves intersect above the pixel size resulting in a not operational design. However, for the EFL of 60 [mm], the green dotted line, representing the minimum entrance pupil diameter needed to prevent any diffraction issue comes before the red line. Therefore, the problem only comes from the geometrical aberrations which are a bit too high at such entrance aperture.

It can be seen that the maximum entrance aperture do not reach 100 [mm] anymore which is due to the design configuration. For instance, for the EFL of 100 [mm], a primary mirror of more than 67 [mm] diameter would require the secondary mirror diameter to be larger than 100 [mm] and therefore oversizing the CubeSat width.

In FIGURE 7.11a the design could be operational if the geometrical aberrations could be lowered by reoptimizing the system. And, in FIGURE 7.11b, the design would need both to lower the geometrical aberration by a little and to reconfigure the design so the red line stands right to the green one meaning a smaller secondary mirror with respect to the pupil entrance diameter.

Third design

The same analysis will be done for the most promising third design. Results are shown in FIGURE 7.12 for each EFL.

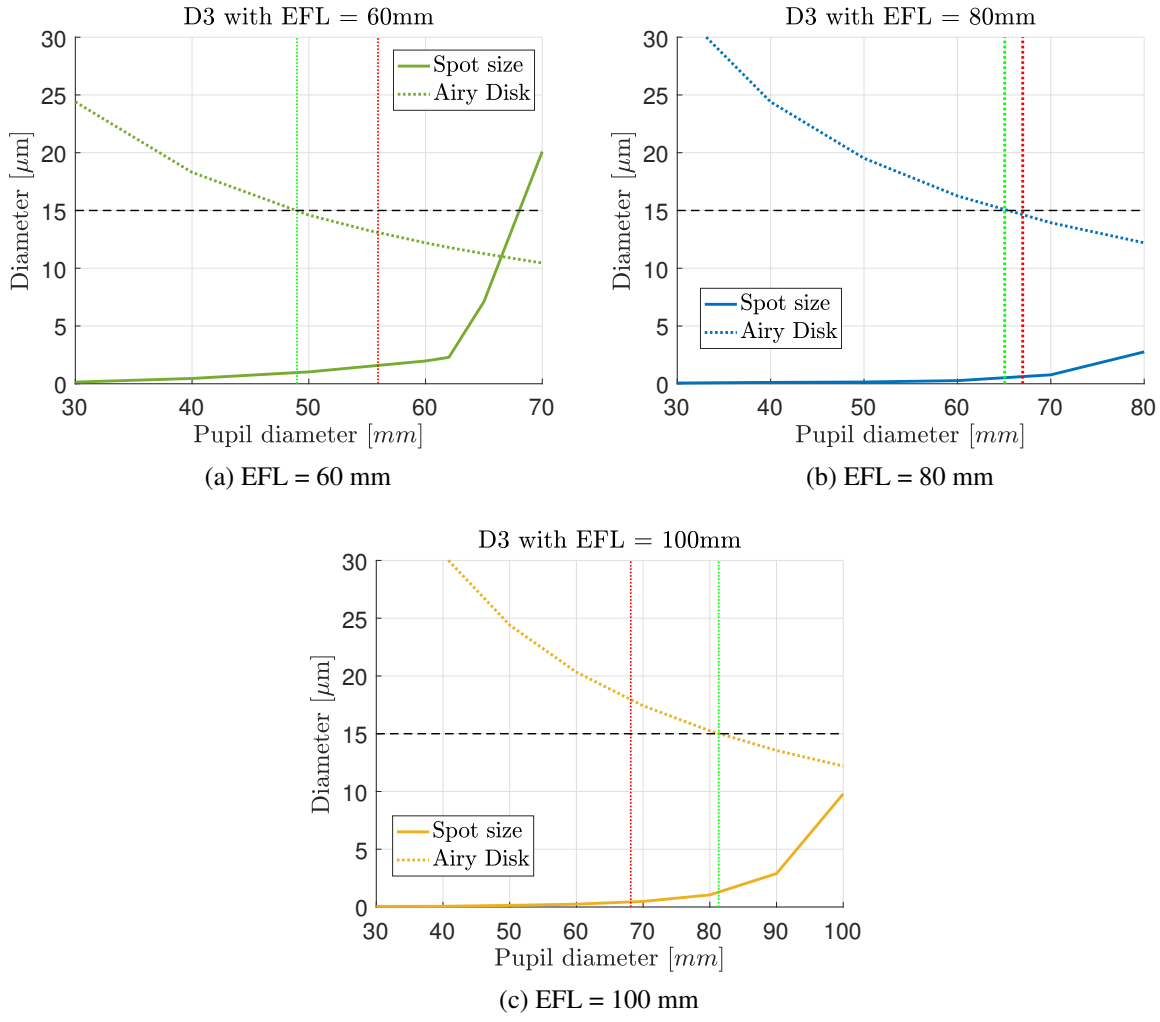

(a) EFL = 60 mm

(b) EFL = 80 mm

(c) EFL = 100 mm

Figure 7.12: D3 : Spot size and airy disk diameters.

This time, the airy disk diameter and the spot size happen below the pixel size (black dotted line), at the same time. It will result in an acceptable design if it happens before the red line, the pupil limit. And this is the case for FIGURE 7.12a and 7.12b. The former has a wider ranger of possible entrance pupil diameter than the latter one having a narrow range, cost to pay for a better GSD. Also, both designs can not be accepted with an entrance pupil diameter below 40 [mm]. At such D_p, the detector would not fit anymore inside the design but that is not too big of a concern. The design will most likely be chosen between the largest possible aperture than in such small ones. Concerning the EFL of 100 mm, the pupil entrance must be over 50 [mm] to allow enough space for the detector.

Actually, this third design proved to be the most influenced by the pupil entrance diameter. Fortunately, this does not demonstrate within the length used in this case. But, up to a certain entrance pupil, the geometrical aberration would suddenly increase tremendously as it can be guessed in FIGURE 7.12a.

Eventually, the TABLE 7.2 is updated below in 7.3 representing the different acceptable design or not.

	Design 1			Design 2		Design 3		
EFL [mm]	160	240	480	60	100	60	80	100
FOV_m [°]	3.44	2.29	1.15	9.17	5.5	9.17	6.88	5.5
GSD_{800} [m]	75	50	25	200	120	200	150	120
GSD_{600} [m]	56.25	37.5	18.75	150	90	150	112.5	90
GSD_{350} [m]	32.81	21.88	10.94	87.5	52.5	87.5	65.63	52.5

Table 7.3: Table representing the working designs so far.

As it can be seen, only the third design presents two acceptable designs both geometrically and diffraction wise: green columns. The red columns represents the non working designss. Design 1 and 2 would not work in the current conditions and optimization. The EFL of 60 [mm] of design 2 is represented in yellow because the image resolution is acceptable but the image quality is not and it is the exact opposite for the EFL of 100 mm from Design 3, therefore represented in yellow as well.

At the end of this section, between both working designs, the EFL of 80 mm is indeed more interesting not only because of its smaller GSD but also because it allows a bigger entrance pupil diameter (up to 67 [mm]) which has other benefits concerning the radiometric budget..

3 Weight & Volume

In this section, the weight and the volume of each design will be studied. Indeed, the optical performances are not the only important parameters when building a telescope. In the field of CubeSats, this section will be of even more importance since the big challenge about CubeSats it too overcome the lack of space and the lighter the better.

The main point is to use the least matter as possible which will both reduce the volume and the mass of the structure. To do so, there exist some complex techniques that allow to empty the mirrors up to 70% of their mass. Indeed, only the used reflecting surfaces are needed, the rest of the mirror is quite superfluous. Moreover, the aperture of each mirror should be as big as possible, as long as the surfaces hit by the rays remain untouched. This is why, the Cassegrain telescope of FIGURE 7.13b (representing the current design 1 for $EFL = 480$ [mm] and $D_p = 80$ [mm]) is definitely preferable to the one in FIGURE 7.13a.

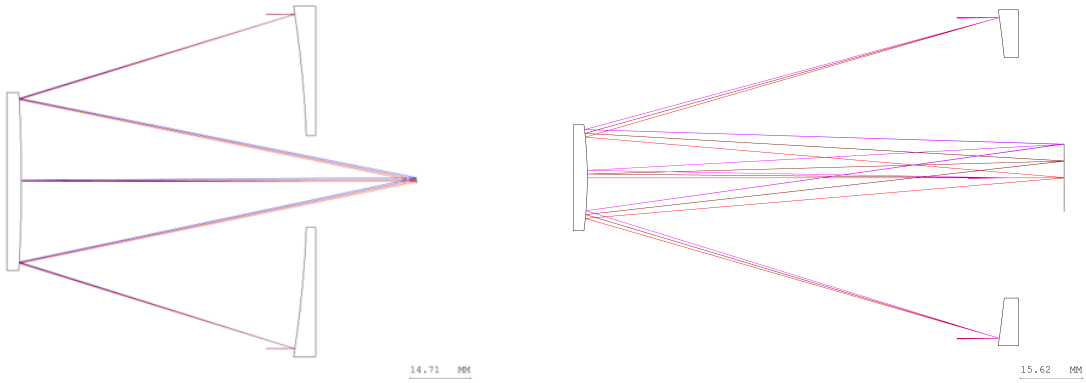

(a) Design 1 : badly optimized (b) Design 1 : smaller and lighter

Figure 7.13: Improvement of Design 1 concerning its weight & volume.

As explained in CHAPTER 4, the thickness has no impact on the optical performances since all the distances are taken with respect to the optical center of the different mirrors. So far, the thickness was only used in order to have a better view of the configuration but it is obviously important to specify it for the manufacture. The smallest thickness possible would be better for the weight and volume but a decent thickness is needed to ensure a minimum rigidity of the mirrors so they can hold themselves straight. In general, it is said the spot of the mirror where the thickness is the smallest should be around one sixth of the mirror's diameter/height, as shown in FIGURE 7.14. This is called the "rule of thumbs".

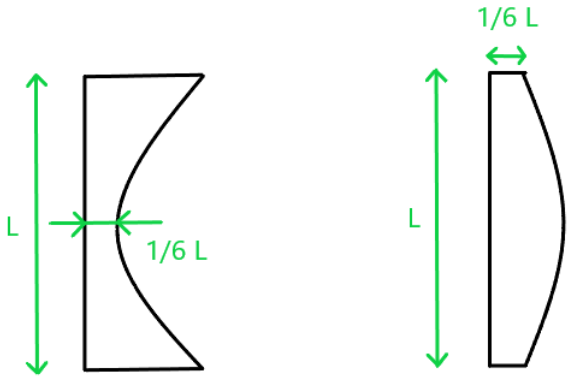

Figure 7.14: Thickness of mirrors compared to length.

In this section, two volumes will be computed. First the volume of the actual mirrors of each system which will eventually gives their weight using the ZERODUR density : $\rho_{Zerodur} = 2.53\ [g/cm^3]$. The gold coating is so thin that it can be neglected in this computation. Then the volume of the whole design, including the light rays' path, will be computed, therefore representing the actual space needed inside the CubeSat to set the telescope.

First design

FIGURE 7.15 is a 3D view of the first design to give a better idea of the actual shape of this first configuration. However, the radius of curvature are not represented in such view, only the thickness of the mirrors and their aperture.

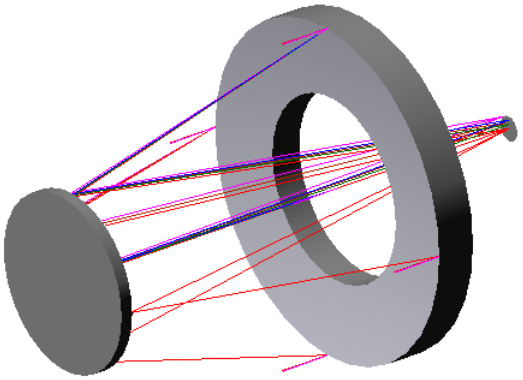

Figure 7.15: Design 1 : 3D view.

The sizes of the mirrors will vary both with the EFL and the entrance pupil diameter (representing the diameter of the primary mirror). At constant aperture, the EFL will still have an impact on both the distances between the mirrors and the focus and on the secondary mirror. At constant EFL, increasing the entrance pupil diameter will only increase the secondary mirror diameter by the same factor. Therefore, the volume, directly translated to the weight, will be computed with respect to the entrance pupil diameter for each EFL. It is represented in FIGURE 7.16 using EQUATION 7.3.

$$W_{D1} = [\overbrace{\pi r_2^2 t_2}^{\text{Secondary mirror}} + \overbrace{\pi\left(r_1^2 - r_2^2\right) t_1}^{\text{Primary mirror}}] \times \rho_{ZERODUR} \times 0.3 \tag{7.3}$$

with

- r_1 and r_2 respectively the radius of the primary and secondary mirror;
- t_1 and t_2 respectively the thickness of the primary and secondary mirror;
- The 0.3 factor representing the fact that the mirrors are emptied of 70% of their mass.

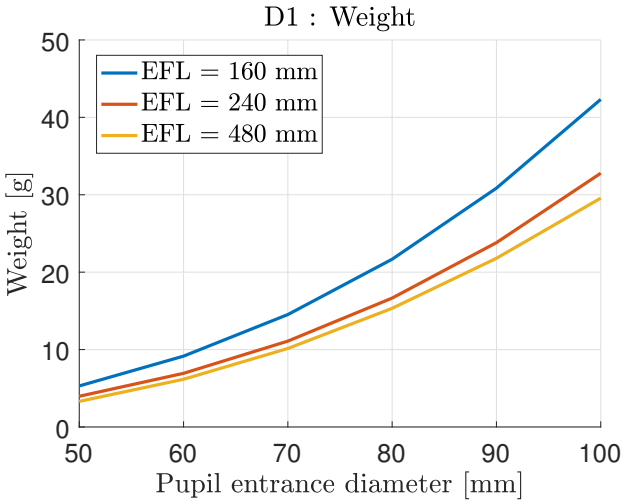

Figure 7.16: Design 1 : Weight.

Since the longer EFL would mean a smaller secondary mirror, the weight slightly decreases with the EFL while it obviously increases with increasing entrance pupil diameter.

Then, the whole volume of such design is computed. This volume is represented in the 2D FIGURE 7.17, it is actually the area surrounded by the green lines and the red square represents the area needed for the detector. In 3D, it will represent a cylinder attached to a small cone on its right end plus a squared box for the detector.

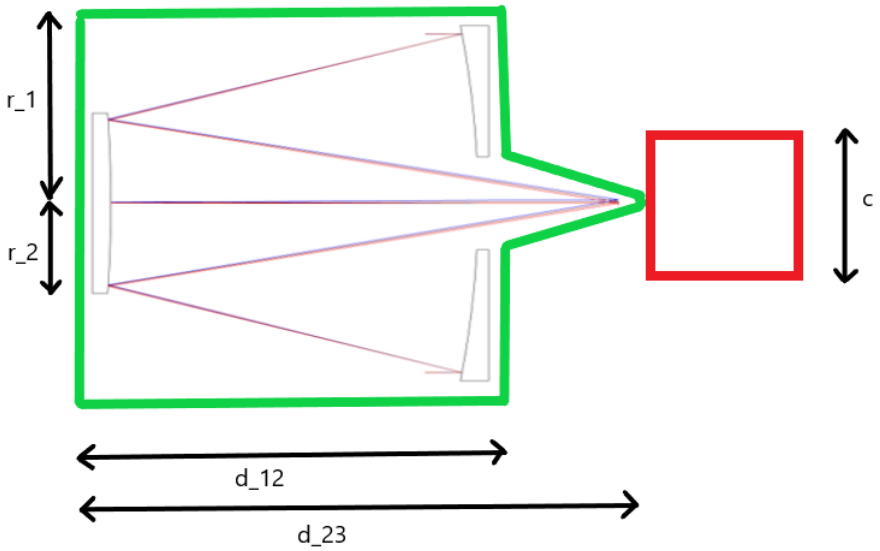

Figure 7.17: D1 : Actual volume needed.

Such area must be drawn by considering the largest possible FoV, when the light rays take the most space. Again, the volumes are represented with respect to the entrance pupil diameter for each EFL in FIGURE 7.18 and their computation was made using EQUATION 7.4

$$V_{D1} = \overbrace{\pi r_2^2 d_{12}}^{\text{Cylinder}} + \overbrace{\pi r_2^2 (d_{23} - d_{12})}^{\text{Cone-shaped}} + \overbrace{c^3}^{\text{Cube}} \tag{7.4}$$

with

- d_{12} is the distance between the primary and secondary mirror;
- d_{23} is the distance between the secondary mirror and the focus plane;
- $c = 0.03$ [dm] represents de detector's side.

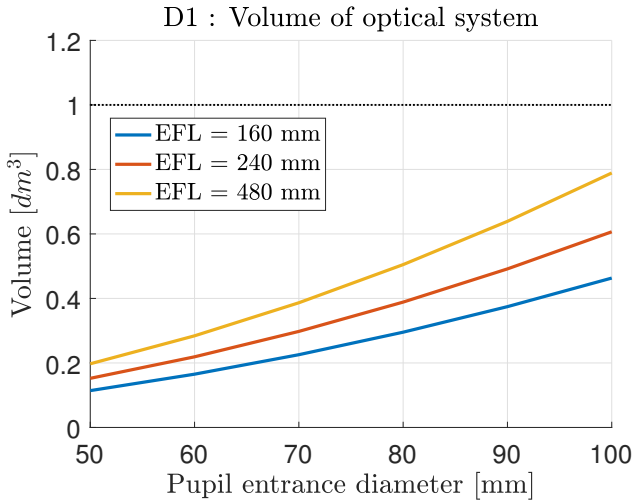

Figure 7.18: D1 : Whole volume of the optical system including detector.

It can be seen that this time, the smallest EFL proves to need less space than the others. The black line representing the volume of 1U of the CubeSat, such a volume is almost reached in the case of an entrance pupil of 10 [cm] for an EFL of 480 [mm]. Indeed, the total volume is strongly influenced by the distance between the mirrors (depending on the EFL) as well as how far the backfocus goes (to a lesser extend).

Second design

The same analysis will be made for this second design. FIGURE 7.19a representing its configuration in 3D and FIGURE 7.19b, a 2D representation of the whole volume needed for the design. Contrarily to the 3D view, the 2D representation actually shows the radius of curvature, used for the volume computations. In 3D, it will represent a cone with a cylindrical base along the thickness of the secondary mirror.

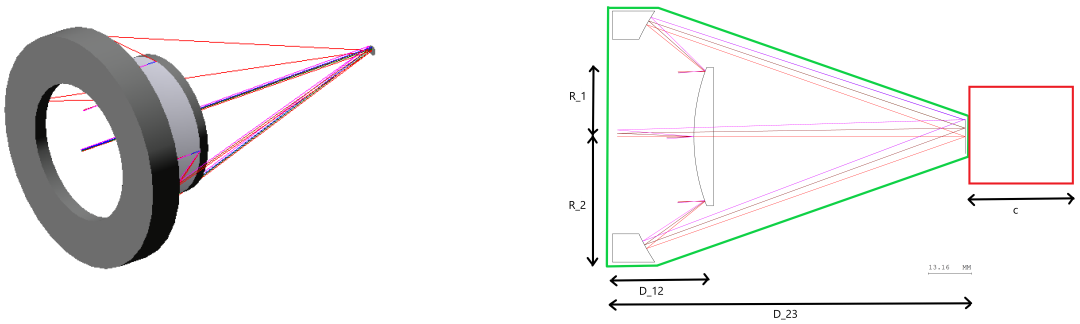

(a) 3D view (b) Actual volume needed

Figure 7.19: Design 2 : Volume analysis.

Then, both the mirrors total weight and the volume of the optical design (including the detector) are respectively represented in FIGURE 7.20a and 7.20b.

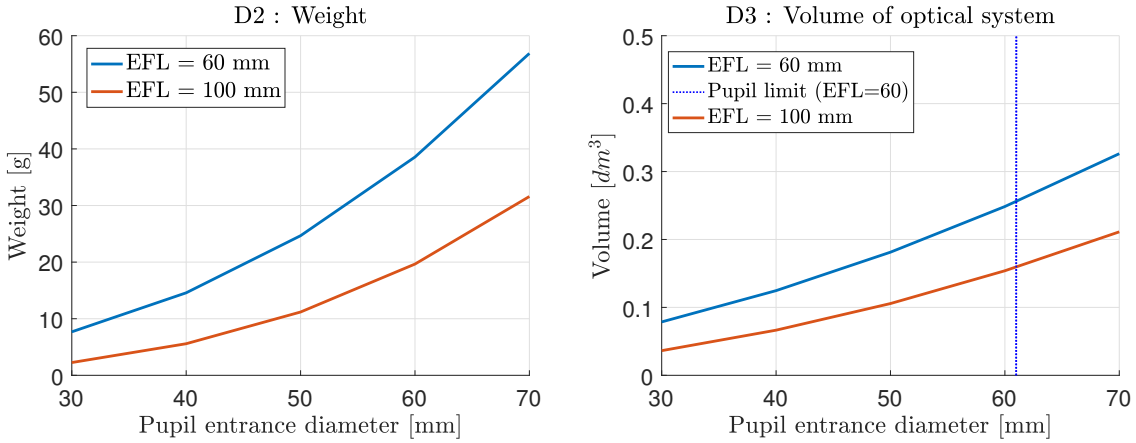

(a) Weight (b) Whole volume needed

Figure 7.20: Design 2 : Volume analysis in graphics.

Concerning their weight, the EFL of 100 [mm] is almost twice as light due to the smaller radius of its secondary mirror and because the weight increases proportionally to the square of the radius. On the other hand, the volume has a cone-shaped, resulting in much smaller volume than the first design which had an important volume, as a cylinder. Again the smaller secondary mirror's radius of the EFL of 100 [mm] implies a smaller volume needed. The vertical blue dotted line represent the pupil limit for the design with EFL of 60 [mm].

Third design

FIGURE 7.21 shows a 3D view of the design representing flat mirrors. However, in this design especially, the radius of curvature are relatively low and it will result in quite different weight than assuming flat mirrors.

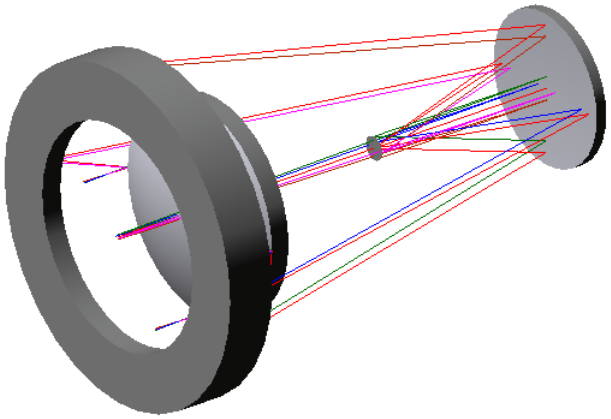

Figure 7.21: D3 in 3D.

The graphics of the weight is plotted below in FIGURE 7.22.

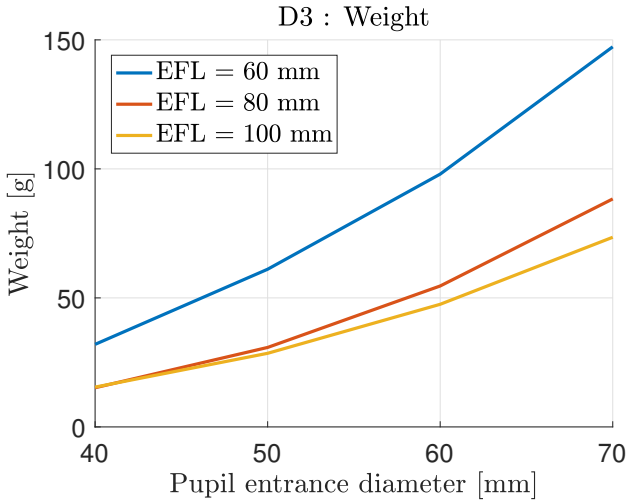

Figure 7.22: Design 3 : Weight.

As expected, the presence of the tertiary mirror does increase the weight compared to the two previous designs.

Then, considering the total volume needed for the optical design, it will be computed as shown in FIGURE 7.23. Contrarily to the previous designs, the whole area surrounding the optical design (green lines) already encompasses the detector space. The detector space inside the optical design is represented by the red lines. This time, the shape of the volume is a kind of truncated cone with a cylindrical basis.

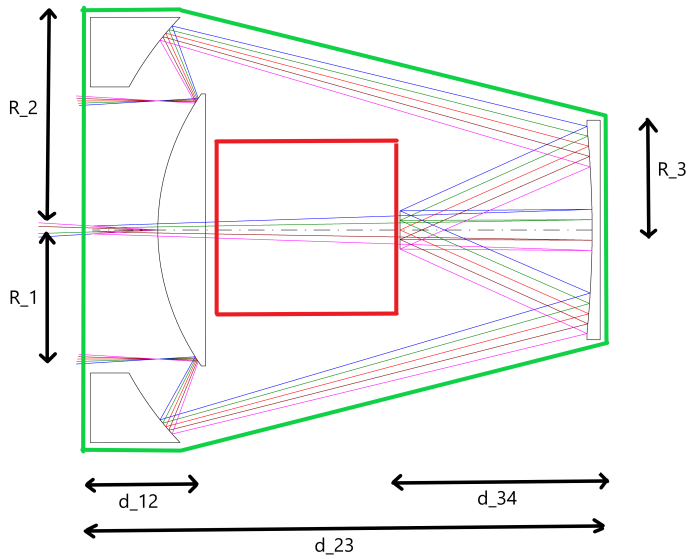

Figure 7.23: Design 3 : Actual volume needed.

The graphic below in FIGURE 7.24 represents the total volume needed for the optical design including the detector.

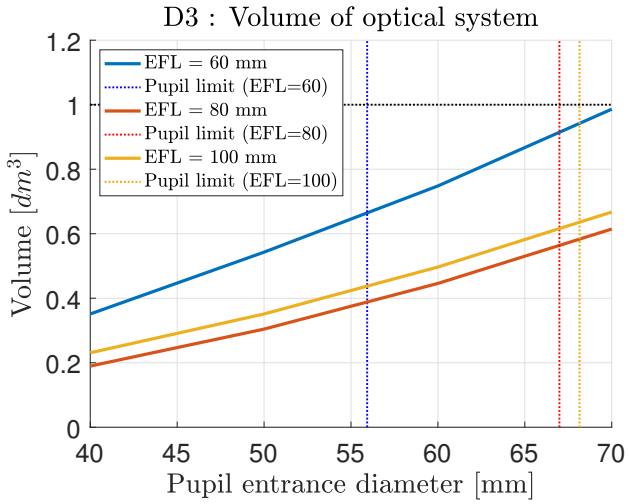

Figure 7.24: Design 3 : Volume needed for the optical system and the detector.

First, it can be seen that the EFL of 80 [mm] is the smallest, due to its whole length of only 115 [mm] compared to the others, both using the maximal length constraint of 140 [mm]. Also, the diameter entrance pupil must be higher than 50 [mm]) so the detector can fit inside the optical design. The vertical dotted lines correspond to the pupil limits of each EFL.

Finally, the average weights and volumes of each design are compared in the following TABLE 7.5 assuming the limit entrance pupil diameter before stepping out of the CubeSat, listed in TABLE 7.4.

	Design 1			Design 2		Design 3		
EFL [mm]	160	240	480	60	100	60	80	100
Pupil limit [mm]	100	100	100	60.33	72.32	55.93	67.04	68.15

Table 7.4: Limit of the entrance pupil diameter for each configuration.

	Design 1	Design 2	Design 3
Average Weight [g]	34.88	35.48	78.51
Average Volume [dm^3]	0.64	0.26	0.58

Table 7.5: Comparison of weights and volumes between designs.

Concerning the weight, the third design is naturally heavier, actually twice as heavy as the other two design which are about the same weight. On the other hand, the volume taken by the third design is not as big as the first one while the second design is three times smaller. Still, if the third design takes that much place, it is mainly due to the fact that its length constraint is not as restrictive than the two others. In the end, the weight of each design is actually really small compared to the weight of the whole satellite. It comes out of this analysis that the second design is the best one when talking about the weight and volume characteristics while the third design is more imposing.

4 Radiometric budget

As described in CHAPTER 5, the computation of the signal at one pixel takes into input the effective surface of the optical design and the optical transmission which will be computed in this section. Then, in order to be able to compare the signal, some assumptions will have to be made concerning the other input parameters involved in the signal computation.

All the following radiometric budget will be computed assuming an average altitude of 600 [km] and its corresponding GSD, depending on the design and its EFL (see TABLE 7.2). Moreover, the pupil entrance diameter used will be the limit pupil of each configuration, as defined in TABLE 7.4.
Then the time integration will simply be computed considering a linear scan as mentioned in CHAPTER 5.

Actually, the only parameters missing in the computation of the SNR are the optical parameters. They will be computed for each design. Then the signal can be computed and eventually the SNR.

First design

The surface of collection of this first design is actually subject to obscuration produced by the secondary mirror standing up front of the primary one. The effective surface is computed following EQUATION **??**.

$$S_{eff} = \pi \left(\frac{D_p}{2}\right)^2 - \pi \left(\frac{D_2}{2}\right)^2 \quad [m^2] \tag{7.5}$$

With D_p corresponding to the entrance pupil diameter, equal to the primary mirror diameter. And D_2 represents the diameter of the secondary mirror, depending on D_p.

Moreover, the FOV corresponding to each EFL are quite low. It can be assumed that all the photons entering the optical system will reach the detector. So, $\tau_O = 1$

Eventually, the signal and the signal to noise ratio are plotted with respect to the GSD for various ground temperatures in FIGURE 7.27.

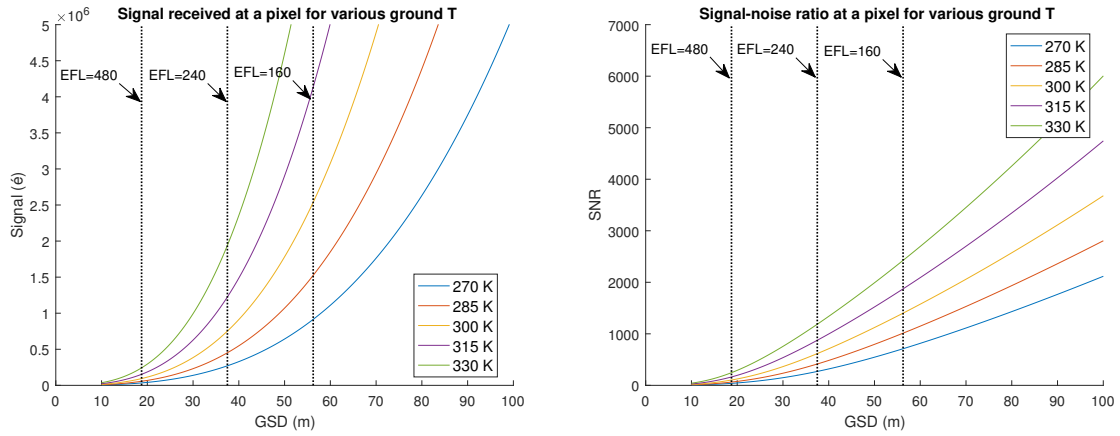

(a) Signal (b) SNR

Figure 7.25: D3: Analysis of the radiometric budget.

Each 3 configurations of the first design are represented by the black dotted lines. Therefore, the signal and SNR are obtained at the intersection between the black dotted lines and the signal/SNR curves, for different ground temperature.

Second designs

The second and third design will present some very similar results concerning the radiometric budget. There will be computed together.

Concerning the collection surface, it is this time directly linked to the entrance pupil diameter since there is not any surface producing obscuration. The EQUATION 7.6 will easily come as

$$S_eff = \pi \left(\frac{D_p}{2}\right)^2 \quad [m^2] \tag{7.6}$$

Then, concerning the transmission of the optical design, since the field angles are large (up to 9.17 °), some photons might be loss through the optical system. This will be computed thanks to a *CODE V* tool, giving the percentage of photons actually reaching the detector. This percentage will be computed as a function of the field angle in FIGURE 7.26.

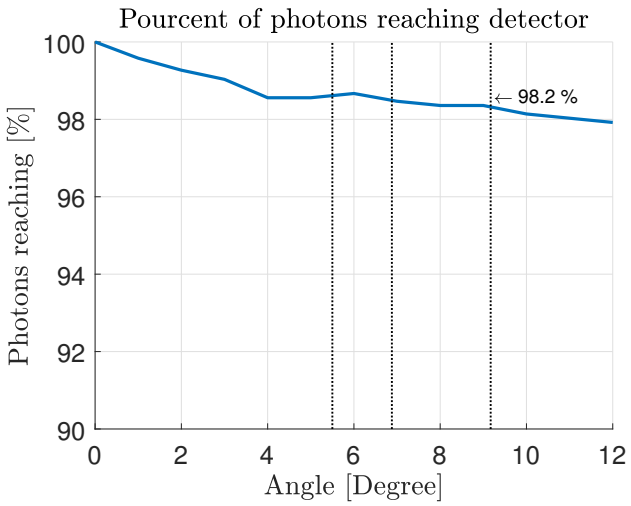

Figure 7.26: D2-3: Optical coefficient of transmission τ_O with increasing FoV

Three FoV were distinguished by black dotted line, corresponding to the FoV needed for each design according to TABLE 7.2. It can be seen that even the worst angle field of 9.17 degrees still has a very efficient transmission coefficient of 98.2%. Therefore, $\tau_O = 0.98$ will be used for the SNR computations, which is a good performance of the optical system.

Eventually, the signal and SNR are computed in FIGURE **??**.

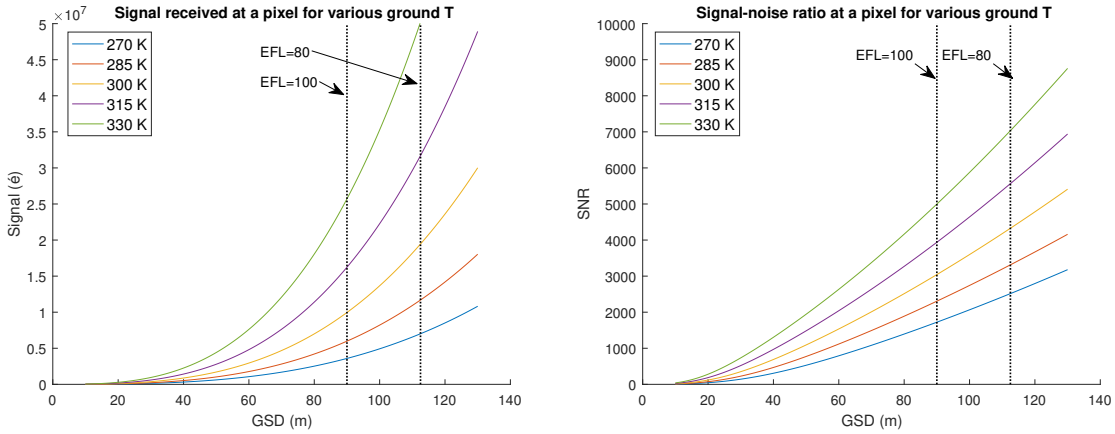

(a) Signal (b) SNR

Figure 7.27: D2 $\simeq$ D3: Analysis of the radiometric budget.

The designs with an EFL of 100 [mm] and of 80 [mm] were represented at their corresponding GSD in black dotted line.

In the end, all three designs actually showed some very similar Signal and SNR values for different GSD even though the entrance pupil diameter is smaller for design 2 and 3. This is due to the secondary mirror, shadowing the collected area of the primary mirror. It actually compensates for the loss in pupil entrance from the two other designs. But when dealing with

the GSD, since design 2 and 3 requires much bigger GSD, their SNR value will be much higher than the one obtained from the first design.
On the other hand, it can be seen that the signal and the SNR strongly increase with increasing ground temperature. This is due to the fact that both the emitted radiance from the Earth and the Sun reflected radiance are much larger. The satellite is therefore more irradiated meaning more photons actually reach it.

Increasing the GSD actually increases the signal a lot and also increases the SNR (eventhough a higher GSD creates a greater noise). Therefore, a good radiometric budget would require the bigger GSD as possible which will go against the philosophy of the optical Engineer, trying to succeed in having the smallest GSD as possible. This represents the main compromise between optical and radiometric performances.

Numerically speaking, the SNR of the designs are really high, therefore a very small acquisition time is indeed in order to take an image of the ground an ensuring a good image free of noises.

5 Design choice

In the end, TABLE 7.6 summarize the different analysis in order to choose the best design for the rest of the study.

Analysis	Design 1	Design 2	Design 3
Geometrical	3	2	1
Diffraction	3	2	1
Weight and volume	2	1	3
Radiometric	3	1	1

Table 7.6: Summary table of CHAPTER 7. The green arrays point out the best design for each analysis individually

As expected, the third design is irrefutably the best choice. Besides being the best design in most analysis it is most of all the only working design concerning both the geometrical aberrations and the diffraction limit. Therefore, it can be used right away for deeper optimization and analysis as it will be done in CHAPTER 8. Then, the design coming in second place is the design 2.

Chapter 8

Optical Design : Deeper analysis

1 Final Design

The third design was chosen so it can now be rebuilt as the final design in order to be as efficient as possible. First, the entrance pupil diameter will be set right below the diffraction limit including a security margin: $D_p = 66$ [mm]. Also, since the EFL is fixed, so is the FoV ($FOV_m \times FOV_n = 6.88 \times 5.504$), represented by the following thorough angle field in TABLE 8.1.

Field position	X coordinate [°]	Y coordinate [°]
1 (0,0)	0	0
2 (0,0.4)	0	1.376
3 (0,0.8)	0	2.752
4 (0.5,0)	1.72	0
5 (1, 0)	3.44	0
6 (0.5, 0.4)	1.72	1.376
7 (1, 0.8)	3.44	2.752

Table 8.1: Final design : angle field.

In order to have a GSD of 100 [m] or less, the altitude of the satellite must not be higher than 533.33 [km] which would corresponds to a swath of 64.2 [km].

Also, the absolute value of the conic constant of each mirror sometimes went up by a lot so this latter was constrained. At the same time, the radius of curvature were checked as well. Both those checkings allow to avoid too complex mirror's shape and to enable a potential manufacture later. Moreover, this allows to have a less sensitive design to tolerances.

Eventually, the final design is represented in FIGURE 8.1 with its two extreme rays implemented.

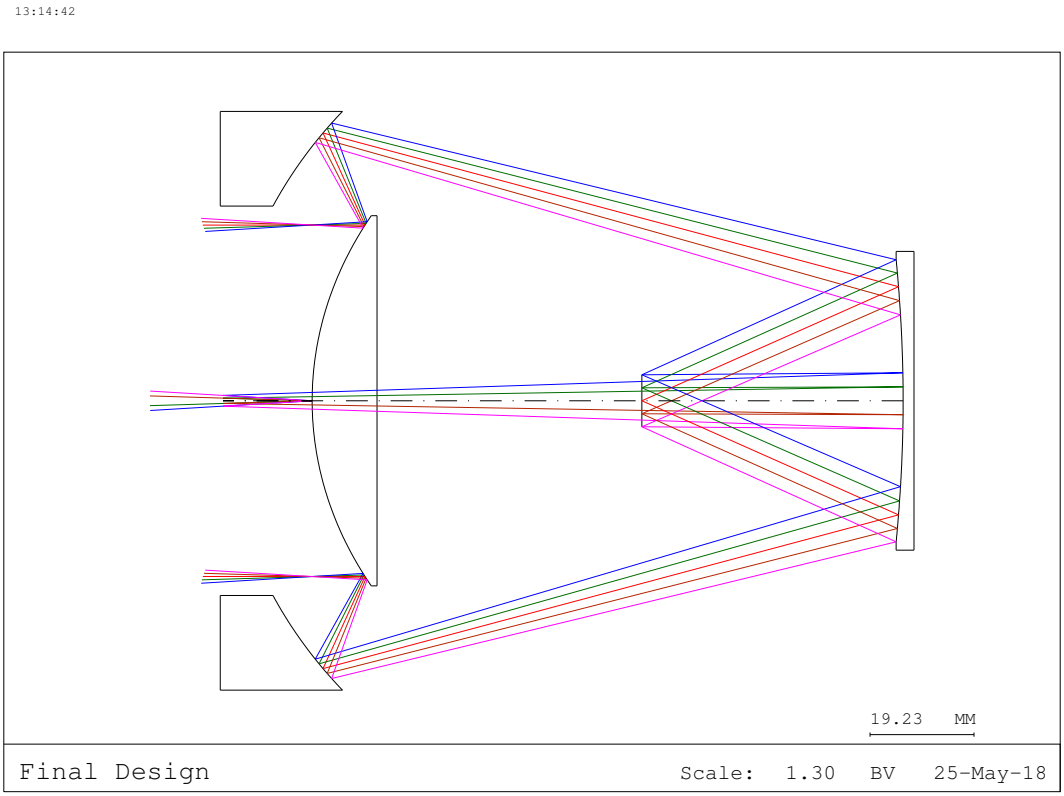

Figure 8.1: Final design with according FoV.

As explained in CHAPTER 7, this choice comes with its disadvantages concerning its weight and volume, listed in TABLE 8.2. However, those properties remain acceptbale. In the field of CubeSat, 1U is usually representing about 1 [kg] and the optical design is way below that weight.

Weight [g]	Volume [dm^3]
267	0.57

Table 8.2: Final design : Weight and Volume.

Now, the performances of this final design will be analyzed.

Spot Diagram

The geometrical aberration can be checked through the spot diagrams represented in FIGURE 8.2.

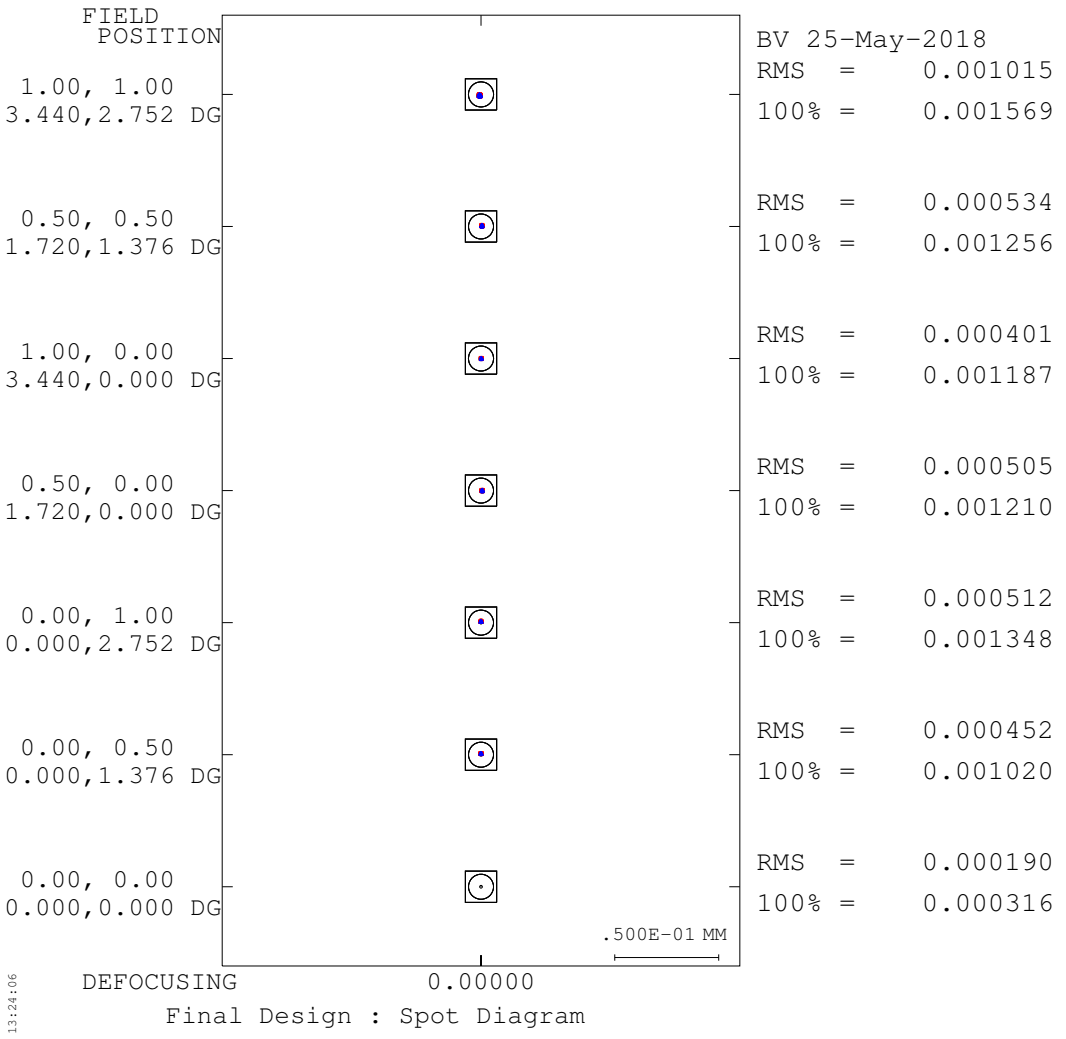

Figure 8.2: Final design : Spot diagrams. With pixel size (square) and Airy disk (circle).

Each one of the seven angle field has its own spot diagram. As explained in CHAPTER 5, this spot size must be smaller than the pixel size for a good image quality. Actually, since the pixel size is represented by the square in the figure, it can right away and easily be observed than every single spot is much smaller. It defines a good image quality (no matter if the rms or 100 % of the spot size is considered). Moreover, the circle actually represents the Airy Disk and it is also smaller than the pixel size, characterizing a possible image resolution diffraction-wise. It can be seen that, again, the worst field is the seventh one, from the very corner, as expected. And that worst field is still ten times smaller than the pixel size.

Encircled Energy

Another way to analyze the geometrical aberrations is thanks to the encircled energy (FIGURE 8.3), which is actually another way than the spot diagrams to present the results obtained.

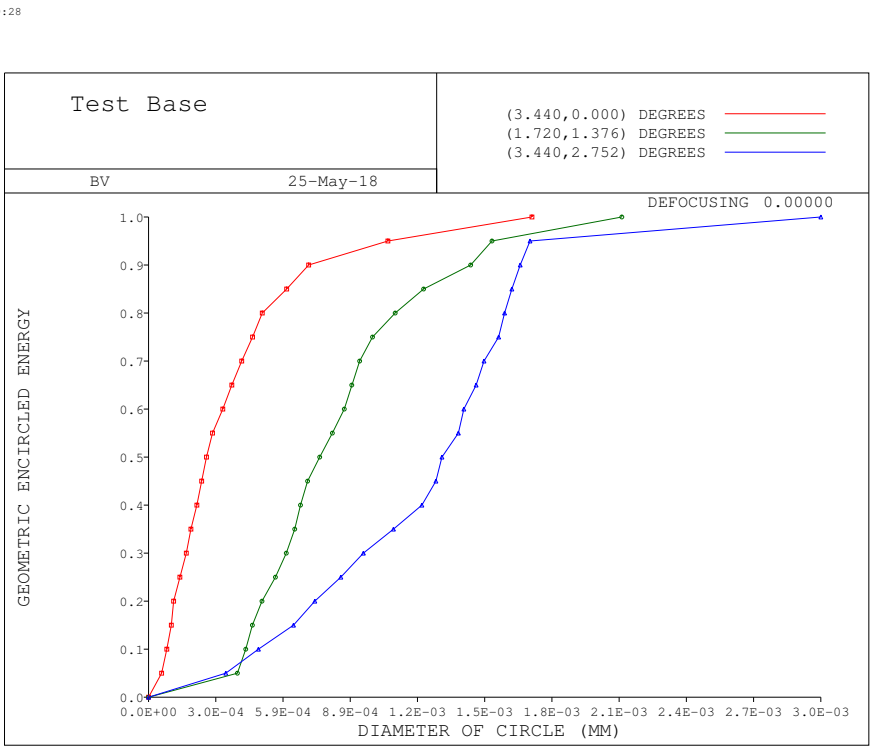

Figure 8.3: Final design : Encircled Energy.

It actually shows the percentage of Energy of each field with respect to the circle's diameter in which that much energy is intercepted. Therefore, the field will reach the number 1 of encircled energy according to the 100% spot size computed in the spot diagrams analysis. However, in this figure, it can be seen that the shape of the curves is actually very steep meaning a lot of energy is focused in the middle of the pixel. It results in little aberrations and great geometrical properties.

MTF

This section is more about the diffraction limit of the design. The Modulation Transfer Function (FIGURE 8.4) represents the contrast between two neighbour pixels (1 being a perfect contrast and 0 meaning no contrast at all).

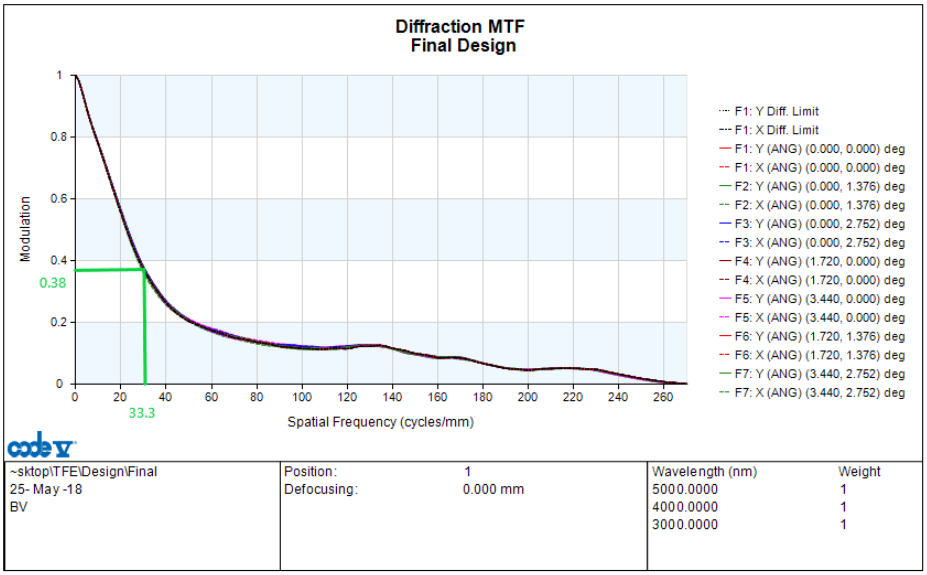

Figure 8.4: Final design : Modulation Transfer Function.

As explained in CHAPTER 3, the minimum frequency needed to distinguish two separate points is given by the Nyquist frequency : $\nu_{Nyquist} = 33.3$. Such a frequency corresponds to a contrast of about 38% for the diffraction limited curve. The good point is that the geometrical aberration are so low that the curve corresponding to the actual design is almost superimposed to the diffraction-limit one, so the best possible contrast for such Airy Disk diameter is actually obtained.

Radiometric budget

2 Tolerances analysis

Now that the final design has been well defined and actually fulfills the mission's goal and requirements, the 4^{th} step of the design process, the tolerances analysis (CHAPTER 6) can get started. In other words, tolerances will be given to some parameters in order to see how much this will influence the whole system.

Once the tolerances are defined, there exist two main methods with different properties to compute the modifications applied to the entire optical design: the Finite Difference (FD) and the Monte Carlo (MC) method. They can both become quite slow if lots of tolerances, fields or type of performances are analyzed. However, the first method provides accurate individual tolerances sensitivities by perturbing the system several times while the second method provides accurate performance prediction but no information about individual tolerance. So, since in this case only a select targeted set of tolerances will be applied at different time, the first method seemed more appropriate. [46]

Before starting the sensitivity analysis, all the parameters must be frozen. Then, the statistical

curves describing the ensued performances will show the modification in the Spot diagrams (simplest tool to analyze the performances). Moreover, a compensator can be specified in order to know the value it should be given in order to counterbalance the modifications due to the tolerances. Usually such compensator would be the displacements of the focus point in each direction. Two kind of analysis will be carried out : the manufacture and the assembly tolerances.

Manufacture tolerances

This first study will assume some errors might be made during the manufacture leading to imperfections. The study will therefore focus on the parameters which are directly linked to the mirrors structures and shapes.

First, tolerances will be applied to the radius of curvature (DLR[1]) of each mirror, the default parameter is 0.0025 [mm] (given by *CODE V*). Actually, in addition to the radius of curvature, the delta fringe (DLF) is usually specified as well. While DLR is a tolerance on the test plate radius, DLF is the power fit of the surface itself to the test plate. Its default parameters is 5 fringes. The FIGURE 8.5 shows the statistical probability of the spot size modification.

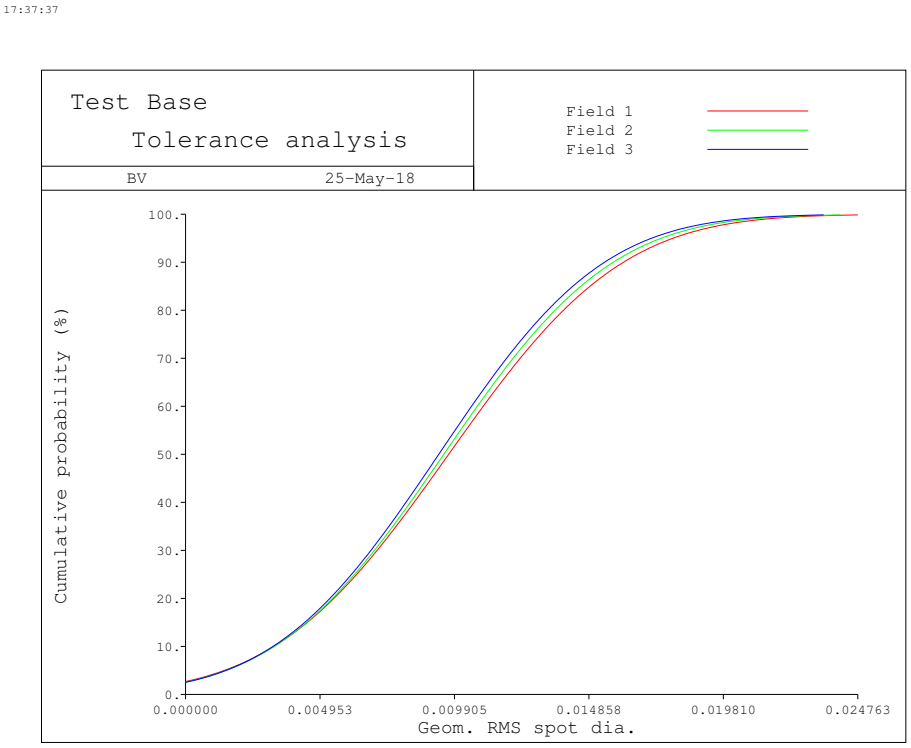

Figure 8.5: Radius of curvature: DLF and DLR sensitivity on spot diagram.

As always, the spot size should remain below the pixel size and it can be seen that it will actually reach the pixel size at a cumulative probability of about 95%. This percentage means that within 95% of the cases, the spot diagram would reach the pixel size explaining the very

[1]Command in *CODE V* to apply the tolerance to the radius of curvature.

weak slope when getting close to the 100%. The tolerances have almost the same impact independently on the field. Then, when analyzing each mirror separately, it appears that most of the loss in performance is actually coming from the tertiary mirror which indeed has a much higher radius of curvature than the two other mirrors. It is actually 10 times more sensitive.

Now, the tolerances will be applied on the conic constant (DAK) of each mirror and the results on the spot diagrams are presented in FIGURE 8.6. The default parameter is 0.001 [mm].

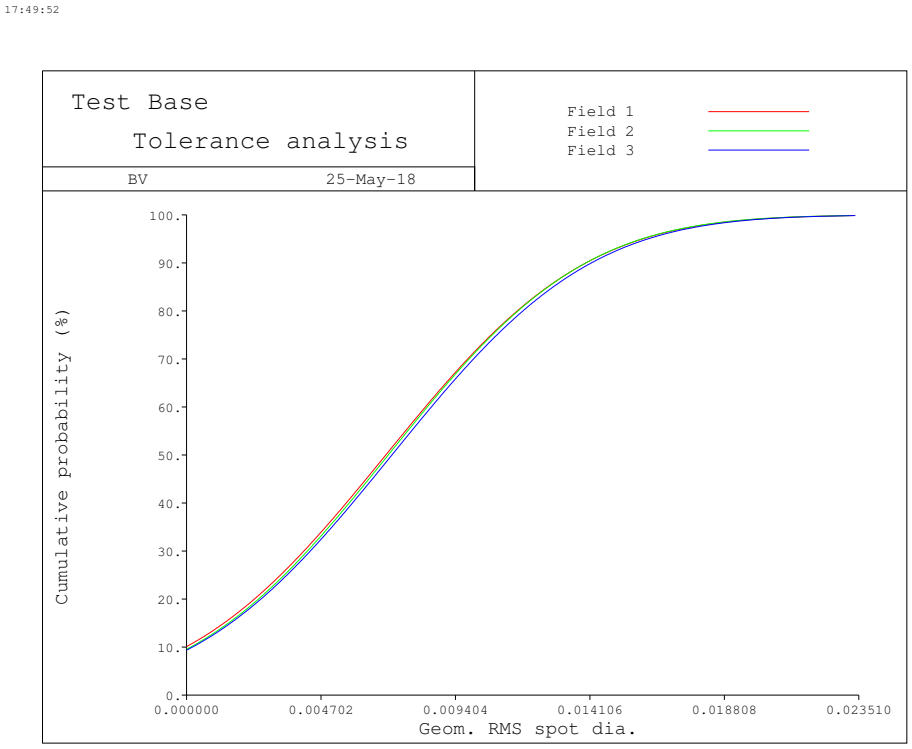

Figure 8.6: Conic constant: DAK sensibility on spot diagram.

This time, the spot diagram reaches the pixel size a bit sooner, at about a 90% of cumulative probability. Again, the fields' curves confuse with each other.

Now, both tolerances will be taken into account at the same time. First with the same default parameters: FIGURE 8.7a. Then with DLR two times tighter and DAK three times tighter: FIGURE 8.7b.

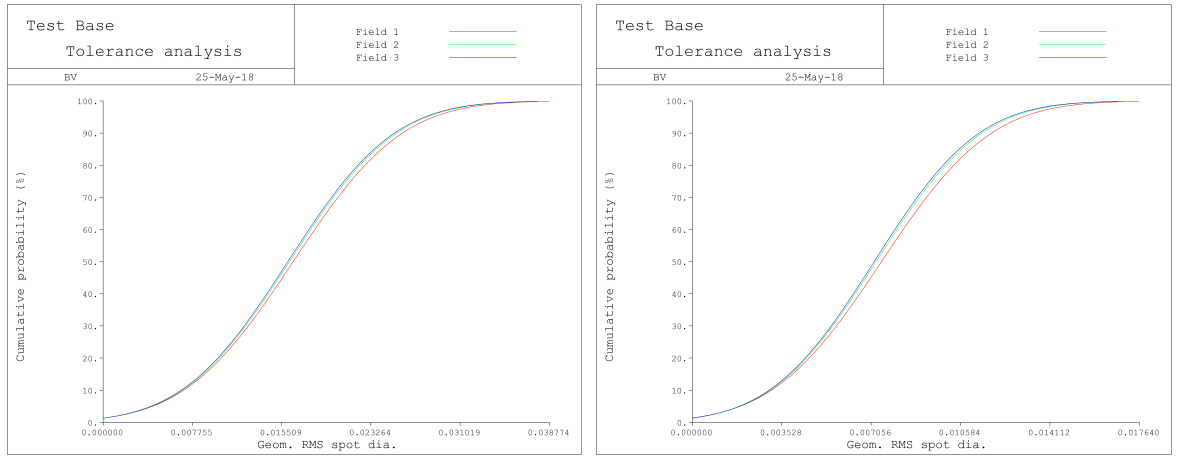

(a) Default parameters (b) Tighter tolerances

Figure 8.7: DLR, DLF and DAK sensibility analysis.

With the default parameters, the pixel size is already reached around 40%, therefore tighter constraints had to be applied to ensure a good image quality as it is the case in FIGURE 8.7b. Also, even though all the curves had the same shape, the total manufacture tolerances are not as simply obtained than by adding the results due to the radius of curvature alone with the ones of the conic constant. It is actually obtained through more complex computations and *CODE V* gratefully computes it by itself.

Assembly tolerances

In addition to the manufacture imperfections, there can also be some assembly imperfections such as the distances between the mirrors or some unwanted tilts in the mirrors position. It actually corresponds to the mirrors alignement which is very important in optical system. Two kind of tolerances will be applied. First, on the displacements of each mirror in the x (DLX) or y (DLY) direction with a default parameter of 0.025 [mm] and then considering a tilt in alpha (DLA) or in beta (DLB) which actually represents a tilt forward or sideways with a default parameter of 0.001 [rad]. They will firstly be analyzed separately in order to see which parameters are more sensitive: FIGURE 8.8a for the displacements and FIGURE 8.8b for the tilts.

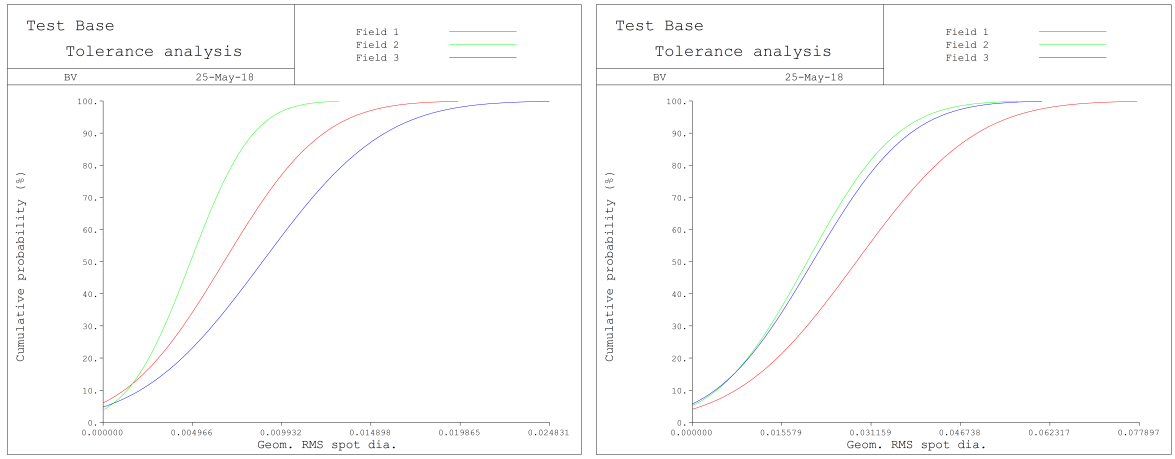

(a) Displacements: DLX and DLY (b) Tilts: DLA and DLB

Figure 8.8: Assembly sensibility analysis.

It can already be seen that the optical design is a lot more sensitive to tilts than displacements. Concerning the displacements, the middle field remains below the pixel size, the zero field is at the edge and the extreme field oversize it at about 85%, so the tolerances should be a bit tighter. Moreover, it is mainly due to the secondary mirror position and then to the primary one while the influence from the tertiary mirror's position is ten times less important. On the other hand, the tilt default tolerances are too big. The geometrical spot size are over the pixel size so tighter tolerances absolutely need to be applied.

The following FIGURE 8.9 shows both tolerances taken into account together. First, FIGURE 8.9a with the default parameters, then FIGURE 8.9 with DLX and DLY twice as tight and DLA and DLB up to 5 times as tight.

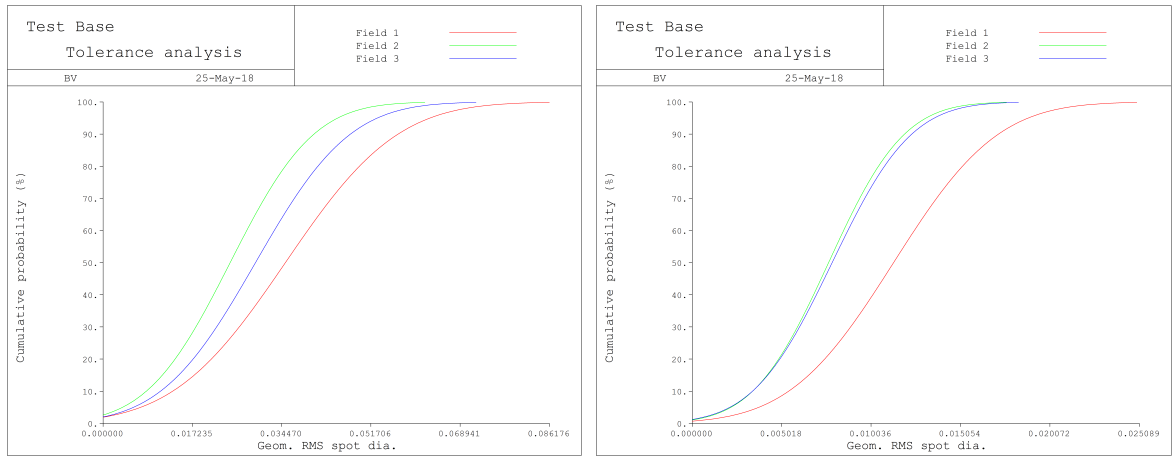

(a) Default parameters (b) Tighter tolerances

Figure 8.9: DLX, DLY, DLA and DLB sensibility analysis.

As expected, the performances with default parameters would become too poor to be accepted

while the performances with the tighter constraints could be used. However, applying tighter tolerances might not be possible in the real life because it would require a very accurate assembly. So this is definitely an issue: the tilt sensitivity is too strong.

3 Distortion

The system engineer said that some measures might have to be taken by tilting the satellite, in order to be able to observe the same spot not only when the satellite is vertically straight up to it. Therefore, it can be studied even at orbits a bit off by tilting the satellite. In the study, it appeared the tilt could go up to a few degrees. It is therefore the job of the optical engineer to study the influence of such a tilt on the optical design.

Actually, the instrument would be rotated vertically by a fixed angular step. The main aberration produced will be the distortion and, more specifically, the barrel distortion, with straight lines bulging outward with increasing distance from the optical axis (CHAPTER 4).

This tilt issue was actually dealt with by using the tolerance tool of *CODE V* by considering the optical system to tilt as a whole while the object remained still. However, this sensitivity analysis gives probabilistic result, so they will not be exactly correct but it will still give a quite general idea of the new performances obtained after the tilt. This is done by setting the tolerances through the command BTX, in radian. FIGURE 8.10 shows the resulting spot diagrams for a tilt of 1°.

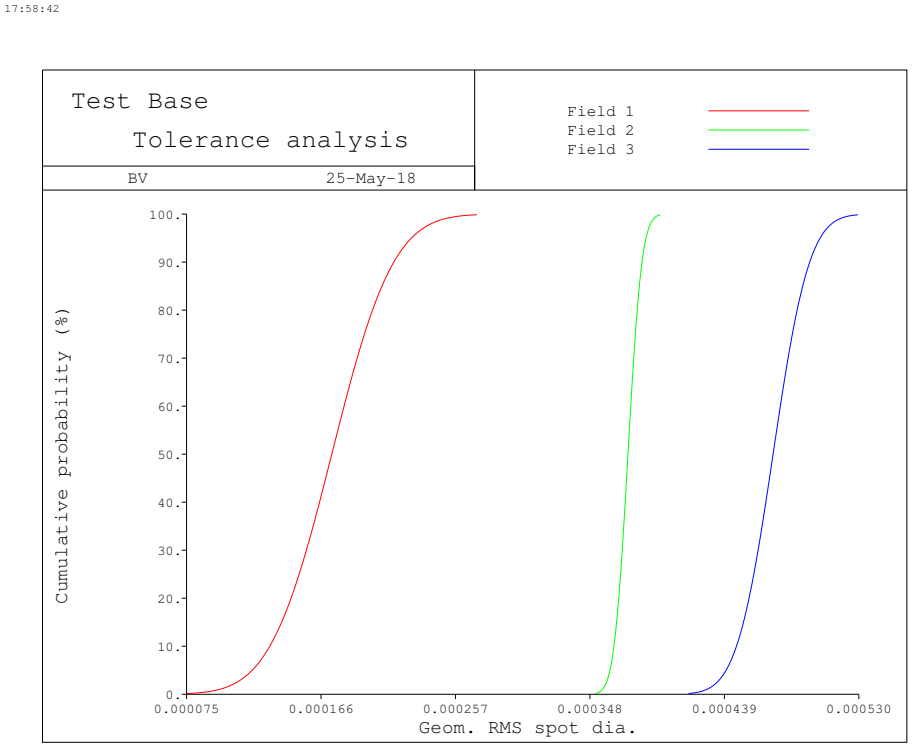

Figure 8.10: Spot diagrams for tilt of 1°.

Such a small tilt angle has almost no influence on the design performances. The same analysis will be made for higher tilts : $5°$ (FIGURE 8.11a) and $10°$ (FIGURE 8.11b).

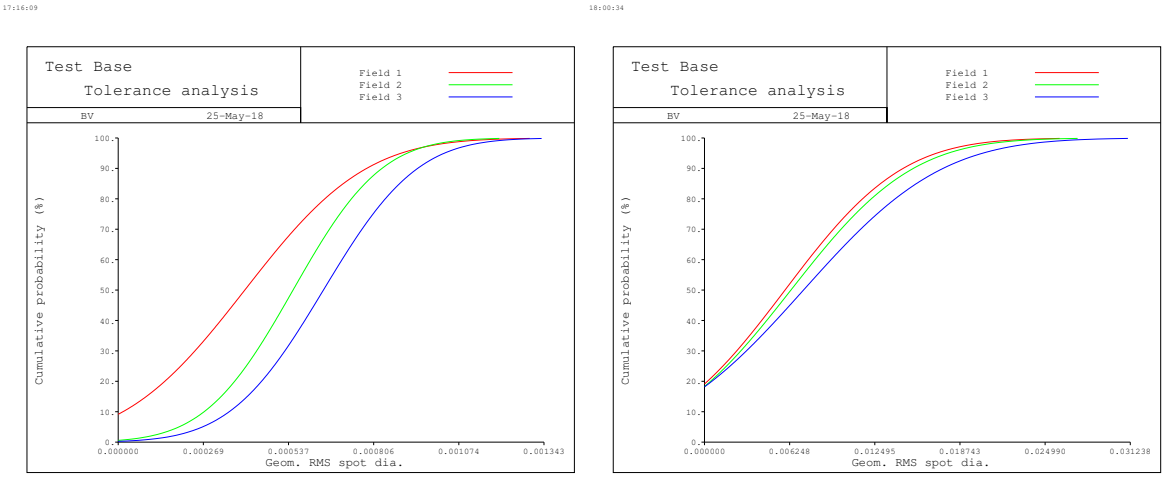

Figure 8.11: Spot diagrams for tilt of $5°$ (left) and $10°$ (right).

Fot the $5°$ tilt, the spot diagram is still acceptable at all time while a tilt of $10°$ would become more troublesome, the spot diagrams reaching the pixel size around 85%.

4 Environmental change

So far, in all the computations, the temperature and the pressure were unchanged through the whole process. This section will take into account a temperature shift to analyze its influence on the performances of the design. Indeed, the space is a harsh environment. The satellite will sometimes be straight in the sun's way and sometimes in eclipses. This will be the job of the thermal engineer to make sure every component of the satellite stays in its operational range of temperatures.

This is actually a kind of sensitivity analysis where the temperature will be modified. Therefore, all the parameters must be frozen beforehand. Then the influence of increase/decrease of temperature will be observed on the spot diagrams. This study will be made by specifying to *CODE V* the material used for the mirrros, the ZERODUR in this cas. Its coefficient of thermal expansion will be used: $\tau_T \simeq 0.1 \times 10^{-6}$ [1/K]. The results are plotted in FIGURE 8.12a. Next to it, FIGURE 8.12b present the same analysis if Aluminum was considered ($\tau_{T,AL} \simeq 20 \times 10^{-6}$ [1/K]).

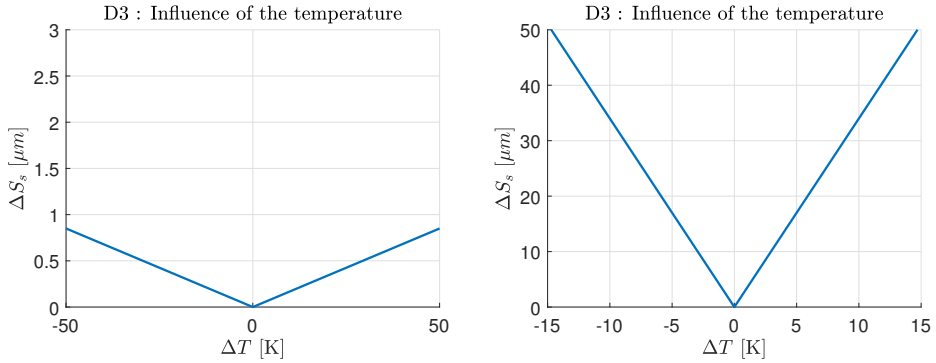

(a) Using ZERODUR (b) Using Aluminum

Figure 8.12: Sensitivity of the optical performances to the temperature.

It can be seen that the performance of the design are not very sensitive to the temperature. A difference of 50 degrees would not even increase the spot size by $1\mu m$. Comparing it with the Aluminum reinforced the choice of ZERODUR over Al made in CHAPTER 5. On the other hand, it should be mentioned that increasing the temperature affects the extreme angle field the most while decreasing the temperature actually affects the zero field more than any others.

Besides the general thermal analysis, a more local thermal issue could occur. Indeed, in this configuration, the detector is inside the optical design and only 3.3 [cm] away from the primary mirror. This situation represents a hot component next to a cold one, resulting in high radiative transfer that should be avoided. The good point is that the detector is actually behind the primary mirror, so, an insulated coating could be applied on its back side since that surface area is not needed for reflection.

5 Detector(s)

As explained about this design configuration, the detector must fit inside the optical design. It was managed for this final design. However, it will not hold still there by itself. It must be held with some filaments which will actually be in the way of the light rays that have not reached the detector sensors yet. This is why the material used must be completely transparent to MWIR wavelength to avoid any loss of performances by modifying the rays initial path.

This final design will then be a totally reflective design suffering from no chromatic aberrations because independant of the wavelength, geometrically-wise. Therefore, the big advantage of reflective optics over refractive optics could be to observe light at other wavelength, especially in the visible (VIS). Indeed, each light rays will be reflected the same way and since the VIS is in smaller wavelength, the Airy Disk diameter would be smaller resulting in a better image resolution. However, the current detector is only working in the MWIR spectrum which mean another detector should be placed to take in the visible light. This could actually be done by adding a surface in the optical system that would be transparent to MWIR but reflective for VIS which is actually the case of the Silicon (Si). Therefore this addition of surfaces would not modified the initial design but could focus the rays into a potential VIS detector, inserted above the tertiary mirror for instance. Furthermore, making a use of the VIS light rays is actually a

way to manage the VIS spectrum which was initially part of the unwanted wavelength for the detector, transforming a source of aberrations into a source of information.

Actually, a lead can be explored by combining design 2 and design 3. This is represented in FIGURE 8.13.

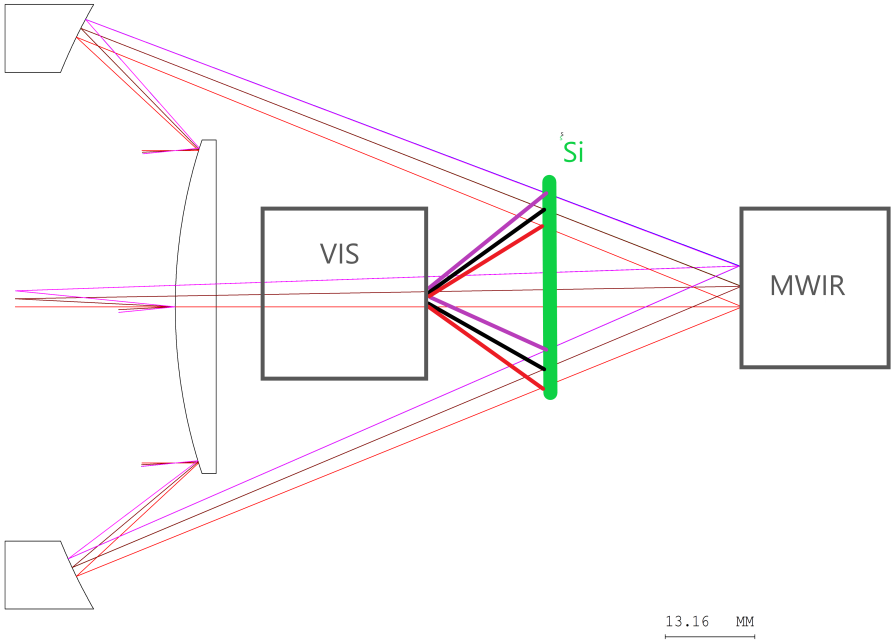

Figure 8.13: Potential design including both MWIR and VIS detectors.

The MWIR rays would follow the path of the design 2, going through the silicon plate and straight to the MWIR detector while the VIS rays, would be reflected by the Silicon plate to the VIS detector, following the same path as the design 3. However, such a configuration could reveal itself to be quite complex to make because the EFL might be different from one range of wavelength to another and it would require every analysis to be run twice. Also, more constraints would come from the space needed for both detectors.

6 Stray light

The stray light means the unwanted light which could interfere with the actual light that is supposed to be observed. The stray light can be of two types: [3]

- In field: It can be due to light from unwanted wavelength or due to reflection on the very edge of the optical components resulting in unplanned reflection. The cross-talk which is any phenomenon by which a signal transmitted on one circuit or channel of a transmission system creates an undesired effect in another circuit or channel. Moreover no surface are 100% reflective meaning some rays will be refracted and can then be reflected on the back surface of the mirrors, through its thickness. Such ray of light are called ghost and they can produce an out-of-focus blur.

- Out of field : it is usually coming from light outside of the field of view representing extra information out of the object that is supposed to be observed. It is called light pollution. It can also be produced by multiple reflections in the optical design.

The out of field stray light can be avoided by different means. A simple way to attenuate the multiple reflection is to paint the inside of the CubeSat structure. Another thing that can be done is to use a baffle system as shown in FIGURE 8.14.

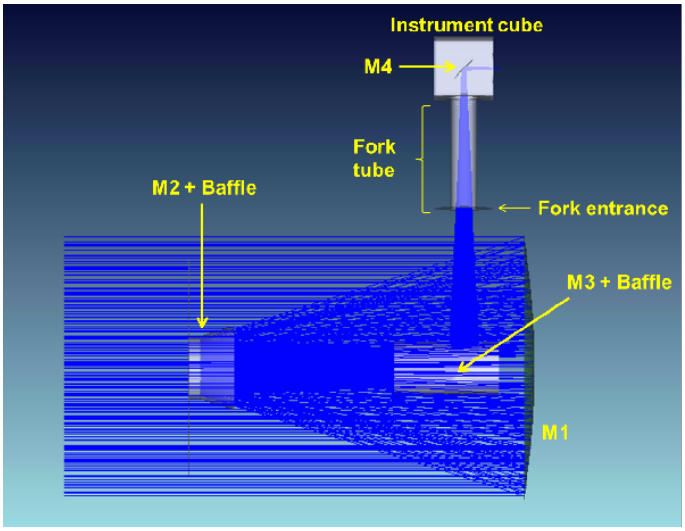

Figure 8.14: Baffle system in an optical design [47].

It can be seen that the baffles are placed close to the mirrors, and even more than one is placed to ensure even less unwanted stray light hit the mirrors. Such a baffle system makes the way for the light to go straight to the detector. It avoids double reflection but, most of all, restrains the light to the wanted field of view by preventing out of field stray light to go through the baffled system.

The baffle system that could be imagined in the final design is roughly represented in FIGURE 8.15.

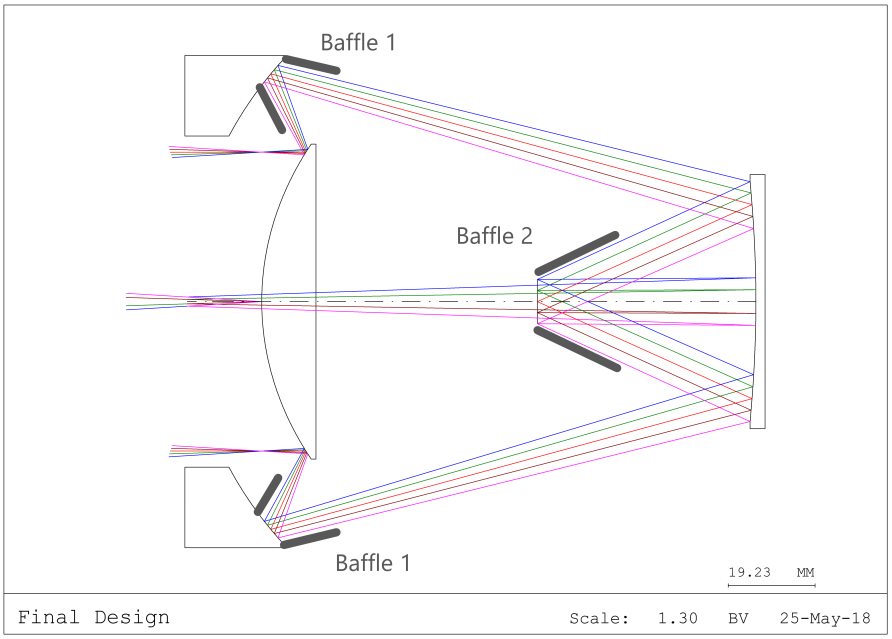

Figure 8.15: Final design : Baffle system.

Two different baffles are used. The first one focusing the light reflected on the circular edge of the secondary mirror which would be all the way around in 3D. The second one which guides the light rays from the tertiary mirror straight to the detector.

7 Jitter

Actually more factors comes into play when analyzing the performances of the optical system. For instance, the jitter inducing image degradation should be taken into account as well, it is the line-of-sight (LOS) movements due to vibrations inside the spacecraft structure. Indeed, if the vibrations are too significant, it will result in a blurry image, so the jitter must be handled properly. Even though the vibrations can be induced from many sources (such as the ADCS, the cooling system, the deployment of the solar panel,..), they can all be resumed in one equation as the MTF_{jitter}, EQUATION 8.1 [20].

$$MTF_{jitter} = e^{-2\pi^2\sigma^2 f^2} \tag{8.1}$$

with σ^2 the LOS jitter variance coming from all sources and f the spatial frequency. Then, this value must be multiplied by the actual MTF of the optical design to obtain the new degraded results. Therefore, a system free of jitter would have its $MTF_{jitter} = 1$. The higher the spatial frequency and the higher the jitter, so, again, the Nyquist frequency, being the smallest acceptable one should be used to avoid as much consequences due to the vibrations as possible. On the other hand the value of σ^2 can hardly be assessed, but should be as low as possible. Eventually, the jitter would result in lowering the MTF and decreasing the image resolution.

Chapter 9

Further study

1 Deployable petals

The diffraction limit has been quite an issue when making the designs and ensure they were operational. Two ways have been presented in order to fix the diffraction problem. Decreasing the EFL but that meant increasing the GSD which was not really a solution. The other way is to increase the entrance pupil diameter, this can be increased over the size of the CubeSat when considering deployable optics. Then of course the design must be well conceived to have low geometrical aberration.

A preliminary study was made, considering deployable optics for OUFTI-NEXT which will have the shape of a Cassegrain telescope. This is actually done by means of two different mechanisms. The first one is about deploying the four petals that will serve as the primary mirror, as shown in FIGURE 9.1. This is done by means of hinge joints.

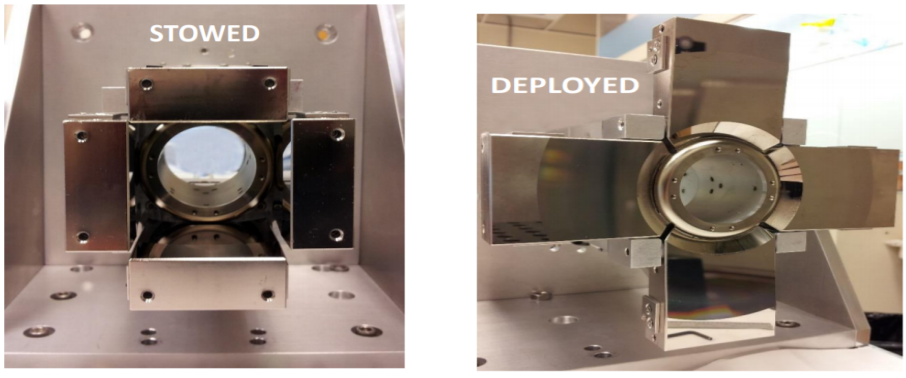

(a) Initial position (b) Final position

Figure 9.1: Deployment of the primary mirror [48].

Then, the second mechanism will be an arm using a prismatic joint in order to bring the small circular secondary mirror up front: FIGURE 9.2

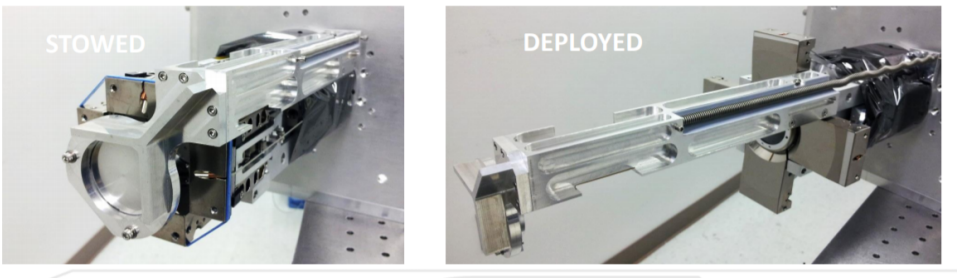

Figure 9.2: Deployment of the secondary mirror [48].

In order to have an idea of how much the mechanism would influence the whole satellite, both mechanisms were implemented into the software SAMCEF FIELD by using some assumptions in order to make the computations easier. For instance, the study will be made in two dimensions, the different elements will be assumed as rigid bodies and the frictions will be neglected. Then it can be represented by the following free-body diagram (FIGURE 9.3).

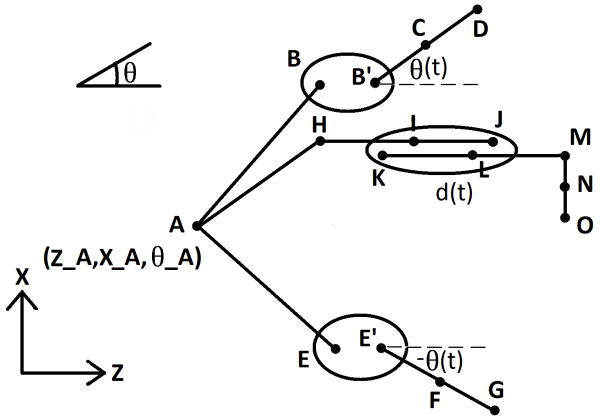

Figure 9.3: Free-body diagram of both mechanisms

The circles represent either the hinges or the prismatic joint where the different motors will be acting to set the mechanisms going. And the node A is the center of gravity representing the whole satellite. The whole purpose of this study will be to analyze by how much the center of gravity will be influenced when the optical system is deployed. This is plotted in FIGURE 9.4a showing its displacements along the $x-axis$ and the $z-axis$ (since working in 2D, it will not be able to move along the $y-axis$) as well as its rotation (positive taking counterclockwise). The energy needed was also analyzed in FIGURE 9.4b.

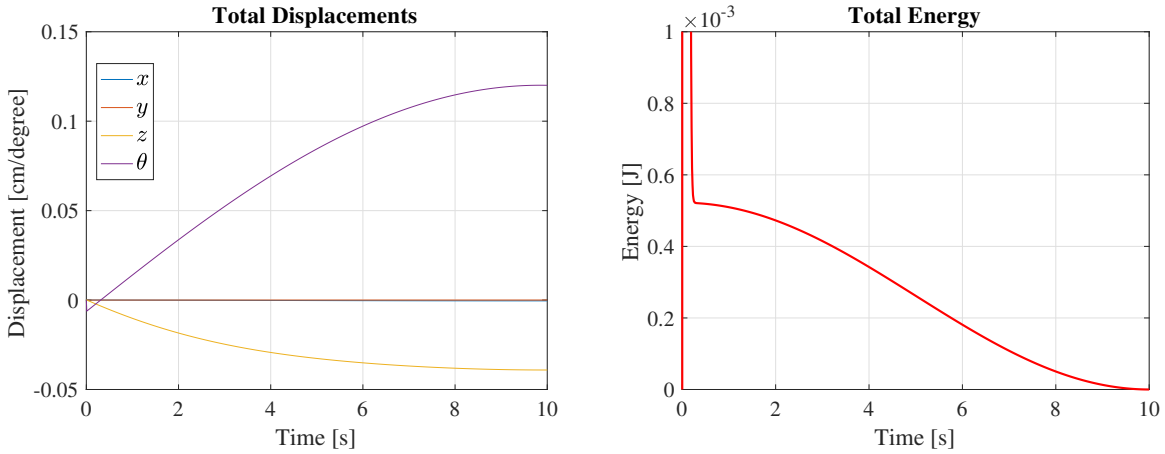

(a) Displacement of the center of gravity

(b) Total energy of the system

Figure 9.4: Influence of the mechanisms on the satellite

As it can be seen, the scales of both graphics are really low. It means the mechanisms do not influence the whole satellite's state by much. The biggest modification would be that the satellite rotates counterclockwise by a little more than $0.1°$ which can easily be counterbalanced by the ADCS of the CubeSat, but still, it is important to know this beforehand. Concerning the Energy, it is only kinetic energy, and there is only a little needed to start up the mechanisms. Anyways, those results must be treated cautiously due to the big assumptions made.

It can still be interesting to see what performance improvements the deployable optics could bring. In the previous case, the petals were assumed to be 10 [cm] long each. Which means the aperture goes up to 30 [cm], three times more than a satellite containing the optical design inside its structure. Therefore, at the diffraction limit, the maximum EFL acceptable would be:

$$EFL = \frac{D_A d}{2.44\lambda} = \frac{0.015 \times 300}{2.44 \times 0.005} = 368.853 \tag{9.1}$$

However, the primary mirror is composed of 4 petals and does not represent a circular mirror anymore which will definitely be very different to implement into *CODE V* and most likely behaves differently than the previous design. The radiometric budget must also be quite different.

Now, if we were to imagine that such an EFL of 368 [mm] could be reached while keeping the spot diagram size below the pixel size [1], then, the graphic from FIGURE 5.5 would become the new graphic plotted in FIGURE 9.5.

[1] Actually, the system is a kind of Cassegrain telescope which is known to reach high EFL and moreover, the secondary mirror distance can be controlled by the second mechanism so it could quite easily go to high EFL.

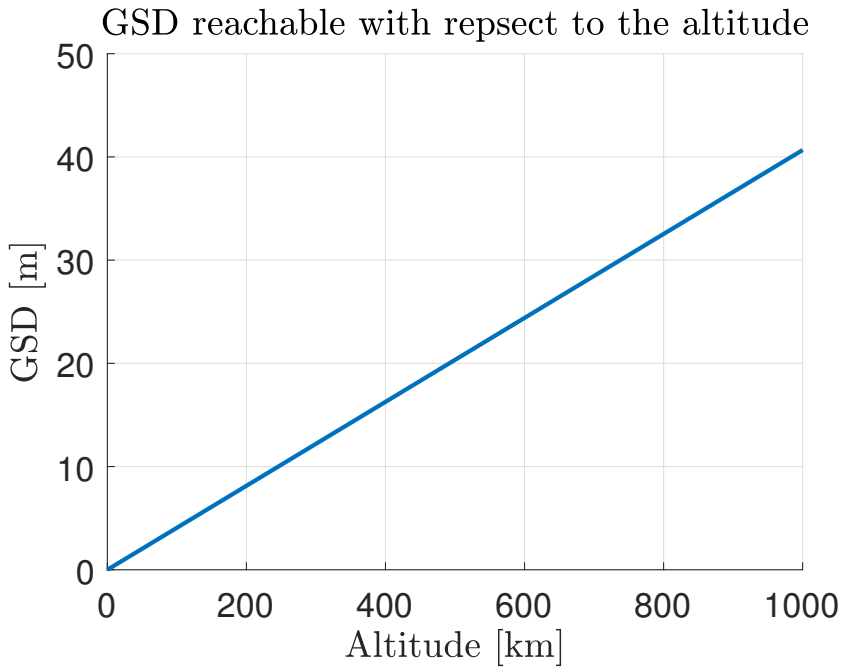

Figure 9.5: Best GSD with respect to the altitude with deployable optic

As it can be seen, the GSD reachable are substantially lower. Indeed, even at an orbit of 600 [km], a GSD of less than 25 [m] could theoretically be reached. The question of getting a GSD lower than 100 [m] would not be an issue anymore at any altitude.

However, bringing new mechanisms in the CubeSat system is always a gamble because it usually brings better performances but if it were to fail, it would mean the entire failure of the whole CubeSat. It must be perfectly well designed so the benefits are worth the risks. But in the case of the demonstrator OUFTI-NEXT, there is no need to consider deployable optics. The goal of the demonstrator is to be a 100% reliable while some risks can be taken on the future CubeSats that will form the potential constellation.

2 More

6U

The possibility of switching to a 6U CubeSat was only considered if a 3U would not be sufficient to fulfill all the mission's requirements. However, as it was shown in CHAPTER 3, in the case of ARKYD-6, the 3U addition do not influence the optical design much. Indeed, this latter still fits in one side of the twice as big CubeSat because the new space will be used for other payloads mostly. Also, a larger CubeSat would allow larger solar panels, radiator and batteries but on the other hand having more payloads requires more energy and more components to keep stable thermally and physically. In the end, the same compromises will have to be made but at larger scale.

Concerning the current optical design fitting in the OUFTI-NEXT 3U CubeSat, the main issue was definitely the diffraction parameter in the scope of reflective optics. Therefore, if a 6U

CubeSat were to be used, its main interest concerning the optical design alone would be to stretched the entrance pupil diameter to more than 1U of width so theoretically a larger EFL could be used within the diffraction limit which will eventually results in a smaller GSD and more accurate images as initially requested.

Thermal image over image resolution

As said in CHAPTER 2, the main goal of the mission is actually to observe the gradient of temperature in agricultural fields which indeed requires a good image resolution but most of all a great thermal resolution. One idea could be to leave aside the image resolution in favour of the thermal one. Therefore, the diffraction limit would not be the main concern anymore and could be "ignored" while only the thermal information would be favoured. Such a strategy would obviously restricts the satellite's possibilities in capturing images but could ensure the actual mission's goal to be reached more easily.

Constellation

OUFTI-NEXT is a demonstrator and its top level requirement is to be a satellite which actually works and will do the job it has been built for. Therefore, the key word when designing it is simplicity. It is much more important to actually get results even if they must be poor in quality and if only a few of them are obtained that not getting any results at all. As its name suggests, a demonstrator is made to prove that some great information could be provided in the event of a constellation. Then, in that constellation, once the OUFTI-NEXT will have proven its worth, the satellite can be improved if needed to obtain even sharper results. Only then, some risks such as deployable optics or sun shield can be considered.

Chapter 10

Conclusion

The aim of this master thesis was the conception of an optical design which could be used for the OUFTI-NEXT project as long as it fulfills the top level requirements of the mission. However, the objectives being too tight, they had to be lightened in order to get a working design.

This project considered reflective optical systems and was actually done in parallel with two other master thesis studying the exact same optical properties but using refractive optics. Therefore, the studies present a trade-off of the optical design which will actually be used for the OUFTI-NEXT project. In an ideal context, both studies should be able to find an operational design. Then, the analysis of the designs is made, giving their different properties and performances. That way, a final choice could more easily made. But in the end, their performances should be quite similar. The best advantage of the reflective optics being the fact that other the Visible spectrum of light could potentially be observed within the same performances.

The main issues in designing an optical system are the geometrical aberration and the diffraction limit. Because of the high wavelengths present in the MWIR window, it was hard to find an working design even after a lot of iterations, going through the optimization tool of a powerful optical software (*CODE V*). Eventually, a design was found (Design 3) fulfilling all the lightened top level requirements. However, that does not mean the design can be use in the actual mission. Indeed, other simulations still need to be made such as the tolerances analysis. Such an analysis describes the sensitivity of the design assuming assembly or manufacture imperfections. Unfortunately, the design was quite sensitive and needed tighter tolerances in order to remain operational.

In other words, the design works well in its perfect configuration but suffers from the tolerances analysis. Moreover, the performances analysis were driven neglecting a few parameters such as the stray lights or the jitter. Such parameters would tarnished the optical design performances even more which were not taken into account in the analysis through this master thesis.

In the end, a deep analysis was made giving an quite accurate preliminary definition of the optical properties. Therefore the general OUFTI-NEXT project is already deep down phase B. And if someone was to take over this work, he should start from the design 3, which still has some room for improvements, mostly concerning the tolerances analysis.

Bibliography

[1] Grabcadcommunity. The Cube Sat (satellite) (1U, 3U .. ..) June 2015. URL: https://grabcad.com/library/the-cube-sat-satellite-1u-3u-1.

[2] Wikipédia. Attitude control. 2018. URL: https://en.wikipedia.org/wiki/Attitude_control.

[3] J. Loicq. Space experiment, slides. 2017-2018.

[4] G. Kerschen. Satellite engineering, slides. 2016-2017.

[5] SLidePlayer. Remote sensing. 2018. URL: http://slideplayer.com/slide/4983795/#.

[6] Jet propulsory Laboratory NASA. CubeSat. 2018. URL: https://www.jpl.nasa.gov/cubesat/missions/.

[7] Planetary ressource. Arkyd-6 mission. 2018. URL: https://www.planetaryresources.com/missions/arkyd-6/.

[8] Thomas S. Pagano. "The CubeSat Infrared Atmospheric Sounder(CIRAS)". In: (2018).

[9] Nanosatellite database. CubeSat Tables of the Nanosatellite Database. 2018. URL: http://www.nanosats.eu/tables.html.

[10] P.Hollingsworth N.H.Crisp K. Smith. Launch and deployment of small satellite systems. Science direct, 2015.

[11] Lori Keesey. Lunar IceCube to Take on Big Mission From Small Package. August 4, 2015. URL: https://www.nasa.gov/feature/goddard/lunar-icecube-to-take-on-big-mission-from-small-package.

[12] IACS/CUA/NASA/GSFC P.E. Clark. "BIRCHES : Mars CubeSat instrument". In: (2018).

[13] C. Barbier. Remote sensing, slides. 2017-2018.

[14] Haystack Observatory. Optical and Radio Astronomy. 2017. URL: https://www.haystack.mit.edu/edu/undergrad/materials/tut3.html.

[15] Imagen-Estilo. Lens Diffraction Limit. 2016. URL: http://www.imagen-estilo.com/Articles/Photography-basics/lens-diffraction-limit.html.

[16] Robert D. Fiete; Bradley D. Paul. Modeling the optical transfer function. August 2014. URL: https://www.spiedigitallibrary.org/journals/optical-engineering/volume-53/issue-08/083103/Modeling-the-optical-transfer-function-in-the-imaging-chain/10.1117/1.OE.53.8.083103.full?SSO=1.

[17] Rutten & van Venrooij. Telescope optics. Willmann-Bell, Inc., January 2006.

[18] Nave R. The Rayleigh Criterion. 2006. URL: http://hyperphysics.phy-astr.gsu.edu/hbase/phyopt/Raylei.html.

[19] Norman Koren. Understanding image sharpness. 2013. URL: http://www.normankoren.com/Tutorials/MTF.html.

[20] Christian KINTZIGER. "Feasibility of a UV imager onboard a Cubesat platform". In: (2013).

[21] Edmund Optics. Pixel Sizes and Optics. 2017. URL: https://www.edmundoptics.eu/resources/application-notes/imaging/pixel-sizes-and-optics/.

[22] AQA AS. Snell's Law, Refraction and Total Internal Reflection. January 2010. URL: https://physi.wordpress.com/2010/01/13/snells-law/.

[23] NASA. IR Atmospheric Windows. 2018. URL: http://coolcosmos.ipac.caltech.edu/cosmic_classroom/ir_tutorial/irwindows.html.

[24] ACEPT W3 Group. Silicon – a Material Transparent to Infrared. 1999. URL: http://www.asu.edu/courses/phs208/phs208_iv/patternsbb/PiN/info/rdg/silicon/index.htm.

[25] Michael S. Basic optics. 2003. URL: http://wiley-vch.e-bookshelf.de/products/reading-epub/product-id/5030654/title/Optical.

[26] Photographylife. Spherical aberration. February 2018. URL: https://photographylife.com/what-is-spherical-aberration.

[27] SlideShare. Aberrations of lenses. August 2013. URL: https://www.slideshare.net/personalp/aberrations-of-lenses.

[28] Edmund Optics. How Aberrations Affect Machine Vision Lenses. 2018. URL: https://www.edmundoptics.com/resources/application-notes/imaging/how-aberrations-affect-machine-vision-lenses/.

[29] Wikipedia. Petsval curvature field. 2018. URL: https://en.wikipedia.org/wiki/Petzval_field_curvature.

[30] Gonzalez Birney and Oesper. Observational astronomy. Cambridge University Press, June 2006.

[31] Russell McMahon. How to read a lens spot diagram. January 2012. URL: https://photo.stackexchange.com/questions/19051/how-to-read-a-lens-spot-diagram.

[32] Wikipédia. Reflecting Telescope. URL: https://en.wikipedia.org/wiki/Reflecting_telescope.

[33] NASA Rob Gutro. James Webb Space Telescope Mirror. December 2009. URL: https://www.nasa.gov/topics/technology/features/jwst_mirror.html.

[34] Schott. Extremely Low Expansion Glass Ceramic. 2018. URL: https://www.schott.com/advanced_optics/english/products/optical-materials/zerodur-extremely-low-expansion-glass-ceramic/zerodur/index.html.

[35] Newport. Optical Mirror Selection Guide. 2018. URL: https://www.newport.com/g/optical-mirror-selection-guide.

[36] Edmund Optics. IR mirrors. 2018. URL: https://www.edmundoptics.eu/optics/optical-mirrors/infrared-ir-mirrors/.

[37] NGENDAKUMANA P. BOZET J-L. Launch Vehicle, slides. 2017-2018.

[38] M. Schaepman H. Wulf. Earth Ressources Satellites. 2015. URL: http://www.geo.uzh.ch/microsite/rsl-documents/teaching/BSc/geo123/2015/GEO123.1_Lecture_08_FS2015_EarthResourceSatellites_dpi220.pdf.

[39] ResearchGate. Atmospheric transmission. November 2017. URL: https://www.researchgate.net/figure/Atmospheric-transmission-in-the-mid-wave-infrared-MWIR-region_fig1_321048132.

[40] Enrico Ghidoli. "Feasibility of Earth Observation in the MWIR Window with Cubesats for Agriculture Monitoring". In: (2017).

[41] Victor Laborde. "Oufti-Next : Radiometric budget". In: (May 2018).

[42] David Brooks. Pyranometer Protocol. January 2008. URL: http://www.instesre.org/Solar/PyranometerProtocol/PyranometerProtocol.htm.

[43] K. Thompson J. Grider. Photon statistics. 2005. URL: https://www.stmarys-ca.edu/sites/default/files/attachments/files/GriderJordanFinalReport_0.pdf.

[44] Zigya. Light : reflection and refraction. 2018. URL: https://www.zigya.com/study/book?class=10&board=cbse&subject=Science&book=Science&chapter=Light+-+Reflection+and+Refraction&q_type=&q_topic=Refraction+of+Light&q_category=&question_id=SCEN10052629.

[45] Wikipedia. Conic constant. 2018. URL: https://en.wikipedia.org/wiki/Conic_constant.

[46] CODEV. CODE V Reference Manual. September 2013.

[47] ResearchGate. TNT Optical initial optical design. 2018. URL: https://www.researchgate.net/figure/TNT-Optical-initial-optical-design-before-baffle-installation-ZEMAX-model_fig1_283085206.

[48] Trent Newswander James Champagne Blake Crowther. CubeSat Image Resolution Capabilities with Deployable Optics. Space Dynamics Laboratory, 2017.